QUANTUM-CHEMICAL INVESTIGATIONS OF SECOND- AND THIRD-ORDER NONLINEAR OPTICAL CHROMOPHORES FOR ELECTRO-OPTIC AND ALL-OPTICAL SWITCHING APPLICATIONS

A Dissertation
Presented to
The Academic Faculty

By

Amalia Agnew

In Partial Fulfillment
Of the Requirements for the Degree of
Doctor of Philosophy in the
School of Chemistry and Biochemistry

Georgia Institute of Technology
August 2006

QUANTUM-CHEMICAL INVESTIGATIONS OF SECOND- AND THIRD-ORDER NONLINEAR OPTICAL CHROMOPHORES FOR ELECTRO-OPTIC AND ALL-OPTICAL SWITCHING APPLICATIONS

Approved by:

Dr. Jean-Luc Brédas, Advisor
School of Chemistry and Biochemistry
Georgia Institute of Technology

Dr. Rigoberto Hernandez
School of Chemistry and Biochemistry
Georgia Institute of Technology

Dr. Seth Marder
School of Chemistry and Biochemistry
Georgia Institute of Technology

Dr. Bernard Kippelen
School of Electrical and Computing Engineering
Georgia Institute of Technology

Dr. Joseph Perry
School of Chemistry and Biochemistry
Georgia Institute of Technology

Date Approved: July 2006

To Aaron, my parents, the Agnew and Leclercq families

ACKNOWLEDGEMENTS

"All progress is precarious, and the solution of one problem brings us face to face with another problem" and *"After climbing a great hill, one only finds that there are many more hills to climb"* are M. L. King and N. Mandela's quotations which appear to be a good description of the scientific research. Fortunately, lots of great people have pushed me from one solution to another one with huge patience.

My first thank you goes to my advisor, *Professor Jean-Luc Brédas* (Georgia Institute of Technology), who has given me the opportunity to complete this dissertation and always believed in me even through life's storms. My second thank you goes to the members of my committee: *Professors Seth Marder and Joseph Perry* (Georgia Institute of Technology) for their teaching and collaboration, and finally to *Professors Bernard Kippelen and Rigoberto Hernandez* (Georgia Institute of Technology) for joining my committee.

This dissertation would have never seen the day without the enormous patience (at so many levels that this pitiful page reserved for acknowledgement could not cover) of *Doctors Egbert Zojer, Karin Schmidt, Steve Barlow* (Georgia Institute of Technology), *Sei-Hum Jang* (University of Washington), *David Beljonne and Victor Geskin* (Université de Mons-Hainaut).

I also would like to thank *Professors Alex K.-Y. Jen, Bruce Eichinger, and Bruce Robinson* (University of Washington) for their collaboration and the opportunity to spend a few days in Seattle.

A huge thank you to the *"brédators"* for the atmosphere they have established in the laboratory, making these past five years great; a special thank you to *Demetrio* and *Sigi* for always coming to my rescue when the high technology would not do what I want it do (a important finding I would like to share with the people living in denial: the problem is often between the screen and the chair).

Finally last but not least, I want to thank my wonderful husband, *Aaron*, who has tremendously helped me in too many ways to be described here, my *mum and dad*, and both the *Agnew and Leclercq families* for believing in me and giving me support.

I would like to end this acknowledgement section on two positive thoughts that will accompany me for the next chapter of my life: *"Imagine each new day is a canvas on which you can paint the most beautiful scene your mind can conceive … then put yourself into the picture"* and *"Education is the most powerful weapon which you can use to change the world"*.

Thank you!

TABLE OF CONTENTS

LIST OF TABLES

LIST OF FIGURES

SUMMARY

The past decades have witnessed the development of new materials with large nonlinear optical (NLO) properties, which have made them attractive candidates for a broad spectrum of applications in the electro-optic and photonic fields (*e.g.*, telecommunications and computing). A deeper understanding of the relationship between, on the one hand, the electrical and (linear and nonlinear) optical properties and, on the other hand, the chemical structure has proven useful for the rational design of new efficient NLO materials. Developing such an understanding has attracted major interest in the scientific community worldwide in both academia and industry.

Traditional electro-optic and photonic technologies based on inorganic materials, such as $LiNbO_3$, face inherent limitations leading the commercial devices based on such materials to approach practical limits. Although organic materials have their own deficiencies, a broader range of intrinsic advantages and potential design suggests that for many applications, organic technologies provide attractive alternatives to those based on inorganic platforms.

The development of commercial devices of high quality has been helped via the establishment of multidisciplinary research teams combining: (i) theoretical modeling using quantum-chemical computational calculations; (ii) organic synthesis; (iii) optical characterization; and (iv) device fabrication. In this dissertation, quantum chemistry is used to evaluate the second- and third-order NLO properties of series of new chromophores. We take advantage of a feedback loop with experimental teams to

understand the relationship between NLO properties and chemical structure, with the hope of assisting the rational design of new and efficient NLO chromophores.

CHAPTER 1 INTRODUCTION

1.1. BASIC CONCEPTS

Optics studies the interaction between an electromagnetic radiation (here, we will concern ourselves only with the electric field of the electromagnetic radiation) and matter (here, we will focus only on the response of the electrons present in the matter). At low radiation intensity, the response of the matter is linear but nonlinear effects are observed under intense radiation, such that generated by a laser. Therefore, in the 1960's, the demonstration of the first working laser by Maiman *et al.* and the observation of second-harmonic generation by Franken *et al.* (by shining a ruby laser onto a quartz crystal) led to the early foundation of the field of nonlinear optics. The interest in nonlinear optics has grown continuously over the past 45 years and covers today a variety of processes ranging from fundamental aspects, including laser cooling and quantum optics, to more applied areas related to information technologies.

The interaction between the electric field of the electromagnetic radiation and the electrons of the matter (leading to their displacements) can be described as a power series in the electric field. For the sake of simplicity, the matter is assumed to be isotropic, lossless, and dispersionless and the total polarization is written (in the electric-dipole approximation) as:

$$\vec{P}_i = \vec{P}_0 + R^{(1)} \sum_j \chi_{ij}^{(1)} \vec{E}_j + R^{(2)} \sum_{jk} \chi_{ijk}^{(2)} \vec{E}_j \vec{E}_k + R^{(3)} \sum_{jkl} \chi_{ijkl}^{(3)} \vec{E}_j \vec{E}_k \vec{E}_l + \ldots \quad [1]$$

where $\vec{P}_i$ is the total polarization; $\vec{P}_0$ is the permanent polarization (in the absence of an electric field); $\vec{E}$ is the applied electric field; $\chi_{ij}^{(1)}$ corresponds to the first-order electrical susceptibility (referred to as the linear optical term); $\chi_{ijk}^{(2)}$ and $\chi_{ijkl}^{(3)}$ correspond respectively to the second- and third-order electrical susceptibilities (referred to as the nonlinear optical terms); and the $R^{(n)}$ terms are the degeneracy factors that depend on the (linear and nonlinear) optical process and the frequencies of the applied electric fields involved in the interaction. The dependence of the induced polarization (linear and nonlinear optical terms) on the applied electric field has drastic consequences for the optical behavior of the matter and can lead to a variety of (linear and nonlinear) optical processes such as the generation of new frequencies.

Each optical process is thus described by electrical susceptibility tensor elements because the electrical susceptibilities are expressed as tensors, which are mathematical constructs allowing one to link two vectors. In general, an n^{th}-order induced polarization, which is due to n interacting electric fields, is described by a (n+1)-rank tensor. The first-order induced polarization term is then written as:

$$\vec{P}_i^{(1)} = R^{(1)} \sum_j \chi_{ij}^{(1)} \vec{E}_j \qquad [2]$$

where i and j run over the Cartesian coordinates x, y, and z. Expanding equation [2] leads to:

$$\begin{pmatrix} \vec{P}_x^{(1)} \\ \vec{P}_y^{(1)} \\ \vec{P}_z^{(1)} \end{pmatrix} = R^{(1)} \begin{pmatrix} \chi_{xx}^{(1)} & \chi_{xy}^{(1)} & \chi_{xz}^{(1)} \\ \chi_{yx}^{(1)} & \chi_{yy}^{(1)} & \chi_{yz}^{(1)} \\ \chi_{zx}^{(1)} & \chi_{zy}^{(1)} & \chi_{zz}^{(1)} \end{pmatrix} \begin{pmatrix} \vec{E}_x \\ \vec{E}_y \\ \vec{E}_z \end{pmatrix} \quad [3]$$

where the χ matrix is a second-rank tensor. Also, the second-order induced polarization is given by a third-rank tensor and consists of 27 elements (since each of the 3 indices i, j, and k can independently take any of the three Cartesian coordinates x, y, and z). Fortunately, the number of independent tensor elements can be reduced by invoking symmetry considerations. Also, for many conjugated chromophores, such as those examined in this dissertation, a few components or even a single component often dominate, which simplifies the analysis. In this dissertation, the second- and third-order induced polarizations are the main focus (because in great demand from the experimental team) and the polarizations of higher order, often much smaller, are ignored.

In the case of a chromophore, in the electric-dipole approximation, the total polarization under non resonant excitation conditions is written as a power series of the electric field:

$$\vec{\mu}_i = \vec{\mu}_0 + R^{(1)} \sum_j \alpha_{ij} \vec{E}_j + R^{(2)} \sum_{jk} \beta_{ijk} \vec{E}_j \vec{E}_k + R^{(3)} \sum_{jkl} \gamma_{ijkl} \vec{E}_j \vec{E}_k \vec{E}_l + \ldots \quad [4]$$

where $\vec{\mu}_i$ is the total dipole moment; $\vec{\mu}_0$ is the permanent dipole moment (in the absence of an electric field); $\vec{E}$ is the applied electric field; the linear (or first-order)

polarizability is given by the tensor α_{ij} and is the molecular equivalent of $\chi_{ij}^{(1)}$; the nonlinear polarizabilities β_{ijk} and γ_{ijkl}, called the second- and third-order polarizabilities (or first and second hyperpolarizabilities), are the molecular equivalents of $\chi_{ijk}^{(2)}$ and $\chi_{ijkl}^{(3)}$, respectively; and $R^{(n)}$ are the degeneracy factors that depend on the (linear and nonlinear) optical process and the frequencies of the applied electric fields involved in the interaction.

Finally, the electrical susceptibilities (linear and nonlinear optical properties of the matter) and the (linear and nonlinear) polarizabilities (linear and nonlinear properties of the chromophore) are related with:

$$\chi^{(n)} \prec \begin{pmatrix} \alpha \\ \beta \\ \gamma \end{pmatrix} Nf \qquad [5]$$

where N (density of chromophores) and f (local field factor) account for the statistical ensemble averages and the intermolecular interactions, respectively.

Specifically, the relationships between $\chi_{ijk}^{(2)}$ and β_{ijk} are challenging and are subject of intensive research; however, simple descriptions based on the oriented gas model exist and have proven to be in many cases a good approximation for the description of poled electro-optic polymers. They are expressed as follows:

$$\chi_{33}^{(2)} = N \frac{\mu^* E_p}{5kT} \beta_{zzz}^* \quad [6]$$

$$\chi_{31}^{(2)} = N \frac{\mu^* E_p}{15kT} \beta_{zzz}^* \quad [7]$$

where the subscripts 33 and 31 of $\chi_{33}^{(2)}$ and $\chi_{31}^{(2)}$ denote the Cartesian coordinates zzz and zxx and the corrected value of β_{zzz}^* is approximated for an electro-optic process to:

$$\beta_{zzz}^* = f_\infty^2 f_0 \beta_{zzz} \quad [8]$$

where f_∞ and f_0 are the Lorentz-Lorentz and Onsager correction field factors for a spherical cavity, respectively, given by:

$$f_\infty = \frac{n^2 + 2}{3} \quad [9]$$

$$f_0 = \frac{\varepsilon_{dc}\left(n^2 + 2\right)}{2\varepsilon_{dc} + n^2} \quad [10]$$

where ε_{dc} is the direct current dielectric constant and n is the refractive index.

Similarly, the corrected value of μ^* is derived from its bare value according to:

$$\mu^* = f_0 \mu \qquad [11]$$

LINEAR OPTICAL TERM

The electric displacement $\left(\vec{D}(\omega)\right)$ in the matter subjected to an electric field $\left(\vec{E}(\omega)\right)$ is defined as the sum of the applied electric field and the induced polarization $\left(\vec{P}(\omega)\right)$:

$$\vec{D}(\omega) = \vec{E}(\omega) + 4\pi\vec{P}(\omega) \qquad [12]$$

When only considering the linear optical term of the induced polarization, equation [12] becomes:

$$\vec{D}(\omega) = \vec{E}(\omega) + 4\pi\chi^{(1)}(\omega)\vec{E}(\omega) = \left(1 + 4\pi\chi^{(1)}(\omega)\right)\vec{E}(\omega) \qquad [13]$$

The term $\left(1 + 4\pi\chi^{(1)}(\omega)\right)$ corresponds to the dielectric constant $\varepsilon(\omega)$ of the medium; when neglecting the magnetic interactions its square root is the refractive index, a parameter that is used to describe how an optical wave propagates into the medium:

$$n(\omega) = \sqrt{\varepsilon(\omega)} = \sqrt{1 + 4\pi\chi^{(1)}}(\omega) \quad [14]$$

The refractive index is a complex number ($n(\omega) = n(\omega) + ik'(\omega)$); the real part that accounts for refraction and frequency dependence describes the dispersion of the medium; the imaginary part describes the absorption of electromagnetic radiation and is related to the linear absorption coefficient $\alpha(\omega)$:

$$k'(\omega) = \frac{\alpha(\omega)c}{2\omega} \quad [15]$$

where c is the speed of the electromagnetic radiation in the vacuum and ω is the oscillating frequency of the applied electric field.

NONLINEAR OPTICAL TERM

Under intense radiation, the response of the matter is nonlinear and the principle of superposition of waves (if two waves of the same frequency and amplitude, A1 and A2, interact in space, the resulting wave has the same frequency as the interacting waves and an amplitude that is the sum of A1 and A2) is no longer applicable; therefore, when two different waves interfere in an NLO material, an energy exchange between them can occur in such a way that some waves vanish and others appear.

The second-order NLO processes arise from the coupling of three photons whose frequencies ω_1, ω_2, and ω_3 are related by the law of conservation of energy: $\omega_1 \pm \omega_2 = \omega_3$, where ω_1 and ω_2 usually correspond to frequencies associated with the incident photons and ω_3 to the frequency associated with the transmitted photon (note that in the case of the parametric oscillator, two photons of frequencies ω_2 and ω_3 can be transmitted from an incident photon of frequency ω_1). Based on the values of frequencies ω_1 and ω_2, the interaction with an NLO material can give rise to various second-order NLO processes such as:

- second-harmonic generation (SHG), for which there is a coupling of two electric fields with identical frequencies ω and the generation of an induced polarization at frequency 2ω;
- the linear electro-optic effect (or Pockels effect), for which an electric field of frequency ω is interacting with a static electric field (zero frequency) and modifies the induced polarization at that same frequency;
- sum-frequency generation (SFG) and difference-frequency generation (DFG).

Both the second-harmonic generation and electro-optic effect are important manifestations of an electromagnetic radiation interacting with matter. The SHG, relevant to new laser technology, is described by the electrical susceptibility tensor elements $\chi_{ijk}^{(2)}(-2\omega;\omega,\omega)$; these write $\chi_{ijk}^{(2)}(-\omega;\omega,0)$ for the electro-optic effect, which has applications in telecommunications and integrated optics. The first frequency argument indicates the frequency of the induced polarization involved in the optical process; due to conventions, this frequency is written with a minus sign so that the sum

of all the frequency arguments is zero, which satisfies the energy conservation conditions.

It is important to note that the field of electro-optics, started well before the field of nonlinear optics. Unfortunately, the two fields use different starting points to describe the action of an electric field, so that a relationship needs to be established in order to connect the two fields. In the framework of electro-optics the refractive index of a material is described as a function of the applied electric field. In contrast, in the framework of nonlinear optics, the starting point is usually to develop the electrical susceptibility into a power series of the applied electric field. Two of the relationships are expressed as:

$$r_{33} = -\frac{8\pi}{n^4}\chi_{33}^{(2)} \qquad [16]$$

$$r_{13} = -\frac{8\pi}{n^4}\chi_{31}^{(2)} \qquad [17]$$

where r_{33} and r_{13} are the electro-optic coefficients, whose relationships to β_{zzz} are obtained by combining equations [6] and [16] (or equations [7] and [17]).

The third-order NLO processes arise from the coupling of four photons whose frequencies ω_1, ω_2, ω_3, and ω_4 are related by the law of conservation of energy: $\omega_1 \pm \omega_2 \pm \omega_3 = \omega_4$, where ω_1, ω_2, and ω_3 correspond to frequencies associated with the incident photons and ω_4 to the frequency associated with the transmitted photon. Based on the

values of frequencies ω_1, ω_2, and ω_3, the interaction with an NLO material can give rise to third-order NLO processes such as:

- third-harmonic generation (THG), for which there is a coupling of three electric fields with identical frequencies ω and the generation of an induced polarization at frequency 3ω;
- the quadratic electro-optic effect (or Kerr effect), for which an electric field of frequency ω is interacting with two static electric fields (zero frequency) and modifies the induced polarization at that same frequency;
- degenerate four-wave mixing.

A third-order NLO process of interest is two-photon absorption (2PA), which corresponds to the simultaneous absorption of two photons of the same energies (degenerate 2PA) or different energies (non-degenerate 2PA), in the presence of intense radiation. Upon 2PA, a chromophore reaches an electronic excited state which is higher than the ground state by the sum of the energies of the two photons absorbed. In 1931, Goeppert-Mayer was the first to propose the possibility that two photons are absorbed simultaneously. The 2PA process has long been regarded as a deleterious effect by the nonlinear optics community, especially in the case of all-optical switching applications where 2PA leads to optical loss and damage. However, as is often the case, what is regarded as detrimental in one field, can be exploited to one's advantage in others; currently, chromophores with large two-photon absorption cross-sections are in great demand and the 2PA process covers a wide range of promising and new applications, which take advantage of two key features:

- High penetration depth. The ability to reach electronic excited states with photons of half the excitation energy improves the penetration in absorbing or scattering media. For a laser radiation of intensity I, the scattering is reduced by a factor of about 16 since the wavelength used for a two-photon (2P) excitation is roughly twice that for a one-photon (1P) excitation. The laser radiation with excitation energy close to the one-photon absorption (1PA) peak of the medium is attenuated along its whole optical path. Hence, in media with a high α, the radiation penetrates the probe only within a short range. In contrast, the laser radiation close to the low 2PA peak usually has an excitation energy well below the 1PA edge where the sample is transparent.
- High spatial selectivity. The rate of simultaneous absorption of two photons depends quadratically on the intensity of an incident laser radiation, which allows for excitation of chromophores with a high degree of spatial selectivity in three dimensions through the use of a tightly focused laser radiation. If a tightly focused laser radiation is used, the intensity is highest at the focus and decreases quadratically with the distance (z) from the focal plane, for distances larger than the Rayleigh length. Thus, the rate at which the chromophores are excited decreases very rapidly (as z^{-4}) with the distance from the focus and the excitation is confined in a small volume around the focus.

Since the 2PA process has only a low probability of taking place (only in the high intensity region of the focal plane, as opposed to the 1PA process, for which absorption can be observed along the whole optical path), the intensity dependence plays a major role.

1.2. MATERIALS OF INTEREST

Although inorganic materials such as $LiNbO_3$ have been the NLO materials of choice for a long time because of their temporal stability, some of their characteristics are not optimal: relatively dense (4.84 g/cm^3), r_{33} of 30 pm/V, relatively low bandwidth (40 GHz/cm), and high driving voltage (3-5 V). Therefore, some efforts have been redirected toward organic materials which, compared to their inorganic counterparts, presented a number of intrinsic advantages: lighter, higher r_{33}, higher bandwidth, and lower driving voltage. The organic materials have been and are extensively investigated for their large second- and/or third-order NLO properties [9].

While all organic materials exhibit third-order NLO properties, symmetry requirements limit the second-order NLO materials and (in the electric-dipole approximation) only those that do not possess a center of inversion exhibit second-order NLO properties. Recall that the induced polarization is expanded into a power series of the electric field (in the electric dipole approximation and considering the NLO molecules to be aligned along their long molecular axis so that the indices i, j, k, and l become x and are removed) as:

$$\vec{P} = \chi^{(1)}\vec{E} + \chi^{(2)}\vec{E}\vec{E} + \chi^{(3)}\vec{E}\vec{E}\vec{E} + ... \qquad [18]$$

The symmetry requirements are easily understood by considering that in an NLO material with an inversion center the second-order induced polarization by two electric

fields pointing in opposite directions are equal in amplitude but have opposite sign $\left(\vec{P}\left(-\vec{E}\right)=-\vec{P}\left(\vec{E}\right)\right)$ and the condition is written as:

$$\vec{P}\left(-\vec{E}\right)=\chi^{(2)}\vec{E}\vec{E}=-\vec{P}\left(\vec{E}\right)=-\chi^{(2)}\vec{E}\vec{E}\rightarrow\chi^{(2)}\vec{E}\vec{E}=-\chi^{(2)}\vec{E}\vec{E}\rightarrow\chi^{(2)}=0 \qquad [19]$$

Therefore, noncentrosymmetry (which should not be equated with anisotropy because a NLO material that is optically anisotropic can still be centrosymmetric) is a necessary condition for second-order NLO materials. Likewise, at the molecular level, the chromophores constituting the second-order NLO material exhibit second-order NLO properties only if centrosymmetry is broken. Therefore, it is imperative to ensure that the noncentrosymmetric chromophores reside in a noncentrosymmetric environment if a large second-order (nonlinear) polarizability (β_{ijk}) is to lead to an observable second-order electrical susceptibility ($\chi_{ijk}^{(2)}$).

Numerous theoretical and experimental studies {10} have been undertaken in order to develop strategies to prevent centrosymmetry in second-order NLO materials. One of the most common has been to orient the second-order NLO chromophores, incorporated into an inorganic or organic polymer matrix host as guest or by covalent attachment, via an electric field poling process of the polymer host {11}. We now discuss this poling in more detail.

The polymer host is heated above its glass transition temperature (T_g) and an electric field is then applied in order to align the chromophores in the polymer host, to which they are covalently attached or in which they are dissolved as guest [12]. The covalent incorporation of the chromophores into the polymer host is preferred over the guest-polymer host system because the sublimation of these chromophores under poling conditions is obviated and the processability problems due to phase separation at high concentration is less likely to happen [12]. The covalent incorporation is achieved by using functionalized chromophores as monomers in the polymerization reaction or by attaching the chromophores to a prefunctionalized polymer host under mild condition. In the former process, the chromophores are either a part of the backbone of the polymer host or a side-chain appendage; both of these procedures involve survival of the chromophores under often harsh polymerization conditions. Therefore, the covalent incorporation by attaching the chromophores to a prefunctionalized polymer host is preferable in many cases [12]. Then, the alignment is frozen in once the polymer host is cooled below T_g and the resulting second-order electrical susceptibility is dependent upon the second-order nonlinear polarizability of the chromophores and their efficiency of alignment (provided no significant relaxation of the system occurs).

If this poling process is to compete with other strategies to prevent centrosymmetry [13], it is necessary to incorporate a high density of chromophores into the polymer host, to achieve a high degree of alignment of the chromophores, and to lock in this alignment for long periods (years) even at elevated temperature (at least $80^{\circ}C$). This alignment is locked in place either by cross-linking of the chromophore-polymer host system or by using polymer host with high T_g (at least 125-150$^{\circ}C$ above the anticipated operating temperature such that over the lifetime of the commercial device the decay of the degree

of alignment of the chromophore alignment is minimized). Therefore, it is necessary to rationally design chromophores that not only present large second-order nonlinear polarizability but also that are thermally robust at a temperature in excess of $200^{\circ}C$ (to withstand the poling process).

1.3. GOALS OF DISSERTATION

The past decades have witnessed the development of new materials with large nonlinear optical (NLO) properties, which have made them attractive candidates for a broad spectrum of applications in the electro-optic and photonic fields (*e.g.*, telecommunication and computing). Specifically, materials exhibiting large second-order NLO properties are exploited in applications such as high-speed optical communications, integrated optics, or optical data processing and storage [{14}]; materials with large third-order NLO properties are used in applications such as all optical switching limiting optical power, upconverted lasing, three-dimensional fluorescence microscopy and microfabrication, two-photon photodynamic cancer therapy, or biological caging [{15}].

A deeper understanding of the relationship between, on the one hand, the chemical structure and, on the other hand, the electronic and (linear and nonlinear) optical properties has proven useful for the rational design of new efficient NLO materials. Developing such an understanding has attracted major interest in the scientific community worldwide in both academia and industry and is helped via the establishment of multidisciplinary research teams. The advantage of the computations is to allow the development of structure-property relationships without having to undertake elaborate organic syntheses or optical characterizations. However, because of the uncertainty in

molecular geometry and the often drastic approximations needed for reasonable efficiency, the success of various calculations can only be evaluated by comparison with experiment. However, as a consequence of differing experimental conditions (for instance, in laser frequencies or solvent polarities), data reported for many of the prototypical NLO organic chromophores show significant discrepancy among them. Thus, it is desirable to establish a uniform database from which many of the aforementioned causes of discrepancy can be eliminated.

The goals of this dissertation are to evaluate the second- and third-order NLO properties of organic chromophores, by using quantum-chemical calculations (discussed in the next chapter) and to take advantage of a feedback loop with experimental teams to understand their relationship to the chemical structure. Specifically, in the context of developing new and efficient primary acceptor end groups for second-order dipolar chromophores, a detailed quantum-chemical investigation is reported on dipolar chromophores incorporating the 4-(dimethylamino)phenyl donor group and a variety of five-membered heterocyclic acceptor groups, including the tricyanofurans (TCF) and the tricyanopyrroles (TCP). New and efficient TCF- and TCP-based dipolar chromophores based on the TCP have been recently synthesized. However, the role of the oxygen atom in the TCF is still unclear. Therefore, a series of dipolar chromophores is investigated, in which the oxygen atom of the TCF is substituted by a variety of other groups X (SiH_2, CH_2, $C{=}CH_2$, NH, C=O, S, $C{=}CHNO_2$, SO, and SO_2) and in which the acceptor group is linked to the 4-(dimethylamino)-phenyl donor group through vinylene or vinylene-thienylene-vinylene π-bridges, in order to understand the extent to which the inductive and resonance effects determine the role of the X group (in terms of the second-order NLO response).

In the context of optimizing the second-order NLO response and determining to which extent the nature of the π-bridge affects it, a detailed quantum-chemical investigation of dipolar chromophores is presented. Here, the second-order NLO responses are evaluated when auxiliary electron-rich thiophene (D') and/or electron-poor thiazole (A') groups are inserted into a variety of positions within the π-bridge and connected with a varying number of vinylene units; in each case, the donor and acceptor groups of the dipolar chromophores are the 4-(dimethylamino)-phenyl and TCF groups.

A detailed quantum-chemical investigation is also reported for third-order dipolar chromophores, for which the two-photon absorption cross-sections are evaluated when auxiliary electron-rich (D') thiophene and electron-poor (A') thiazole groups are inserted into the π-bridge in various positions between the 4-(dimethylamino)-phenyl donor group and TCF. Our objective is to establish the effect on the two-photon absorption cross-section of the order in which the auxiliary groups are inserted into the π-bridge. Finally, the two-photon absorption spectra for a range of bis(acceptor)-substituted bis(dibutoxythienyl)ethene and bis(N-hexylpyrrolyl)ethane quadrupolar chromophores are evaluated and compared to the results of Z-scan and pumb-probe experiments.

CHAPTER 2 METHODOLOGY

The evaluation of the electronic and (linear and nonlinear) optical properties of organic molecules and the understanding of their relationship to the chemical structure by use of quantum-chemical methods [16] are useful tools in the rational design of new efficient NLO chromophores and materials. Therefore, this chapter introduces the basic concepts and important notations for the quantum-chemical methods used in this dissertation.

The non-relativistic, time-independent Schrödinger equation, whose approximate solutions will be exploited here to obtain the electronic properties of a molecule, is written as:

$$H\Psi = E\Psi \qquad [20]$$

where H, the Hamiltonian operator for a material of nuclei and electrons, consists of kinetic and potential energy terms; and Ψ and E correspond to the eigenfunction (total wavefunction) and eigenvalue (total energy) of the investigated molecule, respectively.

If a molecule with M nuclei and N electrons is considered, the Hamiltonian operator is written as (in atomic units):

$$H = -\sum_{i=1}^{N} \frac{1}{2}\nabla_i^2 - \sum_{A=1}^{M} \frac{1}{2M_A}\nabla_A^2 + \sum_{i=1}^{N}\sum_{j>i}^{N} \frac{1}{r_{ij}} + \sum_{A=1}^{M}\sum_{B>A}^{M} \frac{Z_A Z_B}{R_{AB}} - \sum_{i=1}^{N}\sum_{A=1}^{M} \frac{Z_A}{r_{iA}} \quad [21]$$

This Hamiltonian operator includes respectively: a kinetic energy term for the electrons (denoted by indices i and j), a kinetic energy term for the nuclei (denoted by indices A and B), a repulsion term between electrons, a repulsion term between nuclei, and finally a term representing the Coulomb attraction between electrons and nuclei. Also, in equation [21], M_A, Z_A, and Z_B correspond to the ratio of the mass of the nucleus A to the mass of the electron i, the atomic number of the nucleus A, and the atomic number of the nucleus B respectively; the parameters r_{ij}, R_{AB}, and r_{iA} represent respectively the distance between two electrons i and j, the distance between two nuclei A and B, and the distance between one electron i and one nucleus A; and the Laplacian operators ∇_i^2 and ∇_A^2 involve the differentiation with respect to the Cartesian coordinates of the i^{th} electron and the A^{th} nucleus.

Finding and describing approximate solutions to the Schrödinger equation is a major preoccupation of quantum chemists since the birth of quantum mechanics. While it is rigorously solvable for simple cases such as the particle in a box, the harmonic oscillator, or the hydrogen atom, the Schrödinger equation is not solvable exactly in the case of many-particle (many-nucleus and/or many-electron) systems, for which the term describing the nuclear and/or electronic repulsion cannot be accounted for rigorously. Therefore, important approximations are required to be able to solve the Schrödinger equation.

2.1. MAIN APPROXIMATION

2.1.1. BORN-OPPENHEIMER APPROXIMATION

The nuclei are much heavier than the electrons (the proton is 1836 times heavier than the electron) leading them to move more slowly. Therefore, the motions of the nuclei are separated from those of the electrons. Within the Born-Oppenheimer approximation, the kinetic energy term of the nuclei (term of the motions of the nuclei) is neglected and the repulsion term between nuclei is assumed constant. On this basis, the electrons are considered to move in a field of fixed nuclei. Therefore, the Born-Oppenheimer approximation yields a purely electronic Schrödinger equation, whose resolution provides a total wavefunction which depends parametrically on the nuclear coordinates, R, and explicitly on the electronic coordinates, r. The Hamiltonian operator is rewritten as:

$$H = -\sum_{i=1}^{N} \frac{1}{2} \nabla_i^2 + \sum_{i=1}^{N} \sum_{j>i}^{N} \frac{1}{r_{ij}} - \sum_{i=1}^{N} \sum_{A=1}^{M} \frac{Z_A}{r_{iA}} \qquad [22]$$

The repulsion term between electrons prevents the exact resolution of the purely electronic Schrödinger equation, and new approximations are required. Central to the attempts at solving such a problem is the Hartree-Fock (HF) approximation, which plays an important role in quantum chemistry and usually constitutes the first step toward more elaborate approximations.

2.1.2. HARTREE-FOCK APPROXIMATION

In quantum chemistry, there are two fundamentally different approaches to obtain quantitative information about the electronic properties of a material. One of these approaches (that has been more recently introduced in the chemistry community), the Density Functional Theory (DFT) {17}, expresses the total energy of a molecule as a functional of the electronic density. In the other approach, simplified formulations for the total many-particle wavefunction are used leading, via the variational principle, to the HF equations, which are solved in a Self Consistent Field (SCF) iterative procedure.

TOTAL MANY-ELECTRON WAVEFUNCTION

To completely describe one electron, in addition to its spatial wavefunction $\psi_i(r)$, a spin wavefunction $\alpha(\omega)$ for spin up or $\beta(\omega)$ for spin down must be introduced, leading to a total one-electron wavefunction, also called a spin orbital: $\chi_i(\vec{x}) = \psi_i(r)\alpha(\omega)$ or $\chi_i(\vec{x}) = \psi_i(r)\beta(\omega)$. Thus, the total many-electron wavefunction is usually expressed as a combination of spin orbitals; however, the description of the total many-electron wavefunction as a simple product, the Hartree Product (HP), of these spin orbitals violates the antisymmetry principle for fermions: the many-electron wavefunction must be antisymmetric with respect to the interchange of the coordinates $\vec{x}$ (both space and spin) of any two electrons and is expressed as:

$$\phi(\vec{x}_1,...,\vec{x}_i,...,\vec{x}_j,...,\vec{x}_N) = -\phi(\vec{x}_1,...,\vec{x}_j,...,\vec{x}_i,...,\vec{x}_N) \qquad [23]$$

For instance, an antisymmetrized total many-electron wavefunction for a molecule consisting of two electrons (i=1 and j=2), is:

$$\Psi(\vec{x}_1,\vec{x}_2)=(2!)^{-1/2}\left(\chi_1(\vec{x}_1)\chi_2(\vec{x}_2)-\chi_1(\vec{x}_2)\chi_2(\vec{x}_1)\right) \quad [24]$$

When equation [24] is generalized for a molecule consisting of N electrons, one ends up with a single Slater determinant consisting of N spin orbitals:

$$\Psi(\vec{x}_1...\vec{x}_N)=(N!)^{-\frac{1}{2}}\begin{vmatrix}\chi_1(\vec{x}_1) & \cdots & \chi_N(\vec{x}_1)\\ \vdots & \cdots & \vdots\\ \chi_1(\vec{x}_N) & \cdots & \chi_N(\vec{x}_N)\end{vmatrix} \quad [25]$$

In this context, the description of the total many-electron wavefunction is thus based on a single Slater determinant.

HARTREE-FOCK EQUATION

The HF approach consists in finding a set of spin orbitals that gives the best approximate solution to the pure electronic Schrödinger equation of a molecule. This is achieved via the variational principle which states that finding the total many-electron wavefunction minimizing the total energy of the investigated molecule is equivalent to solving its purely electronic Schrödinger equation for the ground state. The total energy of the investigated molecule is written as:

$$\mathrm{E}_0 = \left\langle \Psi_0 \middle| \hat{H} \middle| \Psi_0 \right\rangle \qquad [26]$$

When equation [26] is varied with respect to the spin orbital to obtain a minimum in the total energy, the HF equations are derived into coupled integro-differential equations, from which the best set of spin orbitals is obtained:

$$\left[-\frac{1}{2}\nabla_1^2 - \sum_{A=1}^{M} \frac{Z_A}{r_{1A}} \right] \chi_i(\vec{x}_1) + \sum_{j}^{occ} \left[\int d\vec{x}_2 \left| \chi_j(\vec{x}_2) \right|^2 \frac{1}{r_{12}} \right] \chi_i(\vec{x}_1)$$
$$- \sum_{j}^{occ} \left[\int d\vec{x}_2 \chi_j^*(\vec{x}_2) \chi_i(\vec{x}_2) \frac{1}{r_{12}} \right] \chi_j(\vec{x}_1) = \varepsilon_i \chi_i(\vec{x}_1) \qquad [27]$$

In equation [27], the first term is the one-electron contribution for a single electron 1 in the field of the nuclei; the second term is the Coulomb operator (two-electron contribution), which introduces the average of the repulsion between electron 1 and all others electrons j; and the third term is the exchange operator (two-electron contribution), which expresses the possibility of permuting the cartesian coordinates of the electron 1 and the ones of the other electrons j of the same spin. The Coulomb operator, which does not depend on the spin orbital on which it acts, is a local operator (does not include the instantaneous correlation relative to the motion of two electrons approaching each other) while the exchange operator is a non-local operator.

The HF equations, in which the spin orbitals are involved in the Coulomb and exchange operators, are solved with an iterative SCF procedure. The determination of the best set

of spin orbitals is initiated with a guess of a first set of spin orbitals that is introduced in the Coulomb and exchange operators of the HF equations, which are then solved. Once the various operators are calculated and the HF equations are solved, a new set of spin orbitals is found, which is in turn used in the Coulomb and exchange operators to solve the HF equations again. This iterative SCF procedure is repeated until self consistently is reached and the best set of spin orbitals is then determined.

Although the discussion here is limited to restricted closed-shell molecules, in which all the electrons are paired so that the spin wavefunction is doubly occupied, it quickly becomes very difficult to solve the system of coupled integro-differential equations for large molecules without further approximations concerning the functional form of the spin orbitals.

2.1.3. LINEAR COMBINATION OF ATOMIC ORBITALS APPROXIMATION

The Linear Combination of the Atomic Orbitals (LCAO) approximation consists in expressing the spin orbitals (which correspond to the molecular orbitals (MOs)), the basis set, as a linear combination of basis functions, which tend most of the time to reproduce mathematically the form of the atomic orbitals (AOs):

$$\chi_i(\vec{x}) = \sum_{p=1}^{m} C_{ip}\phi_p(\vec{x}) \qquad [28]$$

where i is the index of the MO; p is the index of the AO; and m corresponds to the number of AOs involved in the expression.

The choice of the set of basis functions is very important and must represent a good compromise between the time and memory space required to run a computational calculation and the accuracy of the theoretical data. A logical choice is the hydrogenoid-type orbitals; however, these have a complex mathematical form. Therefore, the more simple Slater-type orbitals (STOs) are often chosen. In practice, the STOs are complicated to use for molecules made of more than two atoms. Therefore, especially in the case of *ab initio* computational calculations, the STO's are simulated by Gaussian functions; the advantage here is that the product of two Gaussians is a Gaussian, which allows one to obtain compact analytical expressions. A STO cannot be properly described by a single Gaussian function and is represented by a linear combination of several Gaussian functions.

The HF equations are then cast in a matrix form:

$$FC = SCE \qquad [29]$$

with the matrix elements being expressed as:

$$F = \int d\vec{r}_1 \phi_p^*(1) f(1) \phi_q(1) \qquad [30]$$

$$S = \int d\vec{r}_1 \phi_p^*(1)\phi_q(1) \quad [31]$$

$$f(1) = -\sum_{i=1}^{N}\frac{1}{2}\nabla_i^2 - \sum_{i=1}^{N}\sum_{A=1}^{M}\frac{Z_A}{r_{iA}} + \sum_{j}^{occMO}\left(2J_j(i) - K_j(i)\right) \quad [32]$$

In equation [29] F is the Fock matrix (expressed in equation [30]); S is the overlap matrix (expressed in equation [31]); C is the LCAO coefficients matrix; and E is the total energy. The first two terms of the Fock operator $f(1)$ (expressed in equation [32]) constitute the one-electron contribution and the third term corresponds to the two-electron contribution including the Coulomb operator ($J_j(i)$) (equation [33]) and the exchange operator ($K_j(i)$) (equation [34]), whose meanings have been previously discussed:

$$J_j(i)\phi_i(i) = \left[\int \frac{\phi_j^2(j)}{r_{ij}} d\tau\right]\phi_i(i) \quad [33]$$

$$K_j(i)\phi_i(i) = \left[\int \frac{\phi_j(j)\phi_i(j)}{r_{ij}} d\tau\right]\phi_j(i) \quad [34]$$

2.2. SEMI-EMPIRICAL METHODS

The prototypical organic NLO chromophores are generally large and may require quantum-chemical calculations with hundreds of electrons. The computational methods for which all these electrons are taken into consideration explicitly and all the one- and

two-electrons integrals are explicitly calculated without further approximations are called the *ab initio* methods. Such methods when applied to hundreds of electrons are time and memory space consuming. Thus, semi-empirical methods are attractive as they reduce the number of electrons explicitly taken into consideration and the number of one- and two-electron integrals explicitly calculated. In that context, the electronic properties are no longer derived from the fundamentals of quantum mechanics but instead from a combination of theoretical and experimental parameters; the accuracy of the data obtained with semi-empirical methods depends on the quality of the parameterization.

The Zero Differential Overlap (ZDO) approximation consists in neglecting the overlap between different basis functions ($\phi_p(\vec{x})\phi_q(\vec{x}) = \phi_p(\vec{x})^2 \delta_{pq}$), which allows for a major reduction in the number of two-electron integrals to be explicitly calculated. The ZDO approximation is a basic ingredient of many semi-empirical methods, including the Austin Model 1 (AM1) method [18] and the Intermediate Neglect of Differential Overlap (INDO) method [19].

These two semi-empirical methods are extensively used in this dissertation. In both methods, the Fock operator is separated into: one operator for the core electrons (h_c) and one operator for the valence electrons (h_v). The core approximation is such that the valence electrons are assumed to move in a core field constituted of nuclei and electrons of internal layers. This approximation is valid since the core electrons confined in the AOs of low energy do not participate in the chemical bonding, thus not influencing significantly the molecule properties.

2.2.1. AM1 METHOD

The AM1 method [18] is based on the core approximation and the Neglect of Diatomic Differential Overlap (NDDO) method, in which the differential overlap between two basis functions centered on the same atom is taken into consideration. The elements of the Fock matrix are partially determined through the measure of physical properties or based on semi-empirical expressions; the numbers in these expressions are adjusted to reproduce some experimental parameters, such as heat of formation, ionization potential, molecular geometry, and ground state dipole moment.

The geometries of the chromophores investigated here are optimized with the AM1 method as implemented in the AMPAC package.

2.2.2. INDO METHOD

In the INDO method [19], the two-electron integrals involving three or four centers are totally neglected; the values assigned to the one-center two-electron integrals arise from experimental parameters coming from atomic spectroscopy measurements. The two-center two-electron integrals are evaluated through empirical expressions, such as the Mataga-Nishimoto [20] or Ohno-Klopman [21] potentials. The INDO method used is specifically parameterized to reproduce the electronic and linear optical properties of a chromophore.

The electronic properties in the ground state and the electronic excited states (state dipole moments, transition dipole moments, and transition energies) of the chromophores investigated here are evaluated with the INDO method; the spectroscopic

parameterization along with the Mataga-Nishimoto [20] potential are used, as implemented in the ZINDO code [22].

2.3. CONFIGURATION INTERACTION METHOD

Within the HF approximation, the total many-electron wavefunction of a molecule is described with a single Slater determinant, which translates the neglect of electron correlation effects. In other words, the instantaneous interactions between electrons of opposite spins are not taken into consideration in the HF approach. The error committed when neglecting the instantaneous interactions between electrons corresponds to the electronic correlation energy, which is the difference between the exact total energy of the molecule and the HF total energy.

Methods exist for which at least part of the electronic correlation energy is explicitly recovered, which allows one to improve the accuracy of the data obtained. Among these methods, configuration interaction (CI) is conceptually the simplest. The basic idea is to build the total many-electron wavefunction as a linear combination of Slater determinants corresponding to electronic configurations as:

$$\left|\phi\right\rangle = C_0\left|\Psi_0\right\rangle + \sum_{r,a} C_a^r \left|\psi\right\rangle_a^r + \sum_{\substack{a<b \\ r<s}} C_{ab}^{rs}\left|\Psi\right\rangle_{ab}^{rs} + \sum_{\substack{a<b<c \\ r<s<t}} C_{abc}^{rst}\left|\Psi\right\rangle_{abc}^{rst} + \ldots \qquad [35]$$

In equation [35], in addition to the single Slater determinant (obtained with the iterative SCF procedure within the HF approach) taken as reference, the linear combination

consists of Slater determinants resulting from the excitations of one or more electrons from occupied spin orbitals (MOs) to virtual, or unoccupied, ones. A single excitation arises from the promotion of one electron from an occupied MO to an unoccupied one; while a double excitation comes from the promotion of two electrons from occupied MOs to unoccupied ones. The CI coefficients describing the total many-electron wavefunction in the ground state and electronic excited states, as well as the corresponding total energies, are obtained by diagonalizing the CI matrix in the basis of the Slater determinants (by application of the variational principle).

In practice, based on the fact that the number of electronic configurations considered is limited, only a fraction of the electronic correlation energy is recovered, and therefore, the total energies are not exact. Additionally, for practical reasons, the consideration of all the electronic configurations associated to a finite set of basis functions is impossible when the size of a molecule becomes large. Therefore, in order to obtain a practical computational scheme, the CI expression must be truncated. The CI method is defined in terms of single, double, triple, quadruple, and so on interactions. In a single configuration interaction (SCI) scheme, the electronic excited states are described as a linear combination of singly excited Slater determinants; a single and double configuration interaction (SDCI) scheme includes also doubly excited Slater determinants; and a multireference determinant configuration interaction (MRDCI) scheme is such that excited Slater determinants of higher order are obtained by taking not only the ground state Slater determinant but also excited ones as references and then performing single and double excitations on all these references.

In this dissertation, the electronic properties of the second-order NLO chromophores are evaluated with a SCI scheme; however, an MRDCI scheme is necessary to evaluate

those of the third-order NLO chromophores. Since (i) the CI active space is far from being complete and (ii) the actual choice of the CI active space influences the quantitative aspects of the theoretical data, throughout this dissertation, extensive tests of the influence of size of the CI active space are performed to ensure reliability and convergence of the theoretical data. Also, the MOs included in the CI active space are chosen based on their character rather than their number in order to ensure a consistent CI description. In general, in this dissertation, the expansion of the basis set of Slater determinants considered for each series of chromophores investigated here does not modify the composition of the relevant electronic excited states and the computed properties.

2.4. MOLECULAR POLARIZABILITIES

The goals of this dissertation are to evaluate the second- and third-order NLO properties (specifically the second-order polarizabilities and the two-photon absorption cross-sections) of new chromophores and to understand their relationship to the chemical structure.

EVALUATION OF SECOND- AND THIRD-ORDER NLO PROPERTIES

Within the perturbative Sum-Over-States (SOS) [23] method, the second- and third-order polarizabilities (β_{ijk} and γ_{ijkl}) are expressed as:

$$\beta_{ijk}(-\omega_3;\omega_1,\omega_2) \prec \sum_{m,n\neq g} \frac{\langle g|\mu_i|m\rangle\langle m|\mu_j|n\rangle\langle n|\mu_k|g\rangle}{(\omega_{mg}-\varpi_3-i\Gamma_{mg})(\omega_{ng}-\omega_1-\omega_2-i\Gamma_{ng})} - \sum_{n\neq g} \frac{\langle g|\mu_i|g\rangle\langle g|\mu_j|n\rangle\langle n|\mu_k|g\rangle}{(\omega_{ng}-\omega_1-i\Gamma_{ng})(\omega_{ng}+\omega_2+i\Gamma_{ng})} \quad [36]$$

$$\gamma_{ijkl}(-\omega_4;\omega_1,\omega_2,\omega_3) \prec \sum_p \sum_{m,n,p\neq g} \frac{\langle g|\mu_i|m\rangle\langle m|\mu_j|n\rangle\langle n|\mu_k|p\rangle\langle p|\mu_l|g\rangle}{(\omega_{mg}-\omega_4-i\Gamma_{mg})(\omega_{ng}-\omega_1-\omega_2-i\Gamma_{ng})(\omega_{pg}-\omega_1-i\Gamma_{pg})}$$
$$-\sum_{m,n\neq g} \frac{\langle g|\mu_i|m\rangle\langle m|\mu_j|g\rangle\langle g|\mu_k|n\rangle\langle n|\mu_l|g\rangle}{(\omega_{mg}-\omega_4-i\Gamma_{mg})(\omega_{ng}-\omega_1-i\Gamma_{ng})(\omega_{ng}+\omega_2+i\Gamma_{ng})}$$

[37]

where m, n, and p denote the electronic excited states; g denotes the ground state; μ_x (for which x corresponds to i, j, k, and l) is the x component of the state or transition dipole moment; ω is the transition frequency between the ground and electronic excited states considered; and Γ is the damping factor for the electronic excited state considered.

In general, β_{ijk} is dominated by a single diagonal tensor term, along the donor-acceptor axis for dipolar chromophores; with this choice, the long axis component of the dipole moment is positive and the β_{xxx} components defined in this way totally dominate the other tensor elements of β_{ijk}. Therefore, the discussion of the properties and trends of the nonlinear polarizability are limited to these β_{xxx} components.

Although a wealth of semi-empirical methods have been used on organic chromophores with widely different electronic and (linear and nonlinear) optical properties and representative of various classes of NLO chromophores of interest, these semi-empirical methods have rarely been critically compared with one another. Therefore, a collaborative effort {1} with the Eichinger and Robinson groups at the University of

Washington has been undertaken in order to assess the reliability of the HF, INDO, and DFT methods, for which the dipole moment, first- and second-order polarizabilities have been compared (the focus was on the trends rather than on the absolute values).

It has been found that, when used for screening in support of organic synthesis, there is little to recommend one computational method over another. It has been shown that the various computational methods (HF, INDO, and DFT) all give relatively consistent descriptions of the electronic as well as (linear and nonlinear) optical properties for the wide variety of organic chromophores investigated in this collaborative study. Therefore, when used carefully and consistently, any one of these computational methods should provide useful guidance for an experimental investigation.

UNDERSTANDING OF STRUCTURE-PROPERTY RELATIONSHIP

Since the discovery of synthetic dyes in the 1800s, chemists and physicists have been attempting to understand the relationship between chemical structure, electronic structure {24}, and optical properties {25} of organic chromophores. To a great extent, the structure-property relationships for the first-order polarizability (α_{ij}), second-order polarizability (β_{ijk}), and third-order polarizability (γ_{ijkl}) have been treated separately and as somewhat unrelated. However, in an attempt to develop a unified description of the chemical structure and the linear and nonlinear polarizabilities, it has been shown {26} that, for polymethine dyes, they are correlated with a single chemical (geometrical) relevant parameter, the bond length alternation (BLA), which is the difference between the average lengths of C-C single and double bonds, denoted Δr (for more detail on these α-, β-, and γ-BLA surfaces see Ref {26}).

In this dissertation, the structure-property relationships are understood by using the essential-state models. A two-state model [27] is used to analyze the second-order polarizability when a single electronic excited state (e) is strongly coupled to the ground state (g). Therefore, the SOS expression (equation [36]) is reduced to one term; the static long axis component of the second-order polarizability then writes:

$$\beta_{xxx} \prec \frac{\Delta\mu_{eg} M_{ge}^{2}}{E_{ge}^{2}} \qquad [38]$$

where $\Delta\mu_{eg}$ is the change in state dipole moment between (e) and (g); M_{ge} is the transition dipole moment between (g) and (e); and E_{ge} is the transition energy between (g) and (e).

In the same way, a three-term model [28] is used to analyze the third-order polarizability when a single electronic excited state (e) is strongly one-photon allowed and acts as an intermediate electronic excited state for excitation into higher-lying electronic excited states (e'). In that case, the summations over the electronic excited states that are coupled to the ground state (g) is limited to (e) and the summations over the higher-lying electronic excited states go over those few electronic excited states (e') that are strongly coupled to (e). Therefore, the SOS expression (equation [37]) is reduced to three terms: a dipolar term (D) (similar to the two-term model), a negative term (N), and a two-photon term (T); the static long axis component of the third-order polarizability thus writes as:

$$\gamma_{xxxx} \prec \left[\frac{\Delta\mu_{eg}^2 M_{ge}^2}{E_{ge}^3} - \frac{M_{ge}^4}{E_{ge}^3} + \sum_{e'} \frac{M_{ge}^2 M_{ee'}^2}{E_{ge}^2 E_{ge'}^2} \right] \qquad [39]$$

where the first, second, and third terms are the D, N, and T terms respectively (for which $\Delta\mu_{eg}$ is the change in state dipole moment between (e) and (g); M_{ge} is the transition dipole moment between (g) and (e); E_{ge} is the transition energy between (g) and (e); $M_{ee'}$ is the transition dipole moment between (e) and (e'); and $E_{ge'}$ is the transition energy between (g) and (e')).

Some of the chromophores investigated here have a large number of electronic excited states contributing significantly to the SOS expressions, thus preventing the rapid convergence of essential-state models. Therefore, the analysis of the NLO properties is also based on the Finite Field (FF) method {29} in its local contribution version, as proposed by Chopra {30} and developed by Nakano {31}. This computational method, successfully applied to organic chromophores in conjunction with an INDO Hamiltonian {32}, allows one to discern the local contributions of individual chemical segments of the chromophores to the overall β or γ (main advantage).

The FF method in the local contribution version relies on the fact that, by definition, the β_{xxx} and γ_{xxxx} components are respectively the second and third derivatives of the long axis component of the induced dipole moment μ_x with respect to the long axis component of the applied electric field E_x according to the general expression:

$$\vec{\mu}_i = \vec{\mu}_0 + R^{(1)} \sum_j \alpha_{ij} \vec{E}_j + R^{(2)} \sum_{jk} \beta_{ijk} \vec{E}_j \vec{E}_k + R^{(3)} \sum_{jkl} \gamma_{ijkl} \vec{E}_j \vec{E}_k \vec{E}_l + \ldots \quad [40]$$

The electronic part of the β_{xxx} and γ_{xxxx} components is then cast rigorously as the integral over the moments of the second and third derivatives of the charge density (ρ), respectively. In an approximate way, that integral is partitioned into a sum over derivatives of the point charges q_i concentrated on the individual atoms (i):

$$\beta_{xxx} = \left. \frac{\partial^2 \mu_x}{\partial F_x^{\,2}} \right|_{F_x=0} = \int x \left. \frac{\partial^2 \rho(\vec{r})}{\partial F_x^{\,2}} \right|_{F_x=0} d^3\vec{r} \approx \sum_i x_i \left. \frac{\partial^2 q_i^2}{\partial F_x^2} \right|_{F_x=0} = \sum_i x_i q_i^{(2)} \quad [41]$$

$$\gamma_{xxxx} = \left. \frac{\partial^3 \mu_x}{\partial F_x^{\,3}} \right|_{F_x=0} = \int x \left. \frac{\partial^3 \rho(\vec{r})}{\partial F_x^{\,3}} \right|_{F_x=0} d^3\vec{r} \approx \sum_i x_i \left. \frac{\partial^3 q_i^3}{\partial F_x^3} \right|_{F_x=0} = \sum_i x_i q_i^{(3)} \quad [42]$$

where the β_{xxx} and γ_{xxxx} components are partitioned into local contributions or so-called β- and γ-moments, $x_i q_i^{(2)}$ and $x_i q_i^{(3)}$, derived from the so-called β- and γ-charges, $q_i^{(2)}$ and $q_i^{(3)}$. Note that the superscripts (2) or (3) represent the second or third derivative with respect to the applied electric field. In this dissertation, the derivatives are approximated by finite differences obtained from INDO/HF Mulliken charges, with electric fields of zero and ± 5.14×10^8 V/m for the second- order and of zero, ± 5.14×10^8 V/m, and ± 10.28×10^8 V/m for the third- order (1au = 5.1422 10^{11} V/m).

Each moment is dependent on the arbitrary choice of the axis origin, which can make plotting the moments somewhat misleading. Here, in order to display reliably the relative importance of the moments to both the β_{xxx} and γ_{xxxx} components, the origin is consistently set in the middle of the chromophore (leading to opposite x signs at opposite ends). In this context, it is clear that an efficient chromophore should rather have large terminal moments (where the moment arms are large), preferentially of the same sign for a given end, and of opposite signs at opposite ends (to avoid cancellation of moments).

The two-photon absorption cross-sections (δ) are evaluated using: (i) the perturbative SOS method (equation [43]), and/or (ii) the 2PA tensor (equation [44]), which write:

$$\delta \prec \mathrm{Im}\left[\gamma\left(-3\omega;\omega,\omega,-\omega\right)\right] \quad [43]$$

$$\delta \prec \sum_{ij}\left(S_{e'}^{i,i}S_{e'}^{*j,j} + 2S_{e'}^{i,j}S_{e'}^{*i,j}\right) \quad [44]$$

Where $S_{e'}^{i,i}$ writes as:

$$S_{e'}^{i,i} = \sum_{e}\left(\frac{M_{ge}^{i}M_{ee'}^{i}}{E_{ge} - \frac{E_{ge'}}{2}} + \frac{M_{ge}^{i}M_{ee'}^{i}}{E_{ge} - \frac{E_{ge'}}{2}}\right) \quad [45]$$

In the same way, to facilitate the interpretation of the calculated 2PA spectra, approximations are applied to the full SOS expression. In the D and T terms, the 2PA process occurs with respect to (e) and (e'), respectively. In the case of resonance into (e), a two-state model is often appropriate to describe the two-photon peak, while (at least) three states (g, e, e') have to be included in the SOS expression to describe the two-photon peak when the 2PA process occurs into (e'). Within such simplified models, for the D-term (resonance into (e)), assuming that $\Gamma_{ge} < \frac{E_{ge}}{2}$, we derive:

$$\delta_D \prec \Delta\mu_{eg}^2 M_{ge}^2 \qquad [46]$$

For the T-term (resonance into (e')), assuming that $\Gamma_{ge} < \frac{E_{ge} - \frac{E_{ge'}}{2}}{2}$, we find:

$$\delta_T \prec \frac{\left(\frac{E_{ge'}}{2}\right)^2 M_{ge}^2 M_{ee'}^2}{\left(E_{ge} - \frac{E_{ge'}}{2}\right)^2} \qquad [47]$$

CHAPTER 3 SECOND-ORDER NONLINEAR OPTICAL DIPOLAR CHROMOPHORES

It has been shown in the case of polymethine dyes [26] that a unified description, for which the geometric structure is correlated to the (linear and nonlinear) polarizabilities, is established (chapter 2). Specifically, the relationship between the bond length alternation (BLA) and the second-order polarizability (β) is understood within the context of the two-term model (equation [38]), in which three electronic terms contribute to β (the change in state dipole moment ($\mu_{ee} - \mu_{gg}$), the transition dipole moment (μ_{ge}), and the transition energy (E_{ge})). The β-BLA surface has been predicted by Marder et al. [33] and is presented in Figure 1.

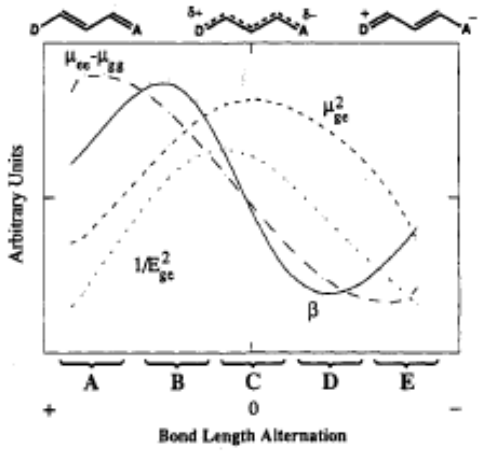

Figure 1: Second-order polarizability (β), change in state dipole moment term ($\mu_{ee} - \mu_{gg}$), transition dipole moment term (μ_{ge}^2), and transition energy term ($\frac{1}{E_{ge}^2}$) as a function of the bond length alternation (BLA) for polymethine dye.

In Figure 1, as a function of increasing degree of ground state polarization, the ($\mu_{ee} - \mu_{gg}$) term starts positive, increases, reaches a positive peak (region A), decreases (region B), continues to decrease, passes through zero at the cyanine limit, becomes negative (region C), then becomes increasingly negative (region D), and exhibits a negative peak (region E); the μ_{ge}^2 and $\frac{1}{E_{ge}^2}$ terms peak at the cyanine limit.

Therefore, β (product of these three terms) is initially positive, then as a function of increasing degree of ground state polarization, first increases, peaks in a positive sense, decreases, passes though zero at the cyanine limit, becomes increasingly negative, peaks in a negative sense, and increases when the ground state of the polymethine dye is dominated by the charge separated polyene-like resonance form.

Although the determination of an optimum pair of an electron-rich (referred to as the primary donor, D) and an electron-poor (referred to as the primary acceptor, A) end groups for a given π-bridge or an optimum π-bridge for a given D-A pair is a difficult task, given the number of possible D-A pairs, π-bridges, and the vast array of accessible organic, inorganic and organometallic structural motifs; however, the qualitative features of the β-BLA surface and the two-term model assist the mapping of such a structure-property relationship.

Based on the β-BLA surface and the two-term model, one of the simplest strategies to design a chromophore with a large β value is to start with a highly delocalized π-bridge (such as a polyene segment or a phenylene vinylene segment) and connect at the ends two different substituents (R_1 and R_2), so that a strong asymmetry is built into the

chromophore if one of the subsistent is a donor group and the other is an acceptor group. Such a chromophore is called a push-pull, or dipolar, chromophore because the donor group is pushing charge toward the π-bridge, while the acceptor group is pulling charge from it. The traditional dipolar chromophore is the para-nitroaniline (pNA): a disubsituted benzene with a donor group (NH_2) and an acceptor group (NO_2) in the para-positions. The investigation of the pNA allowed one to establish that β depends on the strength of the donor and acceptor groups, as well as the length and nature of the π-bridge [11].

There are thus three major strategies to optimize β of a dipolar chromophore:

- to modify the strength/number of the donor and acceptor groups for a given π-bridge;
- to modify the length of the π-bridge for a given D-A pair, or
- to modify the nature of the π-bridge for a given D-A pair.

A combination of these three strategies has proven successful and most dipolar chromophores have been designed following these strategies [34].

3.1. COMPARISON OF STRONG ACCEPTOR END GROUPS

One of the major challenges to optimize β of a dipolar chromophore is the development of new and efficient acceptor groups, which has been the focus of numerous investigations over the past decade [35]. Starting from the NO_2 group of the pNA, strong acceptor groups with a better electron-withdrawing ability and a better overall stability have been developed, such as: 3-(dicyanomethylene)-2,3-dihydrobenzothiophene-1,1-dioxide, referred to as the SDS acceptor group [36]; 1,3-bis(dicyanomethylene)indane, referred to as the TCI acceptor group [37]; N,N'-diethylthiobarbituric acid, referred to as the BBA acceptor group [13]; or tricyanovinyl, referred to as the TCV acceptor group [38]. Their chemical structures are presented in Figure 2.

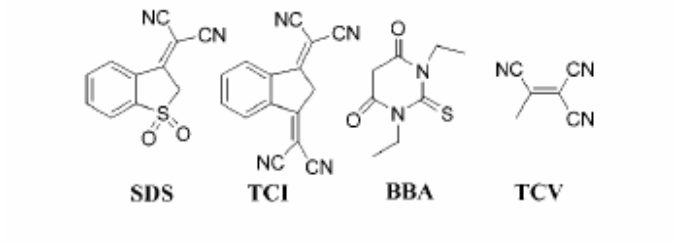

Figure 2: Chemical structures of strong SDS, TCI, BBA, and TCV acceptor groups with better electron-withdrawing ability and better overall stability.

In addition to low solubility and/or lack of chemical and/or thermal stability, a common structural feature in all these strong acceptor groups makes for an important drawback in terms of applications: planarity. Indeed, when these strong acceptor groups are used in the construction of a dipolar chromophore, the entire dipolar chromophore tends to be very planar with a large ground state dipole moment (μ_g). This gives rise to large electrostatic interactions that favor tight antiparallalel pairing of the dipolar chromophores

in the solid state or at high concentration, thus reducing the benefit of the poling process. When these large electrostatic interactions become dominant, the second-order electrical susceptibility ($\chi_{ijk}^{(2)}$) decreases significantly, even more severely when the concentration of the dipolar chromophores is high.

In order to decrease the strength of these large electrostatic interactions, the chemical structures of the strong acceptor groups (SDS, TCI, BBA, or TCV) are modified through the addition of alkyl chains, which lead to the new and effective acceptor groups consisting of five-membered heterocyclic rings substituted with functional groups capable of withdrawing electrons through both inductive and resonance effects. Specifically, 2-dicyanomethyl-3-cyano-4,5,5-trimethyl-2,5-dihydrofuran, referred to as the TCF acceptor group [39] (acceptor group of chromophore **1** in Figure 3), gains popularity as a strong acceptor group suitable for incorporation into a stable dipolar chromophore with a large β value.

Larger β values are obtained for dipolar chromophores substituted with acceptor groups whose chemical structures are related to the TCF. Therefore, the β value of **1** is compared to that of a dipolar chromophore including 2-dicyanomethyl-3-cyano-4,5-trimethyl-5-trifluoromethyl-2,5-dihydrofuran, referred to as the CF_3-TCF acceptor group [39] (acceptor group of chromophore **2** in Figure 3). During the synthesis of the CF_3-TCF, difficulties are encountered originating from the dimerizations of ketols [40] and malononitriles [41], which are found to be the major, factors determining the yield and purity of the acceptor group [42]. Once the CF_3-TCF is synthesized, the inductive and resonance effects of the trifluoromethyl group (CF_3) are investigated, which lead us to expect that these two effects could be further enhanced by replacing the dialkyl group

(CH_3-C-CH_3) in the TCF or (CH_3-C-CF_3) in the CF_3-TCF with a carbonyl group (C=O) which can then participate in the main conjugation path of the dipolar chromophore. Therefore, 3-methyl-4-cyano-5-dicyanomethylene-2-oxo-3-pyrroline, referred to as the TCP acceptor group [3] (acceptor group of chromophore **4** in Figure 3) is synthesized.

Finally, to benchmark the effectiveness of the furan-based (**1** and **2**) and pyrrole-based (**3** to **5**) acceptor groups, they are compared to two previously developed strong acceptor groups, the SDS (acceptor group of chromophore **6** in Figure 3) and the TCI (acceptor group of chromophore **7** in Figure 3), and also to three alternative acceptor groups: acceptor group of chromophore **8**, which is close to the BBA, and acceptor groups of chromophores **9** and **10** in Figure 3.

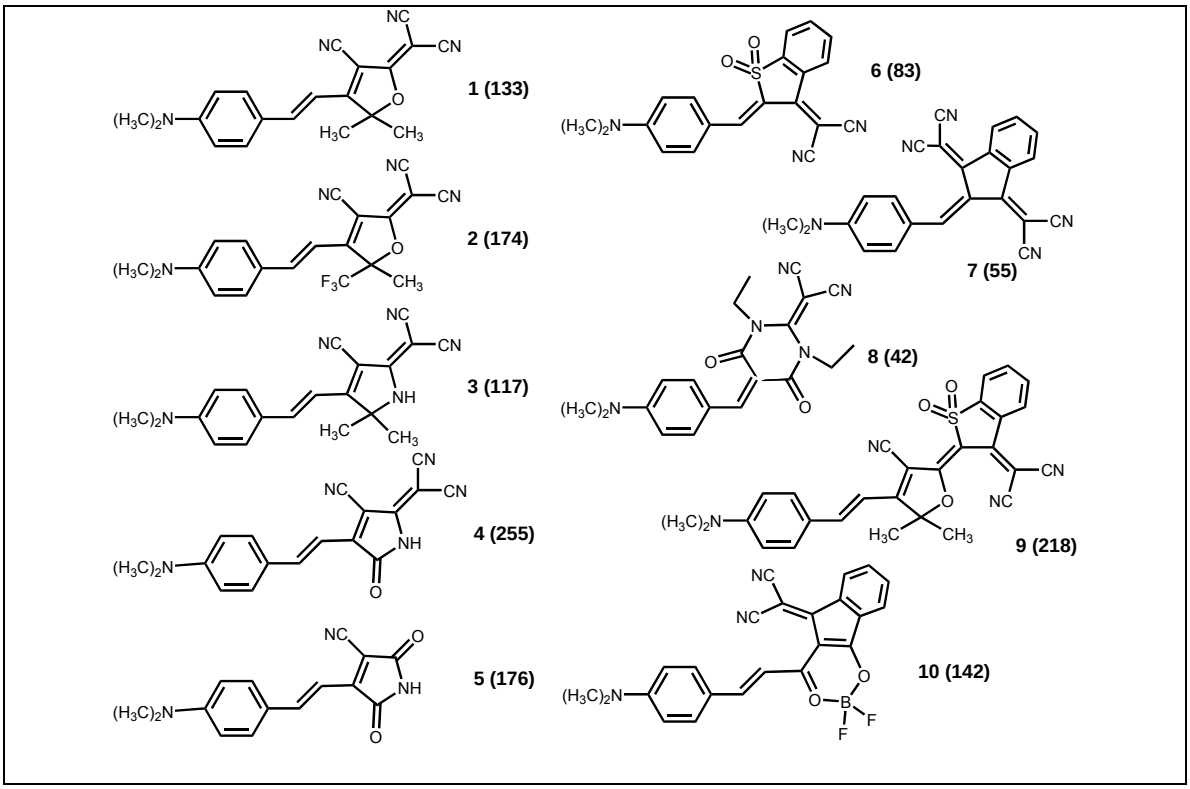

*<u>Figure 3:</u> Chemical structures of dipolar chromophores **1** to **10** substituted with: (i) furan-based (**1** and **2**) and pyrrole-based (**3** to **5**) acceptor groups; (ii) two previously developed strong acceptor groups (**6** and **7**); and (iii) three alternative acceptor groups (**8** to **10**) (the β_{xxx} components from FF method are reported in brackets in 10^{-30} esu).*

The theoretical transition energies (E_{ge}), optical absorption maxima ($\lambda_{\max}$), ground state dipole moments (μ_{gg}), long axis components of the second-order polarizability (β_{xxx}), and product of the β_{xxx} components and the μ_x components are calculated with the SOS and/or FF methods and reported in Table 1.

Table 1: Theoretical transition energies (E_{ge}), optical absorption maxima (λ_{max}), ground state dipole moments (μ_{gg}), static long axis components of the second-order polarizability (β_{xxx}), and product of the β_{xxx} components and the μ_x components calculated with the SOS and/or FF methods for dipolar chromophores **1** to **10**.

	E_{ge} (eV)	λ_{max} (nm)	μ_{gg} (D)	β_{xxx} (10^{-30} esu) SOS	β_{xxx} (10^{-30} esu) FF	β_{xxx} μ_x (10^{-48} esu) SOS
1	3.04	408 561* 584**	14.5	131	133	1725
2	2.93	422 607* 628**	13.3	176	174	2229
3	3.08	402	14.5	116	117	1364
4	2.62	473 691* 732**	9.2	275	255	2383
5	2.76	449	8.6	216	176	1645
6	2.93	423	5.1	99	83	195
7	3.02	411	6.5	68	55	92
8	3.31	374	4.6	45	42	178
9	2.80	442	10.5	207	218	1210
10	2.86	433	6.9	165	142	277
4	***2.62***	***473***	***9.2***	***275***	***255***	***2383***

experimental λ_{max} in toluene * and in chloroform **

For all these dipolar chromophores, the trends and magnitudes obtained for the β_{xxx} components from the FF method are consistent with those obtained with the SOS method. Note that the nitrogen atom of the donor group is substituted with two ethyl groups (CH_3CH_2) in the dipolar chromophores experimentally investigated, while the alkyl groups are replaced with two methyl groups (CH_3) for the sake of simplicity of the quantum-chemical computational calculations.

For **1**, **2**, and **4**, the theoretical optical absorption maxima show a systematic bathochromic shift in the following order: **1** (408 nm = 3.04 eV), **2** (422 nm = 2.93 eV), and **4** (473 nm = 2.62 eV), which is in agreement with the experimental optical absorption maxima (as shown in Table 1).

For **1**, a β_{xxx} component of 133×10^{-30} esu is calculated and increases by 31% when one CH_3 group in the TCF is replaced by one CF_3 group (β_{xxx}(**2**) = 174×10^{-30} esu). This increase in the β_{xxx} component between **1** and **2** can be understood in terms of the inductive electron-withdrawing effect of the CF_3 group relative to that of the CH_3 group. A much larger change in the β_{xxx} component (increase by almost a factor of 2 compared to **1**) is obtained for **4** (β_{xxx}(**4**) = 255×10^{-30} esu). To determine which of the structural modifications of the acceptor group (replacement of the furan by a pyrrole or substitution of the dialkyl group ($C(CH_3)_2$) with a C=O group) is principally responsible for this increase, a dipolar chromophore based on another acceptor group is investigated, in which only the oxygen atom is replaced by a nitrogen atom (acceptor group of chromophore **3** in Figure 3). The β_{xxx} component (β_{xxx}(**3**) = 117×10^{-30} esu) does not change significantly compared to **1**. Consequently, the replacement of the $C(CH_3)_2$ group by the C=O group appears to be the principal structural modification responsible for the large β_{xxx} component in **4**. Although it has the highest β_{xxx} component among **1** to **5**, **4** might not be very attractive when the transparency-nonlinearity tradeoff is considered (as can be deduced from the 65 nm (correspond to 0.42 eV) red-shifted linear absorption maximum of **4** compared to **1**).

The experimental β values of **1**, **2**, and **4**, which are measured by Hyper-Rayleigh Scattering at an excitation wavelength of 1900 nm in the Jen group at the University of Washington, are compared with the theoretical β_{xxx} components. The experimental β values of **1**, **2**, and **4** show systematic enhancement in the order of **1** (452 ± 5 × 10^{-30} esu) < **2** (493 ± 22 × 10^{-30} esu) < **4** (1290 ± 179 × 10^{-30} esu), as do the theoretical β_{xxx} components; however, the experimental β value of **4** is almost three times as large as that of **2**, while it is almost twice as large in theory. This discrepancy is not very surprising because the absolute magnitudes of the experimental β values are expected to exceed the theoretical β_{xxx} components because of dispersion, resonance, and solvent effects. Nevertheless, the experimentally observed trend is consistent with the theoretical trends.

Finally, as expected, in **5**, where a C=O group replaces the dicyanovinylene group ($C=C(CN)_2$) of **4**, the β_{xxx} component is 45% lower than in **4** while remaining significantly larger than in **1**.

To benchmark the effectiveness of the furan- and pyrrole-based acceptor groups, they are compared to dipolar chromophores based on the two previously developed SDS (**6**) and TCI (**7**). In spite of their longer π-bridges, the β_{xxx} components for **6** and **7** are significantly smaller than in the furan- and pyrrole-based dipolar chromophores, which underlines the high potential of these acceptor groups. Also, **8**, which is close to the BBA, presents a rather small β_{xxx} component.

Finally, two alternative acceptor groups are tested: (i) **9**, which can be regarded as the condensation product of the ketone precursor to the TCF with the SDS; and (ii) **10**, where the acceptor group is an hybrid of 1,3,2-(2H)-dioxaborine with the TCI. Dioxaborines are known to yield new and efficient acceptor groups for nonlinear optics [{43}] and electron transport [{44}] applications. For **9** and **10**, the β_{xxx} components are in the same range as **4** and **1**, respectively; the acceptor groups and resulting molecular masses are, however, significantly larger than in the former dipolar chromophores.

In order to understand the molecular origin of the trends observed for the β_{xxx} components, the β-charges, also called the local contributions, obtained from the FF method are discussed and plotted for **1**, **2**, **4**, and **5** in Figure 4.

1

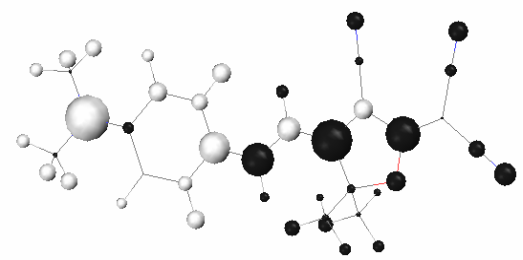

2

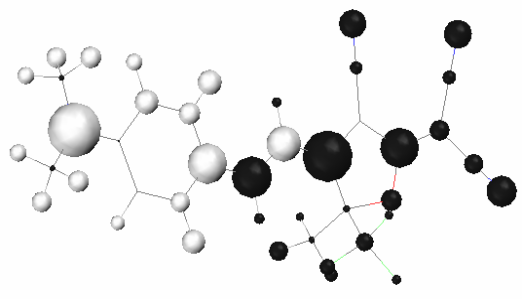

4

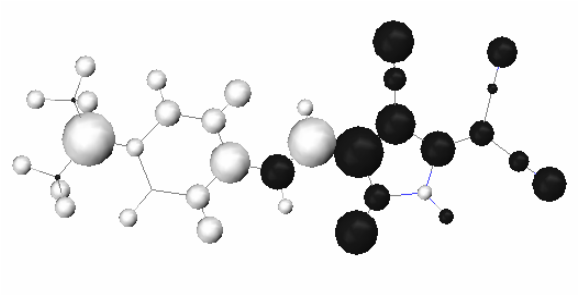

5

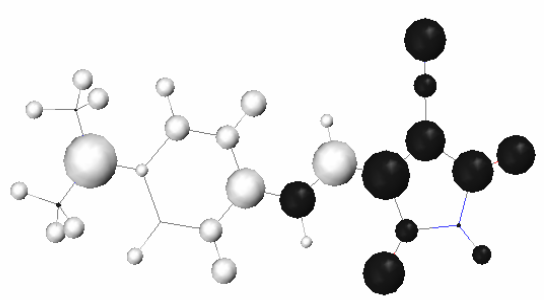

*<u>Figure 4:</u> Second derivatives of the atomic charge (β-charges) for dipolar chromophores **1**, **2**, **4**, and **5** (from top to bottom). The circle size is proportional to the magnitude of the β-charge and the circle shading indicates its sign (positive β-charges are in black circles and negative ones in white).*

The acceptor groups display positive β-charges, while the donor groups display negative ones. Only small variations in the magnitude of the β-charges are observed in the donor group with the nitrogen atom having the largest β-charge, while the patterns remain qualitatively similar in all the dipolar chromophores (**1**, **2**, **4**, and **5**). Overall, the pattern of the β-charges reflects an efficient charge transfer between the donor and acceptor groups, without any significant cancellation of the β-moments on neighboring atoms.

To analyze the β_{xxx} components of **1**, **2**, **4**, and **5** in more detail, it is instructive to compare the β-charge distributions. Note that, although the β_{xxx} components are determined not by the β-charges themselves but by their moments, a direct comparison of the β-charges is reasonable here since, for **1**, **2**, **4**, and **5**, the size and shape are similar and the moment arms are practically the same. The variations in the magnitude of the β-charges are directly induced by the acceptor groups, as the sum of the negative and positive β-charges over the whole chromophore has to be zero. Qualitative differences are clearly seen among the acceptor groups, for which the atom numbering in the five-membered heterocyclic ring is indicated in Figure 5.

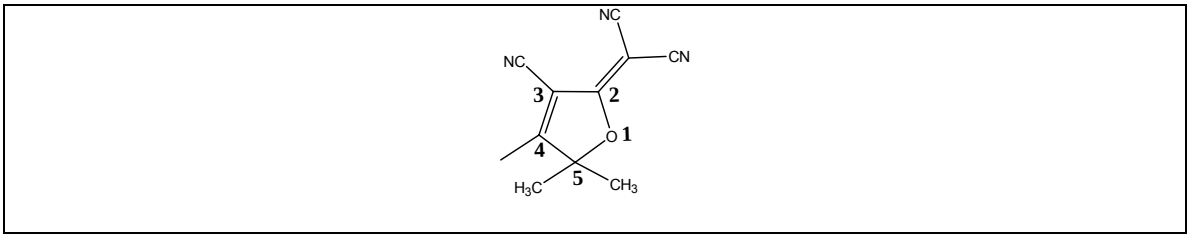

Figure 5: Chemical structure of TCF with atom numbering.

We find that: (i) in **1**, the largest β-charges are on the carbon atoms in positions 2 and 4 of the furan, while the β-charges on the cyano groups (CN) are relatively small; note,

however, that the CN groups in the $C=C(CN)_2$ group still give rise to appreciable β-moments, due to their larger distance from the center of the dipolar chromophore; (ii) in **2**, the situation remains qualitatively the same with somewhat larger β-charges on the carbon atom in position 4 of the furan, the CN groups, and the atoms forming the CF_3 group; (iii) significantly stronger modifications are observed in **4**: the increase in β-charges on the two CN groups is much larger (being even larger for the CN group in position 3 of the furan); the most striking change is, however, observed at the C=O group, which provides a much more significant contribution to the β_{xxx} component than the two CH_3 groups in **1**; and (iv) in **5**, the large β-charges on both C=O groups and at the carbon atoms in positions 2 and 5 partially account for the still appreciable β_{xxx} component. Overall, the plots in Figure 4 suggest that position 1 of the five-membered heterocyclic ring is the most suitable for further structural modifications of the acceptor group to achieve even larger β_{xxx} component.

The β-charges obtained from the FF method are plotted for **6** to **10** in Figure 6.

6

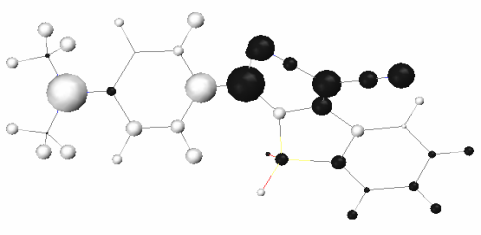

7

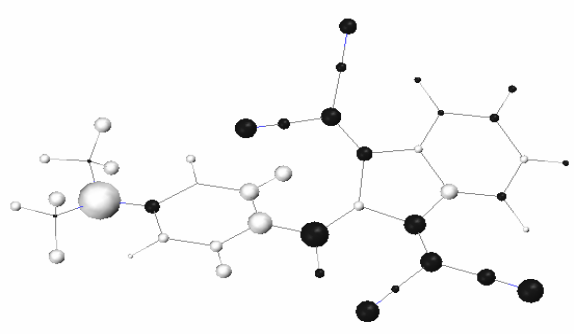

8

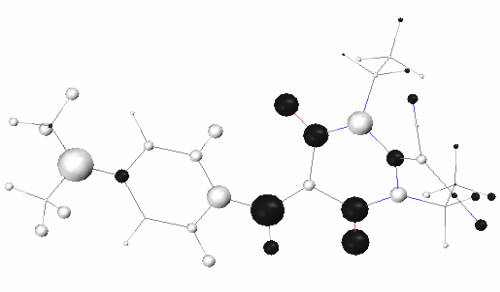

9

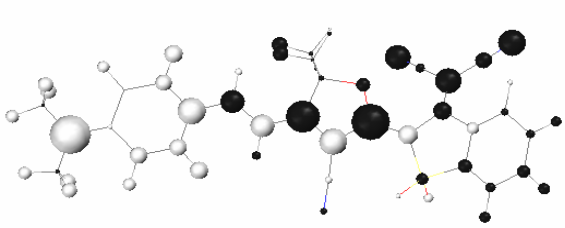

10

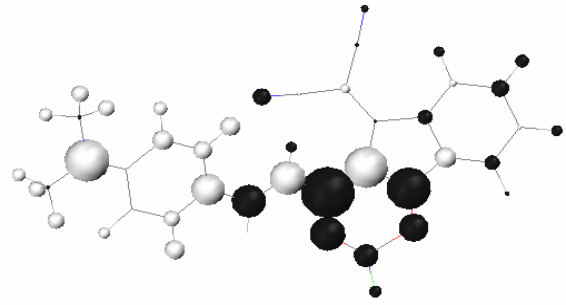

*<u>Figure 6:</u> Second derivatives of the atomic charge (β-charges) for dipolar chromophores **6** to **10** (from top to bottom). The circle size is proportional to the magnitude of the β-charge and the circle shading indicates its sign (positive β-charges are in black circles and negative ones in white).*

In **6** to **8**, only small parts of the acceptor groups are active and they are usually relatively far from the end of the dipolar chromophore (in **6** and **7**, the most active segment is the $C=C(CN)_2$ group; in **8**, the C=O group). The rest of the acceptor group is characterized by either very small β-charges or, in some cases, even opposite-sign β-charges. The main observation in **8** is that the $C=C(CN)_2$ group hardly makes any contribution; this can be related to the reduced π-bridge induced by the strong bending of the saturated part of the heterocyclic ring.

In **9**, large β-charges are found only in the furan and on the $C=C(CN)_2$ group of the acceptor group; the rest of the heterocyclic ring is again relatively inactive. In **10**, all the β-charges are concentrated on the dioxaborine. The rest of the acceptor group of **10** appears to be relatively inactive; therefore, the β_{xxx} component is calculated for an analog of **10** carrying a simple dioxaborine as the acceptor group (**10'**). It is found that the β_{xxx} component decreases from 142×10^{-30} esu (**10**) to 105×10^{-30} esu (**10'**); this reduction results from two effects: (i) the decrease in the magnitude of the β-charges on the atoms forming the dioxaborine; and (ii) the loss of the β-charges on the part of the acceptor group that is removed; the latter is the most important effect because those atoms are further from the center of the dipolar chromophore, thus leading to larger β-moments.

Finally, the β_{xxx} component shows a nearly three-fold increase in going from **6** to **9**, that is upon addition of a furan ring. The latter can be considered as part of the π-bridge and displays alternating β-charges. Their magnitude on the donor and acceptor groups are similar in **6** and **9**; however, there occurs a larger cancellation of the β-moments within

the π-bridge of **9** because of the alternating β-charges. Therefore, the β_{xxx} component increase from **6** to **9** is simply due to an increase of the length of **9**.

In the absence of electrostatic interactions, the electro-optic coefficient (r_{33}) of a polymer host is directly proportional to β and to the degree of alignment in a noncentrosymmetric fashion of the dipolar chromophores induced by an applied poling electric field. Thus, it is expected that the improvement in the β_{xxx} component of **4** over **1** should translate directly into changes in r_{33} in the polymer host. However, a significant drawback of **4** is the formation of large electrostatic interactions due to the planar chemical structure of the TCP.

Preliminary results on the poling of TCP-based dipolar chromophores have shown that the introduction of bulky substituents on the acceptor group via a methylene linkage to the N-H position does not prevent the formation of these large electrostatic interactions between the dipolar chromophores, resulting in a r_{33} only comparable to the one of **2**. Analysis of the structural differences between the TCF-, CF_3-TCF-, and TCP-based dipolar chromophores suggests that bulky substituents both above and below the main conjugation path of **4** are necessary for an efficient electric field induced degree of alignment of the dipole moments, especially at high concentration (concentration correspond to the loading density).

Moreover, careful studies on the modes (distance and degree of overlap between dipolar chromophores in the polymer host) and the strength of these electrostatic interactions should proceed to guide the rational design of dipolar chromophores for a polymer host.

Bulky substituents should be designed to reduce the dimerization energy between the dipolar chromophores for efficient poling.

Nevertheless, a preliminary r_{33} for **4** doped in an amorphous polycarbonate polymer host using a simple reflection technique is reported to be 51 pm/V at 1550 nm with 20 wt% dipolar chromophore loading density when poled at 65 V/μm. The poling conditions with other polymer hosts are ongoing and some preliminary measurements suggest that r_{33} of **4** with a FTC π-bridge is comparable to the one of **2** with the more efficient CLD π-bridge.

In summary, the Sum-Over-States (SOS) and Finite-Field (FF) methods have been used in order to evaluate the second-order polarizability of dipolar chromophores incorporating a variety of strong five-membered heterocyclic acceptor groups. To obtain a clear picture of the relationship between the second-order polarizability and the chemical structure, the local contributions FF method has been applied. The long axis components of the second-order polarizability calculated with the different methods are self consistent and are expected to reflect the major features of the evolution of the second-order polarizability. In general, the TCF- and TCP-based dipolar chromophores are found to yield second-order polarizabilities superior to many strong acceptor groups previously developed; this is explained by the fact that in the latter groups, significant parts of the acceptor group appear to be relatively inactive in terms of local contributions. In general, the FF method in its local contribution version has allowed us to provide an explanation for why the TCF- and TCP-based dipolar chromophores are good candidates for optoelectronics and photonics since the pattern of local contributions

reflects an efficient charge transfer from the donor group to the acceptor group, nearly without cancellation of β-moments on neighboring atoms.

3.2. INFLUENCE OF COMPETING INDUCTIVE AND RESONANCE EFFECTS FROM OXYGEN ATOM OF TCF-BASED DIPOLAR CHROMOPHORES

The TCF has been increasingly used as a strong acceptor group; for example, the TCF is part of 2-dicyanomethylene-3-cyano-4-{2-[E-(4-N,N-di(2-acetoxyethyl)-amino)-phenylene-(3,4-dibutyl)thiene-5]-E-vinyl}-5,5-dihydrofuran, referred to as the FTC dipolar chromophore (in Figure 7), which possesses large β value and excellent overall (chemical and thermal) stability [45]. In addition, Robinson et al. [45] have previously suggested that the superior chemical stability of the FTC (with respect to a nucleophilic attack) to that of other dipolar chromophores with larger β values is rationalized by considering two effects: (i) the inductive (σ) electron-withdrawing effect, for which the electronegativity of the carbon atom of the $C=C(CN)_2$ group (to which the oxygen atom is attached) is more positive than that of the same carbon atom if the oxygen atom is replaced by a CN group or a CF_3 group, increasing the strength of the TCF; and (ii) the resonance (π) electron-donating effect, through which the lone pair of the oxygen atom can contribute electron density to the adjacent carbon atom reducing the strength of the TCF.

However, there have been no reports of systematic investigations of the electron effect of the oxygen atom of the TCF relative to other groups X (divalent moieties) that can potentially be incorporated into the five-membered heterocyclic ring. Therefore, the systematic investigation of a wide range of five-membered heterocyclic ring acceptor groups based on the TCF, in which the oxygen atom at the position 1 is replaced with

other groups X with varying inductive and resonance electron-withdrawing and electron-donating effects, is of interest in this chapter.

The effect on β of the group X occupying the position 1 of the TCF (in Figure 7), is investigated using chromophores **1** to **10**, in which the dibutyl groups (C_4H_9) of the vinylene-thienylene-vinylene π-bridge of the FTC are replaced by two hydrogen atoms (H), and also in which, the nitrogen atom of the donor group is substituted with two CH_3 groups rather than two R groups in order to simplify the quantum-chemical computational calculations. The groups X considered here are: SiH_2, CH_2, $C=CH_2$, NH, C=O, S, O, $C=CHNO_2$, SO, and SO_2. In order to establish if the trends observed for **1** to **10** are independent of the chemical structure, and, thus, whether they can be translated as new guidelines for the rational design of new and efficient acceptor groups, the systematic investigation is extended to: (i) chromophores **11** to **20**, for which the π-bridge connecting the 4-(dimethylamino)-phenyl donor group and the TCF is a vinylene (the latter being the only structural difference between **1**-**10** and **11**-**20**); and (ii) chromophores **21**-**30**, for which the TCF of **11**-**20** is replaced by the TCP whose nitrogen atom at the position 1 of the pyrrole of the TCP is replaced with the same range of groups X used for **1** to **20**.

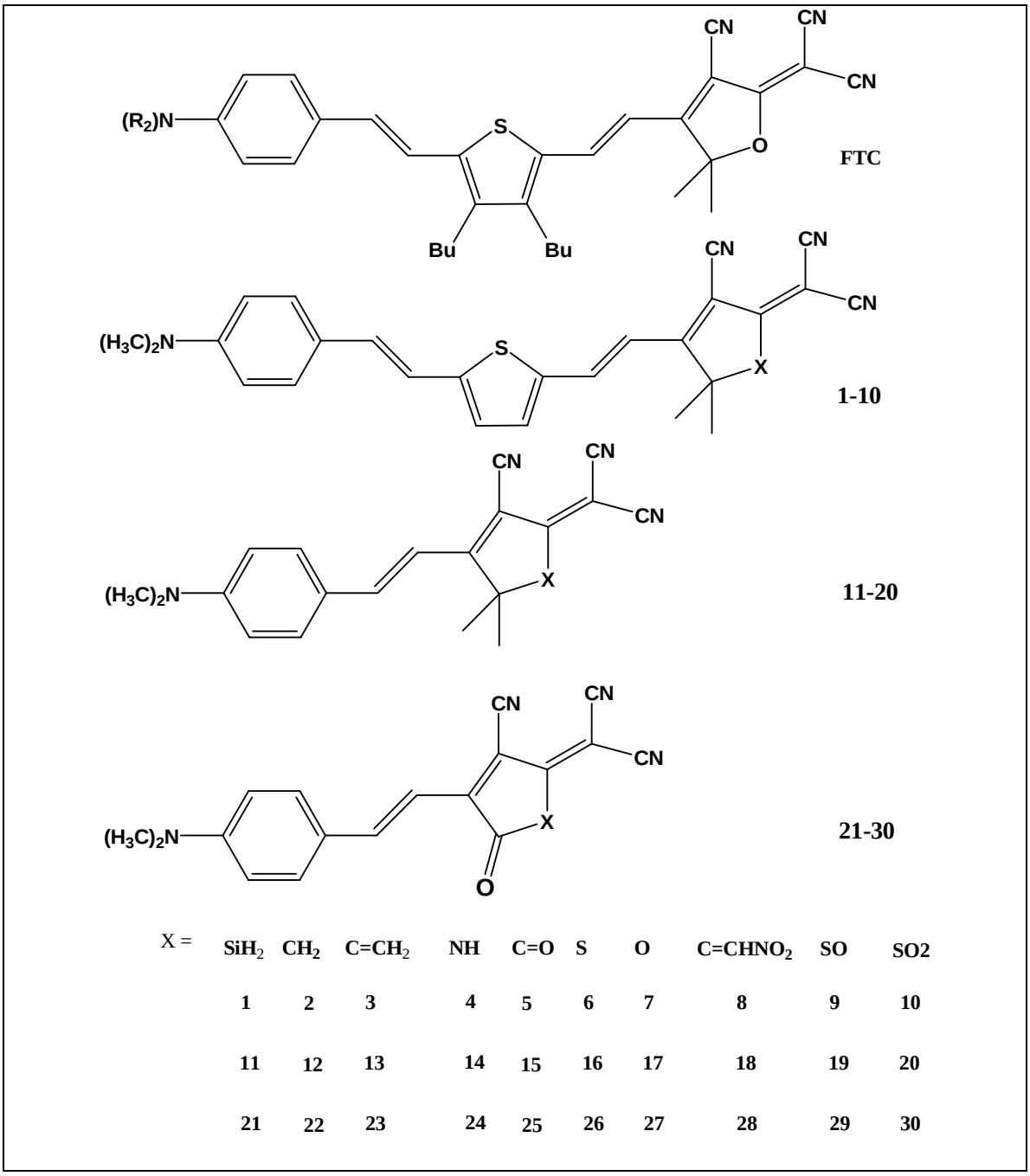

X =	SiH_2	CH_2	$C{=}CH_2$	NH	C=O	S	O	$C{=}CHNO_2$	SO	SO2
	1	2	3	4	5	6	7	8	9	10
	11	12	13	14	15	16	17	18	19	20
	21	22	23	24	25	26	27	28	29	30

*Figure 7: Chemical structures of dipolar chromophores **1** to **30**.*

The theoretical long axis components of the second-order polarizability (β_{xxx}) calculated with the SOS and FF methods and second-order polarizabilities (β) calculated with the

two-term model for **1** to **10**, **11** to **20**, and **21** to **30** are respectively reported in Tables 2, 3, and 4.

Table 2: Theoretical static long axis components of the second-order polarizability (β_{xxx}) calculated with the SOS and FF methods and second-order polarizabilities (β) calculated with the two-term model for dipolar chromophores **1** to **10**.

	position 1 group X	β_{xxx} (10^{-30} esu) SOS	β_{xxx} (10^{-30} esu) FF	β (10^{-30} esu) TWO-STATE MODEL
1	SiH_2	301	336	539
2	CH_2	314	355	552
3	$C=CH_2$	350	387	614
4	NH	290	330	495
5	CO	443	487	822
6	S	321	362	561
7	O	320	368	553
8	$C=CHNO_2$	489	543	888
9	SO	379	430	669
10	SO_2	476	536	815
8	***$C=CHNO_2$***	***489***	***543***	***888***

Table 3: Theoretical static long axis components of the second-order polarizability (β_{xxx}) calculated with the SOS and FF methods and second-order polarizabilities (β) calculated with the two-term model for dipolar chromophores **11** to **20**.

	position 1 group X	β_{xxx} (10^{-30} esu) SOS	β_{xxx} (10^{-30} esu) FF	β (10^{-30} esu) TWO-STATE MODEL
11	SiH_2	145	140	287
12	CH_2	140	140	274
13	$C=CH_2$	170	160	325
14	NH	116	117	195
15	CO	225	203	444
16	S	144	140	278
17	O	131	133	244
18	$C=CHNO_2$	205	187	341
19	SO	176	167	344
20	SO_2	226	209	418
20	***SO_2***	***226***	***209***	***418***

Table 4: Theoretical static long axis components of the second-order polarizability (β_{xxx}) calculated with the SOS and FF methods and second-order polarizabilities (β) calculated with the two-term model for dipolar chromophores **21** to **30**.

	position 1 group X	β_{xxx} (10^{-30} esu) SOS	β_{xxx} (10^{-30} esu) FF	β (10^{-30} esu) TWO-STATE MODEL
21	SiH_2	293	263	525
22	CH_2	290	263	542
23	$C=CH_2$	288	264	509
24	NH	275	255	550
25	CO	375	327	474
26	S	323	286	582
27	O	307	277	594
28	$C=CHNO_2$	334	301	446
29	SO	389	339	176
30	SO_2	476	405	682
30	***SO_2***	***476***	***405***	***682***

The theoretical transition energies (E_{ge}), ground state dipole moments (μ_{gg}), electronic excited state dipole moments (μ_{ee}), changes in state dipole moments ($\Delta\mu_{eg}$), and transition dipole moments (M_{ge}) are calculated with the INDO/SCI method for **1** to **10**, **11** to **20**, and **21** to **30** and are reported in Tables 5, 6, and 7 respectively.

Table 5: Theoretical transition energies (E_{ge}), ground state dipole moments (μ_{gg}), electronic excited state dipole moments (μ_{ee}), changes in state dipole moment ($\Delta\mu_{eg}$), and transition dipole moments (M_{ge}) calculated with the INDO/SCI method for dipolar chromophores **1** to **10**.

	E_{ge} (eV)	μ_{gg} (D)	μ_{ee} (D)	$\Delta\mu_{eg}$ (D)	M_{ge} (D)
1	2.50	13.4	20.1	9.4	12.4
2	2.49	14.1	20.9	9.1	12.7
3	2.48	13.9	21.6	10.2	12.6
4	2.52	15.2	21.5	8.6	12.5
5	2.37	14.4	25.5	12.1	12.8
6	2.49	14.8	22.7	9.5	12.5
7	2.48	15.6	23.1	8.9	12.8
8	2.34	12.7	25.3	13.3	12.5
9	2.43	16.0	26.2	10.8	12.5
10	2.33	17.6	28.8	11.7	12.7

Table 6: Theoretical transition energies (E_{ge}), ground state dipole moments (μ_{gg}), electronic excited state dipole moments (μ_{ee}), changes in state dipole moment ($\Delta\mu_{eg}$), and transition dipole moments (M_{ge}) calculated with the INDO/SCI method for dipolar chromophores **11** to **20**.

	E_{ge} (eV)	μ_{gg} (D)	μ_{ee} (D)	$\Delta\mu_{eg}$ (D)	M_{ge} (D)
11	3.04	12.5	19.1	8.3	11.7
12	3.03	13.3	19.3	7.5	12.0
13	2.98	13.2	20.4	9.2	11.6
14	3.08	14.5	18.9	5.8	11.7
15	2.83	13.2	24.0	11.5	11.5
16	3.03	13.8	20.9	8.0	11.7
17	3.04	14.5	20.5	6.7	12.0
18	2.84	16.3	26.6	12.0	9.9
19	2.96	15.2	24.5	9.8	11.5
20	2.85	15.9	26.5	10.6	11.7

Table 7: Theoretical transition energies (E_{ge}), ground state dipole moments (μ_{gg}), electronic excited state dipole moments (μ_{ee}), changes in state dipole moment ($\Delta\mu_{eg}$), and transition dipole moments (M_{ge}) calculated with the INDO/SCI method for dipolar chromophores **21** to **30**.

	E_{ge} (eV)	μ_{gg} (D)	μ_{ee} (D)	$\Delta\mu_{eg}$ (D)	M_{ge} (D)
21	2.63	7.8	19.1	12.4	11.2
22	2.66	8.8	20.5	12.2	11.6
23	2.67	8.5	20.0	12.4	11.2
24	2.62	9.2	21.6	12.9	11.2
25	2.57	10.6	22.2	11.7	10.7
26	2.57	9.5	22.5	13.1	11.2
27	2.63	11.0	23.5	12.4	11.9
28	2.61	12.4	24.0	11.8	10.5
29	2.44	12.4	18.0	6.2	8.5
30	2.33	13.5	27.1	13.6	10.8

For all these dipolar chromophores, the trends and magnitudes obtained from the SOS method for the β_{xxx} components are consistent with those obtained with the FF method and compared with the β values obtained using the two-term model later on in this chapter.

In order to understand the extent to which the inductive and resonance effects determine the role of the group X in **1**-**30**, it is helpful to plot the β_{xxx} components as a function of numerical parameter quantifying either of these two effects. Of the various scales of numerical parameter that are devised to describe the abilities of a substituent to affect a variety of thermodynamic and kinetic variables, the Taft σ_I scale [46] as one to which the β_{xxx} components can be successfully compared since this scale is designed to quantify inductive effects, without interference from resonance effects. By plotting computed

dipolar chromophore electronic and NLO properties versus the Taft σ_I coefficients, it is hoped to distinguish whether the role of the group X can be rationalized in terms of purely inductive effects, or whether resonance effects must also be invoked. In contrast, many other scales of numerical parameter, such as the traditional Hammett σ scale based on the ionization of benzoic acids, depend on a combination of inductive and mesomeric effects. The groups X are chosen to cover a wide range of inductive electron-withdrawing and electron-donating abilities as follows (Taft σ_I coefficient in parentheses): SiH_2 (-0.10), CH_2 (-0.05), $C=CH_2$ (+0.05), NH (+0.09), C=O (+0.20), S (+0.23), O (+0.27), $C=CHNO_2$ (+0.38), SO (+0.50), and SO_2 (+0.60) [47]. Some of these dipolar chromophores are not practical synthetic targets; however, the principal aim in this chapter is to understand the inductive and resonance effects of the group X in these dipolar chromophores by examining a wide range of groups X, rather than to rationally design new and efficient dipolar chromophore.

The β_{xxx} components calculated with the SOS method are plotted versus the Taft σ_I coefficients for **1** to **10** and **11** to **20** in Figure 8.

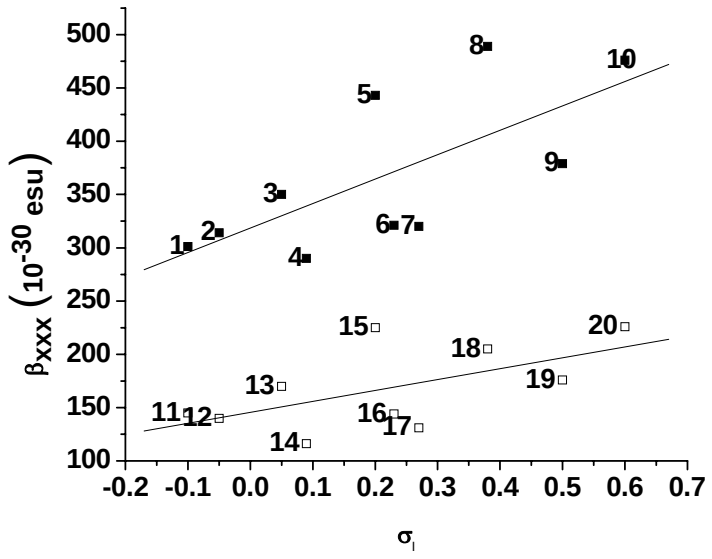

Figure 8: Theoretical static long axis components of the second-order polarizability (β_{xxx}) *calculated with the SOS method as a function of the Taft* σ_I *coefficient associated with the group X for dipolar chromophores* ***1*** *to* ***10*** *(black square) and* ***11*** *to* ***20*** *(white square). These dipolar chromophores are numbered in order of increasing Taft* σ_I *coefficient. The lines are linear least square regressions (with R=0.70228 for* ***1****-****10*** *and 0.59372 for* ***11****-****20*** *that are expected), which have no physical significance and are provided as guides to the eyes, showing the overall increase of the* β_{xxx} *component as a function of the Taft* σ_I *coefficient.*

For the dipolar chromophores with both vinylene-thienylene-vinylene and vinylene π-bridges (**1** to **10** and **11** to **20** respectively) the β_{xxx} components increase with the Taft σ_I coefficients, i.e. with increasingly inductive electron-withdrawing ability of the group X, as indicated by the linear least square regressions indicated on the plot of Figure 8; for example, for X = SiH_2 (σ_I = -0.10), the β_{xxx} component is 301×10^{-30} esu for **1** and 145×10^{-30} esu for **11**, whereas for the corresponding X = SO_2 (σ_I = +0.60) analogues, the β_{xxx} component is 476×10^{-30} esu for **10** and 226×10^{-30} esu for **20**. Although the β_{xxx} component increases by a similar factor (ca. 60%) from **1** to **10** as from **11** to **20**, the

magnitude of the β_{xxx} component is consistently larger in the vinylene-thienylene-vinylene series, as expected from the longer π-bridge in this series.

Relative to the linear least square regressions for either **1**-**10** or **11**-**20** series, some groups X (especially C=O and C=$CHNO_2$) lie above this line, while some others (especially NH and O) lie beneath it. The groups X lying significantly above the line are those known to be electron-withdrawing in a resonance sense (π electron-withdrawing groups), whereas those significantly below the line are π electron-donating groups. To gain some insight into the mechanism by which the π electron-withdrawing or electron-donating groups affect the β_{xxx} component within the framework of the SOS method, it is necessary first to identify which electronic excited states contribute to the β_{xxx} component and the orbital descriptions of the appropriate transitions.

As well as the converged SOS β_{xxx} component, Tables 2, 3, and 4 also include the β values obtained using the two-state model, considering only the lowest-lying electronic excited state. A significant discrepancy between the converged components and the two-state model values exists, indicating that other electronic excited states contribute significantly to the β_{xxx} component, which essentially converges on the inclusion of an additional electronic excited state (not necessarily the second electronic excited state). The two-state model values are however plotted as a function of the Taft σ_I coefficients for **1** to **10** in Figure 9.

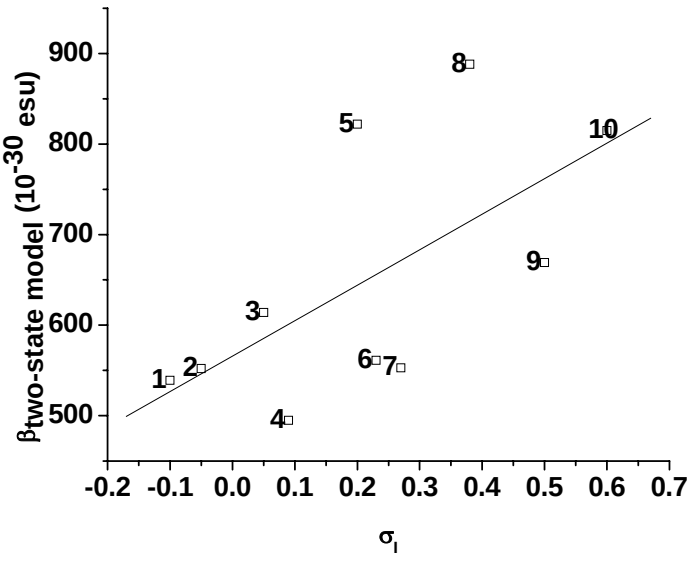

*<u>Figure 9:</u> Theoretical second-order polarizabilities (β) calculated with the two-state model (considering only the first electronic excited state) as a function of the Taft σ_I coefficient associated with the group X for dipolar chromophores **1** to **10**. The line is a linear least square regression (with R=0.63795 for **1**-**10** that is expected), which has no physical significance and is provided as guide to the eyes, showing the overall increase of the β_{xxx} component as a function of the Taft σ_I coefficient.*

However, as shown in the plot of Figure 9, the trend in the two-state model values closely follows that of the converged components, indicating that the trends in β are well-understood by considering only the first electronic excited state. Therefore, the effect on β of the resonance electron-withdrawing or electron-donating effect based on the electronic terms entering the two-state model is investigated, specifically the transition energy (E_{ge}), and the change in state dipole moment ($\Delta\mu_{eg}$).

For **1** to **10**, the lowest energy transition in the linear absorption spectrum is calculated to be between 2.33 and 2.50 eV (ca. 500 nm) and essentially corresponds to the promotion

of an electron from the highest occupied π-molecular orbital (HOMO) to the lowest unoccupied π-MO (LUMO). For **11** to **20**, the lowest energy transition, also essentially a HOMO to LUMO transition, is calculated to be between 2.83 and 3.08 eV (ca. 400 nm). Since (i) the trends in the converged components are mirrored by the two-term model values; and (ii) the first electronic excited state for these dipolar chromophores is well-described as a HOMO to LUMO transition, the resonance electron-withdrawing or electron-donating effects of the groups X upon β is rationalized by examining the frontier π-MOs (HOMO and LUMO) calculated with the INDO/SCI method. They are presented for **1**, **4**, and **5** in Figure 10.

1 HOMO

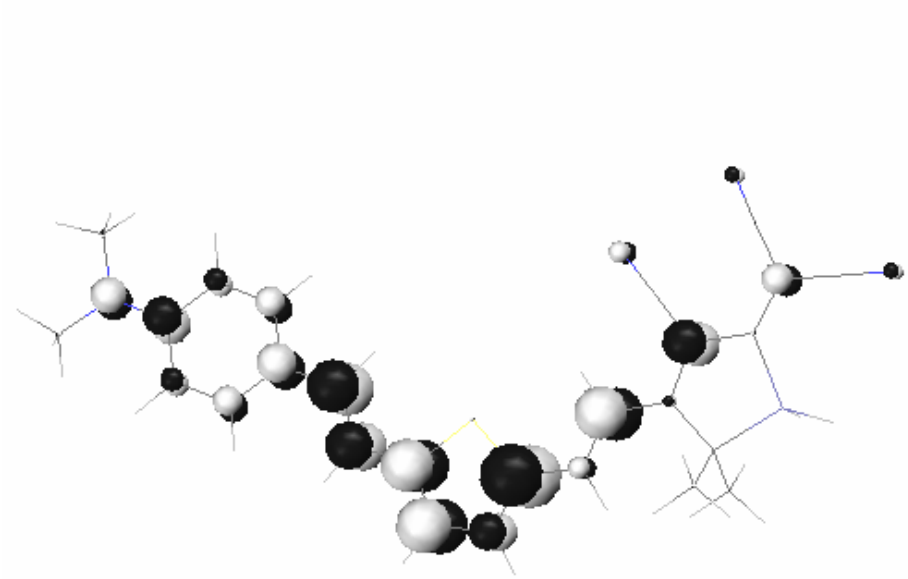

*Figure 10: Theoretical frontier π-MOs (HOMO and LUMO) calculated with the INDO/SCI method for dipolar chromophores **1**, **4**, and **5**.*

1 LUMO

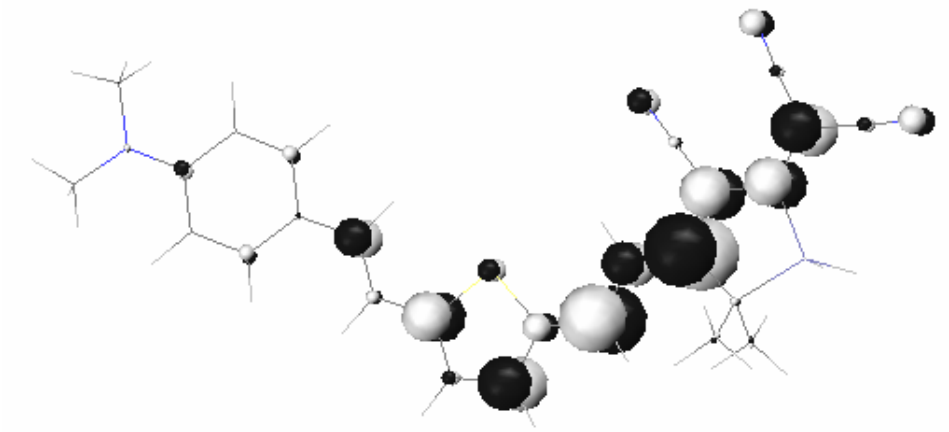

4 HOMO

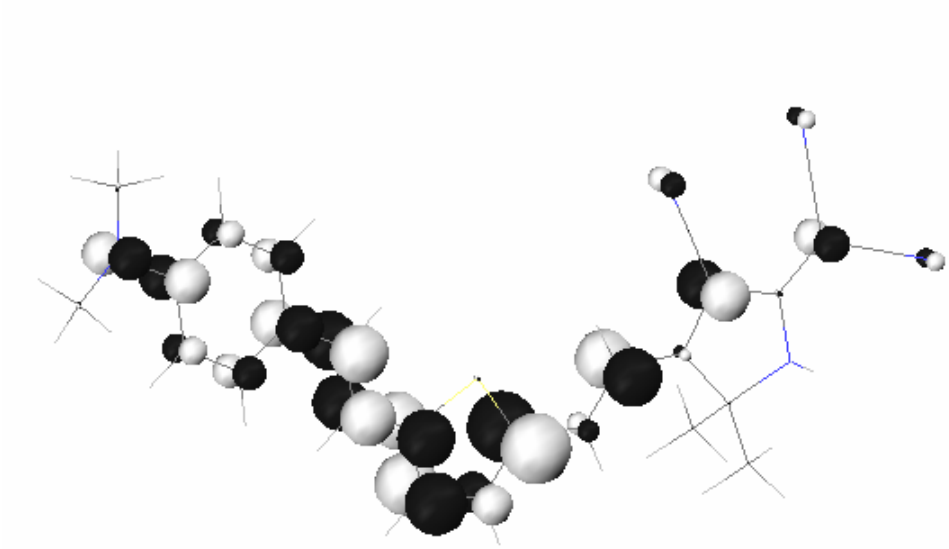

Figure 10: continued.

4 LUMO

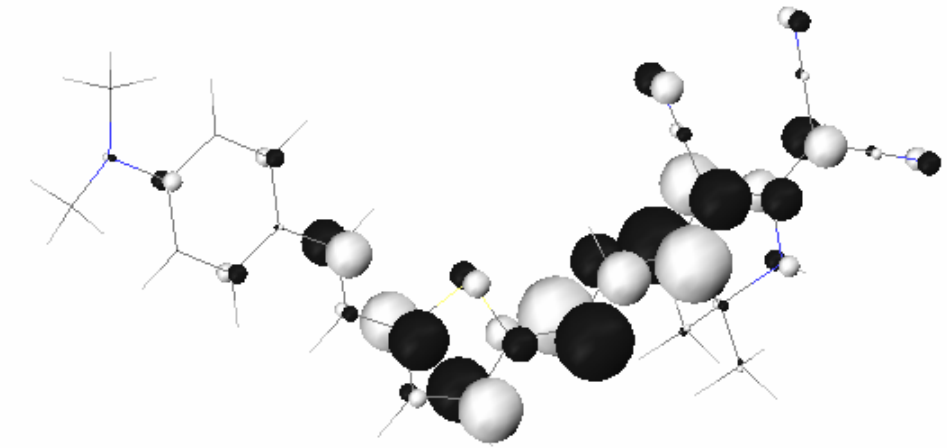

5 HOMO

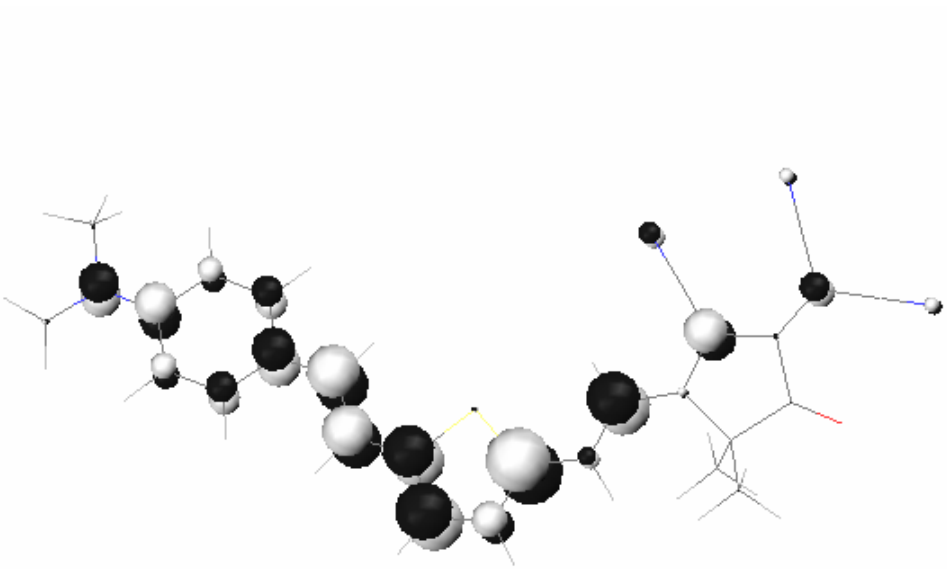

Figure 10: continued.

5 LUMO

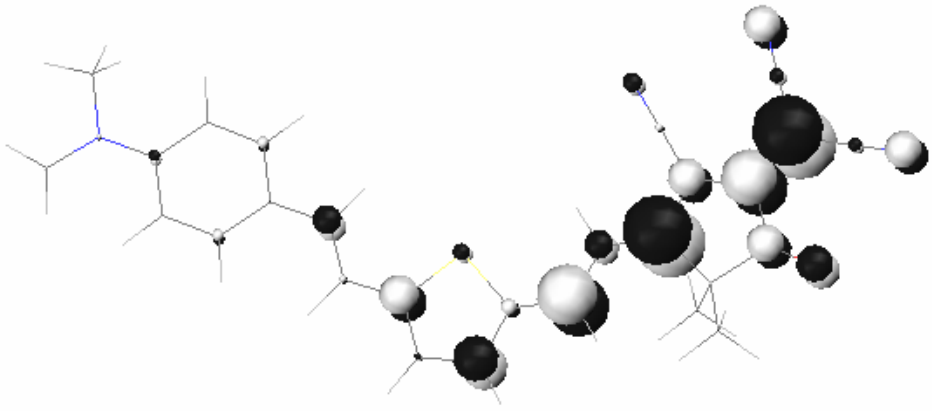

Figure 10: continued.

The chromophore **1** serves as an illustrative example of a dipolar chromophore for which the resonance effects of the groups X are neither expected nor evident in the calculated frontier π-MOs (HOMO and LUMO) (similar behavior for **2**, **9**, and **10**); there are no contributions to either HOMO and LUMO at the site of the group X. The chromophore **5** serves as an illustrative example of a dipolar chromophore where the group X is a π electron-withdrawing group (similar behavior for **3** and **8**), while chromophore **4** is an illustrative example of a dipolar chromophore where the group X is a π electron-donating group (similar behavior for **6** and **7**). The HOMO of **4** and **5** are qualitatively similar to that of **1**, with no contribution at the site of the group X. However, the LUMO of **5** is regarded as resulting from an in-phase combination of the LUMO of **1** and the local LUMO of the group X. In general from energy considerations a π electron-donating

group is expected to contribute more significantly to the HOMO than the LUMO. However, the HOMO of **1** has essentially zero coefficient at the position on the carbon atom of the π-bridge adjacent to the group X, i.e. there is a node corresponding more-or-less to this position. The LUMO of **4** shows a small contribution at the site of the group X and is described as an out-of-phase combination of the LUMO of **1** the local HOMO of the group X. The frontier π-MOs (HOMO and LUMO) energies are calculated with the INDO/SCI method and are plotted as a function of the Taft σ_I coefficients in Figure 11.

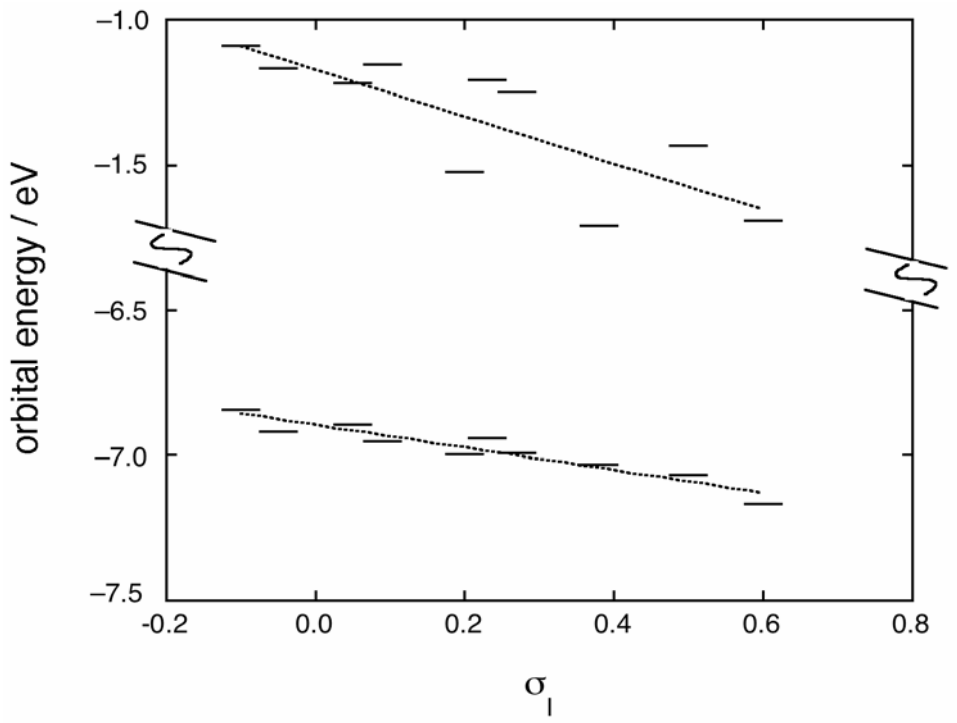

*Figure 11: Theoretical frontier π-MOs (HOMO and LUMO) energies calculated with the INDO/SCI method: HOMO (lower set of data) and LUMO (higher set of data) as a function of the Taft σ_I coefficients associated with the group X for dipolar chromophores **1**to **10** (lines representing linear least square regressions as guides to the eyes).*

The HOMO energies decrease relatively smoothly with the Taft σ_I coefficients, consistent with a principally inductive effect from the group X on this MO. The LUMO

energies decrease more steeply and considerably less smoothly than those for the HOMO energies. The more steep decrease is consistent with the location of the group X at the acceptor group of the dipolar chromophore where the LUMO is concentrated. The scattered LUMO energies are attributable to the resonance effects of the group X discussed above; the LUMO of a π electron-withdrawing group of the groups X, such $C{=}CHNO_2$, lie lower in energy than the linear regression, whereas those of the π electron-donating group of the groups X, such as O, lie above this linear regression.

Thus, relative to a dipolar chromophore of comparable inductive electron-withdrawing ability (σ_I coefficient), but with no resonance character, a π electron-withdrawing group stabilizes the LUMO, leading to a lower E_{ge} and a higher β_{xxx} component than otherwise expected, whereas a π electron-donating group destabilizes the LUMO, leading to a higher E_{ge} and a lower β_{xxx} component than otherwise expected.

The theoretical transition energies (E_{ge}) and changes in state dipole moment ($\Delta\mu_{eg}$) calculated with the INDO/SCI method are plotted as a function of the Taft σ_I coefficients for **1** to **10** in Figure 12.

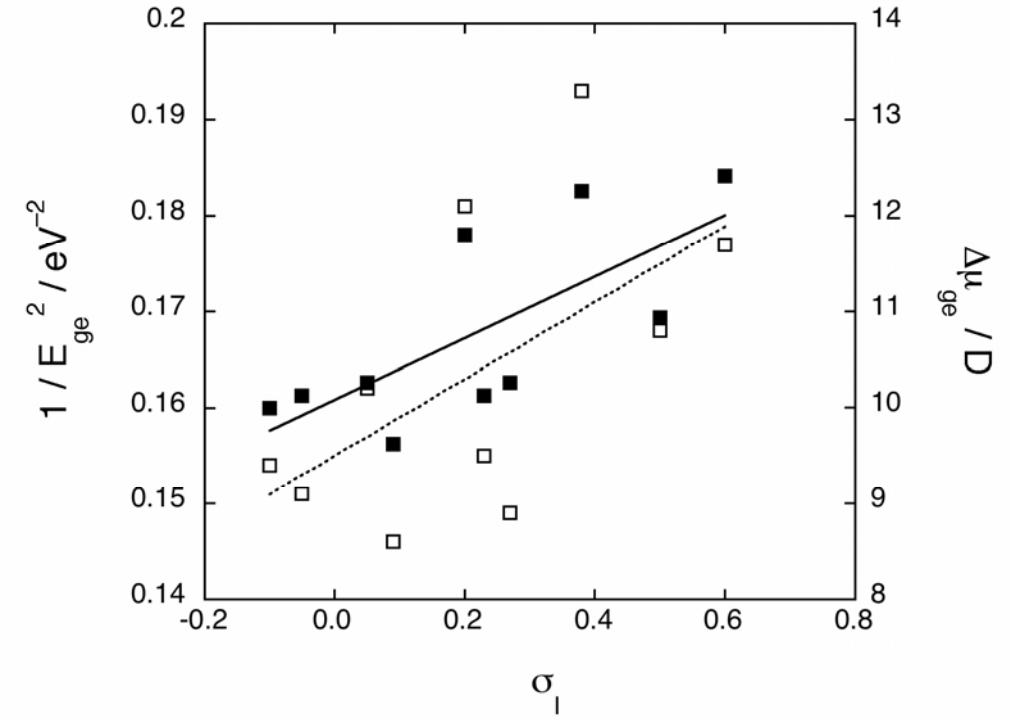

*<u>Figure 12:</u> Theoretical transition energies ($\frac{1}{E_{ge}^2}$) (solid square) and changes in state dipole moment ($\Delta\mu_{eg}$) (open square) calculated with the INDO/SCI method as a function of the Taft σ_I coefficient associated with the group X for dipolar chromophores **1** to **10**.*

As also shown in Figure 12, the change in state dipole moment varies with the Taft σ_I coefficient in a fashion closely paralleling with the reciprocal of the transition energy, with $\Delta\mu_{eg}$ larger than expected with a π electron-withdrawing group and smaller with a π electron-donating group; thus, the trends in $\Delta\mu_{eg}$ and $\frac{1}{E_{ge}^2}$ reinforce one another to give the observed trend in the two-term model values. The transition dipole moments (μ_{ge}) show relatively insignificant variation with the chemical structure (ca. 12.6 D for **1** to **10** and 11.5 D for 11 to **20**). The orbital origin of the trends in $\Delta\mu_{eg}$ is less obvious than that

in $\frac{1}{E_{ge}^2}$; however, the increased values in the dipolar chromophores with a π electron-withdrawing group is partly traced to increased delocalization of the LUMO onto the group X, leading to a greater concentration of the LUMO towards the acceptor group of the dipolar chromophore. In the case of the dipolar chromophores with a π electron-donating group, there appears to be a subtle reduction in the LUMO coefficients at the nitrogen atoms of the $C=C(CN)_2$ group relative to those on the π-bridge. Qualitatively similar trends are observed for **11**-**20**.

This systematic investigation is also extended to **21** to **30**, for which the converged components and the two-term model values are plotted as a function of the Taft σ_I coefficients in Figure 13. As found in **1**-**10** and **11**-**20**, the converged components increase with the Taft σ_I coefficients, although the details of the trend differs markedly. In contrast to **1**-**10** and **11**-**20**, the two-term model values follow a completely different trend than the converged components, indicating that higher-lying electronic excited states make significant contributions to the β_{xxx} component and that the effects of the group X on these contributions differ from those made to the first electronic excited state.

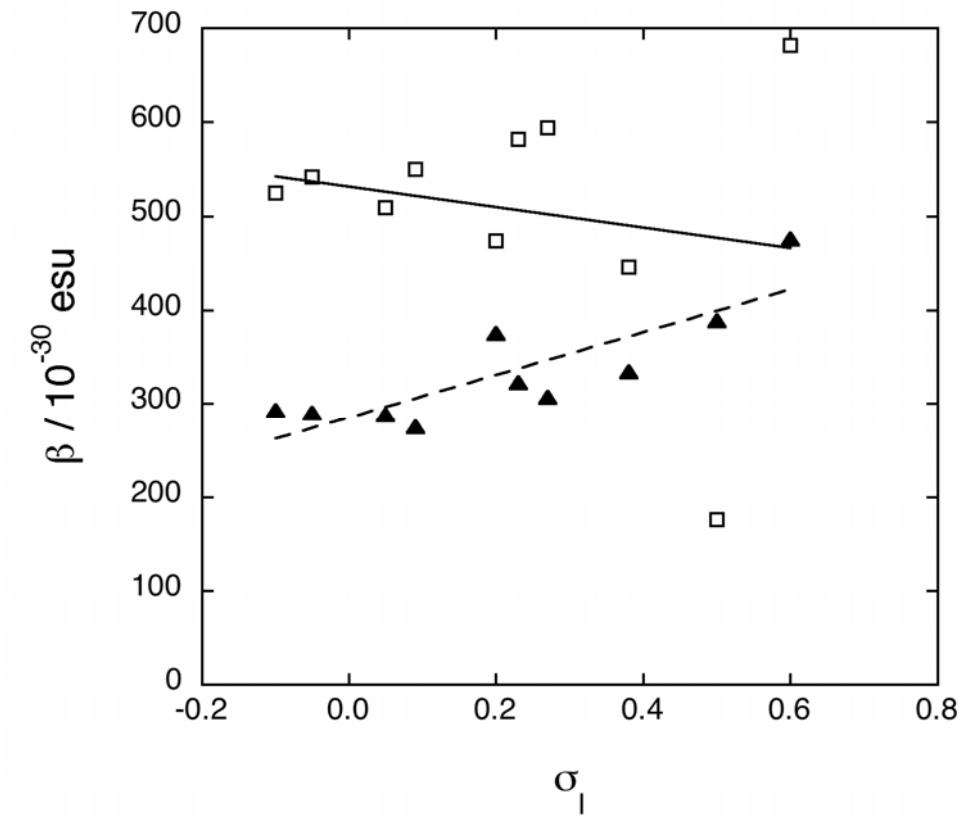

*Figure 13: Theoretical static long axis components of the second-order polarizability (β_{xxx}) calculated using the SOS method (linear regression as broken line) and second-order polarizability (β) calculated with the two-term model (considering only the first electronic excited state) (linear regression as solid line) as a function of the Taft σ_I coefficient associated with the group X for dipolar chromophores **21** to **30**.*

In summary, for dipolar chromophores with the TCF where the oxygen atom is replaced by a variety of groups X, the second-order polarizability increases as the inductive electron-withdrawing ability of the group X increases (cf. SiH_2, CH_2, SO, and SO_2); however, there is a deviation from this trend when the group X possesses either a π electron-donating or electron-withdrawing character. The π-acceptor groups X (C=O and $C=CHNO_2$, and to a lesser extent $C=CH_2$) have higher second-order polarizability than expected based on the inductive electron-withdrawing character of these groups X alone. Since the trends in second-order polarizability is well-described using the two-

state model, the origin of these increased second-order polarizabilities are traced by stabilizing contributions from the local LUMOs of these fragments to the molecular LUMO, leading to reduced transition energies and increased change in state dipole moment. The local HOMOs π-donor of the groups X (NH, S, and O) contribute to the molecular LUMO in a destabilizing fashion, leading to increased transition energies, reduced change in state dipole moment, and reduced second-order polarizability.

3.3. EFFECT ON SECOND-ORDER POLARIZABILITY OF LENGTH OF π-BRIDGE OF DIPOLAR CHROMOPHORES

Previous theoretical [48] and experimental [49] studies have demonstrated a significant enhancement of the β value when the length of the π-bridge is extended. Therefore, in this chapter, this general guideline for the rational design of new and efficient dipolar chromophores for the second-order NLO applications is tested in a specific case: the TCP-based dipolar chromophore, for which the 4-(dimethylamino)-phenyl donor group is connected to the TCP by a polyene segment (π-bridge) containing 0 to 14 vinylene units (n corresponds to the number of vinylene units). The chemical structure is presented in Figure 14.

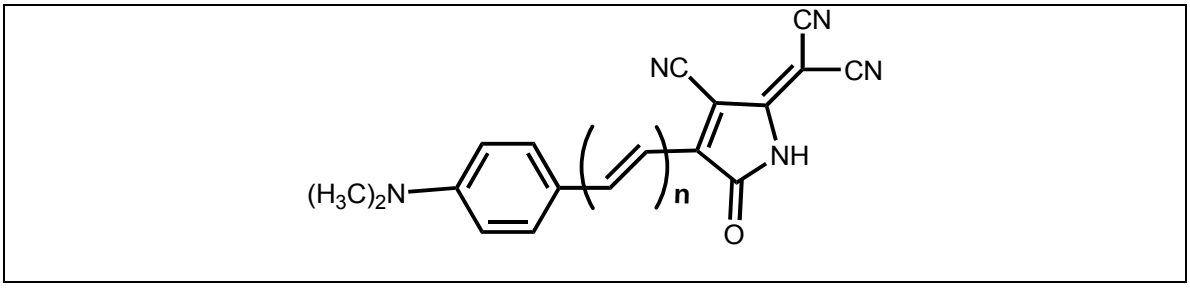

Figure 14: Chemical structure of TCP-based dipolar chromophore.

The theoretical transition energies (E_{ge}), optical absorption maxima ($\lambda_{\max}$), ground state dipole moments (μ_{gg}), long axis components of the second-order polarizability (β_{xxx}), and product of the β_{xxx} components and the μ_x components are calculated with the SOS method and are reported in Table 8. In order to obtain reliable and converged β_{xxx} components, the CI active space (involved in the SCI scheme) must be scaled with the molecular size of the dipolar chromophore because the length of the π-bridge varies; for

instance, the CI active space involves the 24 highest occupied and 24 lowest unoccupied π-MOs for a number of vinylene units (n) = 0, while it consists of the 44 highest occupied and 44 lowest unoccupied π-MOs for n = 10.

Table 8: Theoretical transition energies (E_{ge}), optical absorption maxima (λ_{max}), ground state dipole moments (μ_{gg}), static long axis components of the second-order polarizability (β_{xxx}), and product of the β_{xxx} components and the μ_x components calculated using the SOS method for TCP-based dipolar chromophores.

	n	E_{ge} (eV)	λ_{max} (nm)	μ_{gg} (D)	β_{xxx} (10^{-30} esu) SOS	β_{xxx} μ_x (10^{-48} esu) SOS
	0	2.77	447	8.2	150	1146
	1	2.62	473	9.2	275	2383
	2	2.54	488	9.9	395	3704
	3	2.48	500	10.4	516	5105
	4	2.44	508	10.8	622	6380
	5	2.41	513	11.1	708	7464
	6	2.40	517	11.3	776	8335
	7	2.39	519	11.4	827	9017
	8	2.38	520	11.5	867	9547
	9	2.38	520	11.6	892	9913
	10	2.38	521	11.6	914	10233
	12	2.38	521	11.5	939	10489
	14	2.38	520	11.5	955	10696
	14	***2.38***	***520***	***11.5***	***955***	***10696***

For the sake of simplicity, the β_{xxx} components are plotted as a function of n in Figure 15.

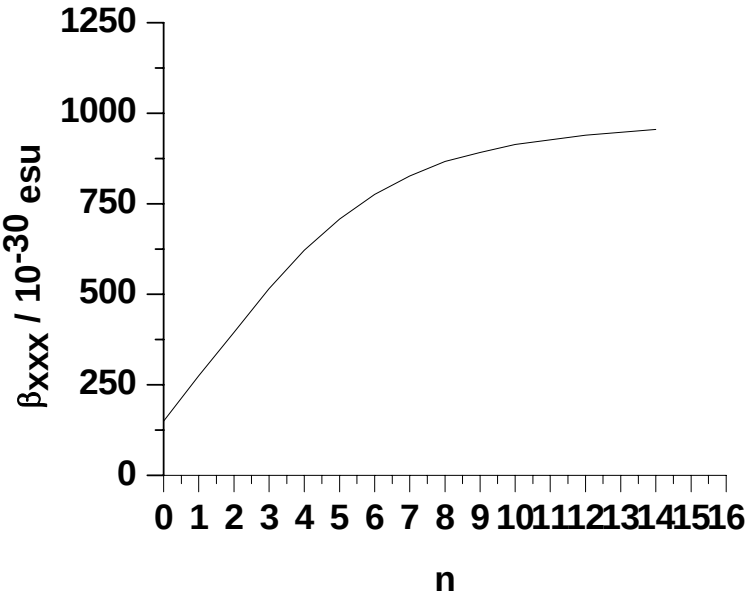

Figure 15: Theoretical static long axis components of the second-order polarizability (β_{xxx}) calculated with the SOS method as a function of n for TCP-based dipolar chromophores.

The β_{xxx} components increase with n and reaches saturation for n = 10 (corresponds to the region A in Figure 1). In order to establish if the number of vinylene units at which the saturation occurs is independent of the chemical structure; the β_{xxx} components are calculated for another dipolar chromophore, for which the polyene π-bridge (containing 0 to 14 vinylene units) is end-capped by a methoxy group (OCH_3), the donor, and a cyano group (CN), the acceptor. Its chemical structure is presented in Figure 16.

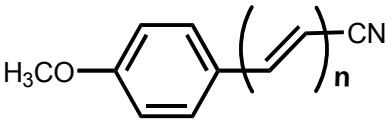

Figure 16: Chemical structure of dipolar chromophore with weaker D-A pair than TCP-based dipolar chromophore presented in Figure 14.

The β_{xxx} components calculated with the SOS method are plotted as a function of n in Figure 17.

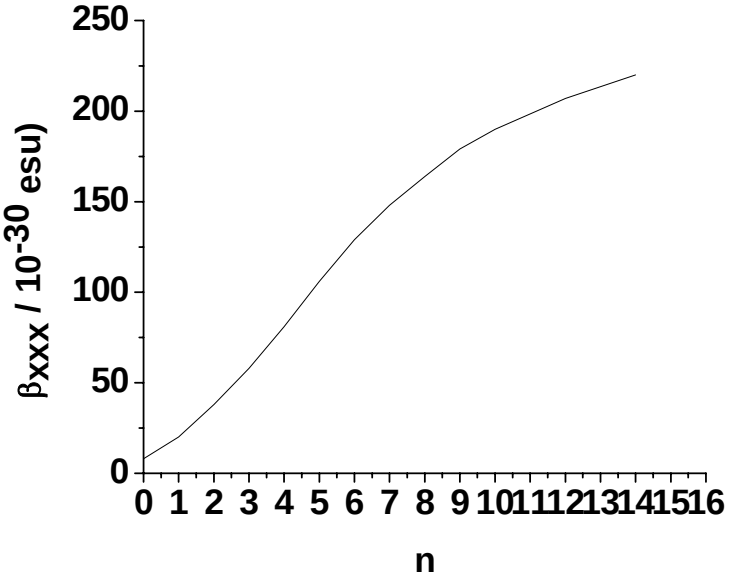

Fgure 17: Theoretical static long axis components of the second-order polarizability (β_{xxx}) calculated with the SOS method as a function of n for dipolar chromophores with weaker D-A pair than TCP-based dipolar chromophore presented in Figure 14.

When the π-bridge consists of 14 vinylene units, in contrast to the TCP-based dipolar chromophore, the β_{xxx} components of the dipolar chromophore with the weaker D-A pair are still increasing and saturation is not yet reached (correspond to an earlier stage of

region A in Figure 1). Therefore, it is important to bear in mind that the effect on the β_{xxx} component of the length of the π-bridge in dipolar chromophores seems to be chemical structure dependent, and a much more involved investigation must be done to extract new guidelines for the rational design of new and efficient dipolar chromophores.

3.4. EFFECT ON SECOND-ORDER POLARIZABILITY OF NATURE OF π-BRIDGE OF DIPOLAR CHROMOPHORES – INSERTION OF ONE AUXILIARY DONOR OR ACCEPTOR

An ideal prototypical dipolar chromophore for second-order NLO applications must have a large β value (best satisfied by a long delocalized π-bridge end-capped by strong donor and acceptor groups) and must also be chemically and thermally stable. Various strategies were used to improve the overall stability of the dipolar chromophores in which the donor and acceptor groups end-capped a conjugated polyene π-bridge. Although relatively short polyenes gave reasonable overall stability and β value, extended polyenes were typically not sufficiently stable to withstand the poling process at a temperature greater than $200^{\circ}C$ [13].

The rigid locking of the conformation of the extended polyene by incorporation into a ring system [50] was anticipated to increase the overall stability by preventing the decomposition related to a *cis-trans* isomerization and by steric protection of the polyene. This strategy was first applied to polymethine dyes, and more recently, to lock some or all of the vinylene units of the dipolar chromophores by their incorporation into ring systems. In several cases, the comparison of ring-locked and traditional polyenes clearly demonstrated greater overall stability for the former, with β values in the ring-locked polyenes comparable to those in the traditional ones.

In the context of improving the overall stability of the dipolar chromophores, in addition to rigid lock the conformation of the extended polyene by incorporation into a ring system, the vinylene units of the polyene were replaced by aromatic rings [51], which led to more

stable and practical dipolar chromophores. For instance, a benzene-1,4-diyl (para-phenylene) bridging unit was regarded as having the same effective conjugation length as a diene π-bridge. However, the degree of ground state polarization in a dipolar chromophore with such a bridging unit was typically reduced relative to the diene analog because of the aromatic stabilization energy associated with the neutral resonance form; the presence of the phenylene bridging unit usually interferes with an efficient intramolecular charge transfer, the significant aromatic stabilization of such a bridging unit favoring electron localization, shielding the donor and acceptor groups, and decreasing the β value.

In this context, replacing a phenylene bridging unit with less aromatic heterocyclic ring offered a potential compromise between the β value and the overall stability. The replacement of one or both phenylene bridging units of a stilbene π-bridge with more easily delocalizable heterocyclic rings has been studied both experimentally and theoretically [52]. Such heterocyclic rings were regarded as auxiliary electron-rich (donor, D') or electron-poor (acceptor, A') groups. For instance, a thiophene-2,5-diyl bridging unit offered a good compromise whereby the overall stability of the diene π-bridge was increased by incorporation into a ring system, but where the degree of ground state polarization was less disrupted than with a benzene-1,4-diyl bridging unit because of the lower aromaticity of the thiophene bridging unit. Although the dipolar chromophores containing a thiophene π-bridge have attracted widespread interest because their β values were superior to those of the corresponding aryl analogues, a detailed understanding of the structure-property relationships for the closely related dipolar chromophores containing a thiazole π-bridge was still lacking.

Breitung *et al.* {52} have investigated a series of dipolar chromophores, whose chemical structures are presented in Figure 18, that contained a stilbene π-bridge (chromophores **1** and **5**), a thiophene π-bridge (chromophores **4**, **8**, and **11**), and a thiazole π-bridge (chromophores **2**, **3**, **6**, **7**, **9**, and **10**).

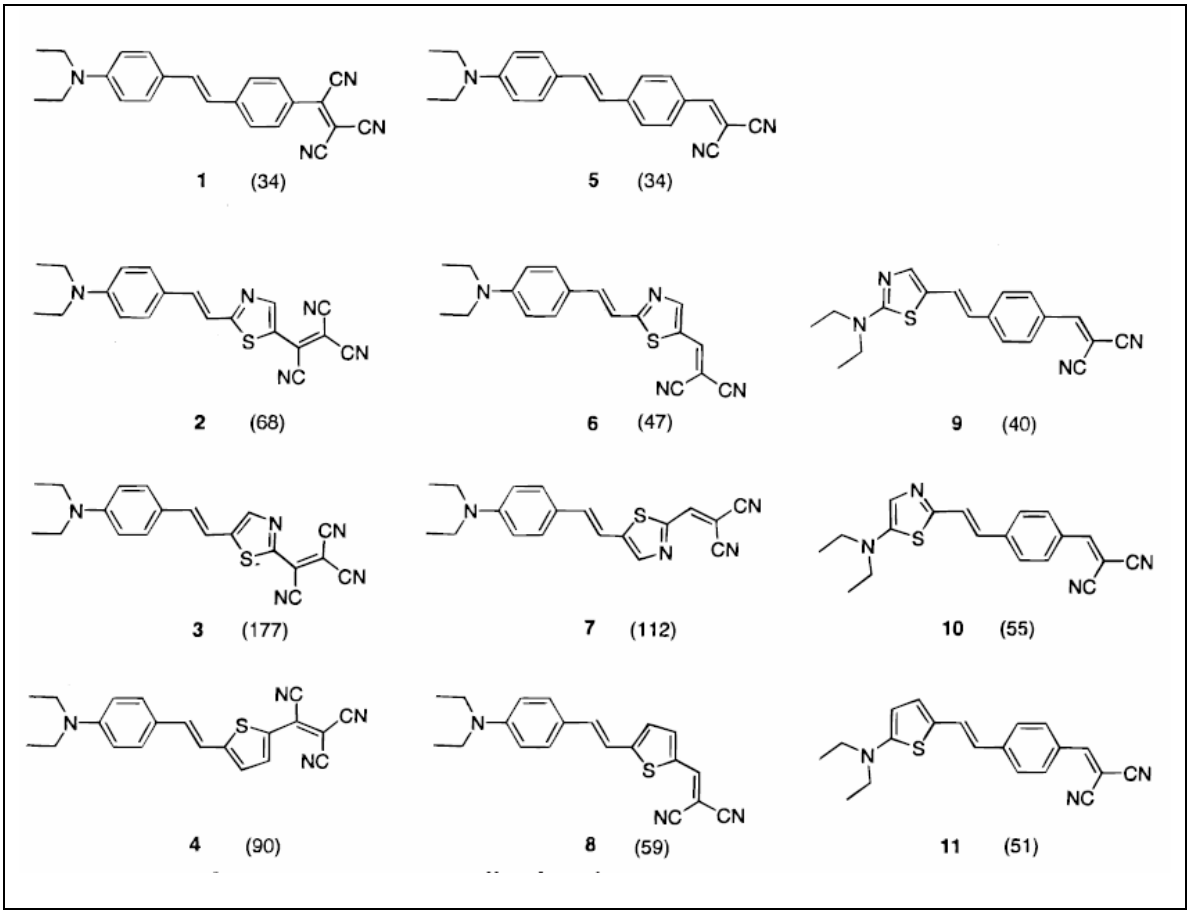

*<u>Figure 18:</u> Chemical structures of dipolar chromophores **1** to **11** (the β values calculated by Breitung in Ref. {52} are between parentheses).*

From Breitung's work, three main observations were made:

- the dipolar chromophores containing a thiazole π-bridge display larger β values than their aryl analogues (cf. **2** and **3** vs. **1**; **6**, **7**, **9**, and **10** vs. **5**);
- the magnitude of the increase of the β value depends on the regiochemistry of the thiazole bridging unit (cf. **2** vs. **3**; **6** vs. **7**; **9** vs. **10**). Therefore, the incorporation of a thiazole bridging unit into a stilbene π-bridge introduces two distinct elements of regiochemistry: (i) the replacement of the phenylene bridging unit adjacent to the donor group yields only a small increase in the β value (cf. **9** or **10** vs. **5**), and the relative orientation of the thiazole bridging unit within the dipolar chromophore does not have a substantial effect (cf. **9** vs. **10**); and in contrast (ii) the replacement of the phenylene bridging unit adjacent to the acceptor group affords a larger increase in the β value (cf. **2** or **3** vs. **1**; **6** or **7** vs. **5**), and the relative orientation of the thiazole bridging unit within the dipolar chromophore plays a substantial role in determining the β value (cf. **2** vs. **3**; **6** vs. **7**);
- in the matched case (see definition below), the β values of the dipolar chromophores containing a thiazole π-bridge are larger than in the aryl analogues and also larger than in the dipolar chromophores containing a thiophene π-bridge (cf. **3** vs. **4**; **7** vs. **8**; **10** vs. **11**).

When the dipole moment of the thiazole bridging unit reinforces the molecular dipole, as in the case of **3**, **7** and **10**, the β value is maximized and we refer to this situation as the "matched" case; conversely, we refer to **2**, **6**, and **9** as the "mismatched" case. The critical issue of the regiochemistry of the thiazole bridging unit ("matched" vs.

"mismatched") has not been articulated previously. Ironically, most of the dipolar chromophores containing a thiazole π-bridge described in the literature represented the "mismatched" cases and only the dipolar chromophores reported by Moylan {53}, Varanasi {54}, and Wurthner {55} corresponded to the "matched" cases.

In this chapter, Breitung's work extends to more complex dipolar chromophores using modified donor and acceptor groups to develop new guidelines for the rational design of new efficient NLO chromophores. The β_{xxx} components are calculated with the SOS method for Breitung's chemical structures: (i) as reported in Ref. {52}; (ii) when the TCV and the dicyanovinyl acceptor group are replaced by the TCF; and (iii) when the TCV and the dicyanovinyl acceptor group are replaced by the TCP. The β_{xxx} components are plotted as a function of the dipolar chromophores **1** to **11** in Figure 19.

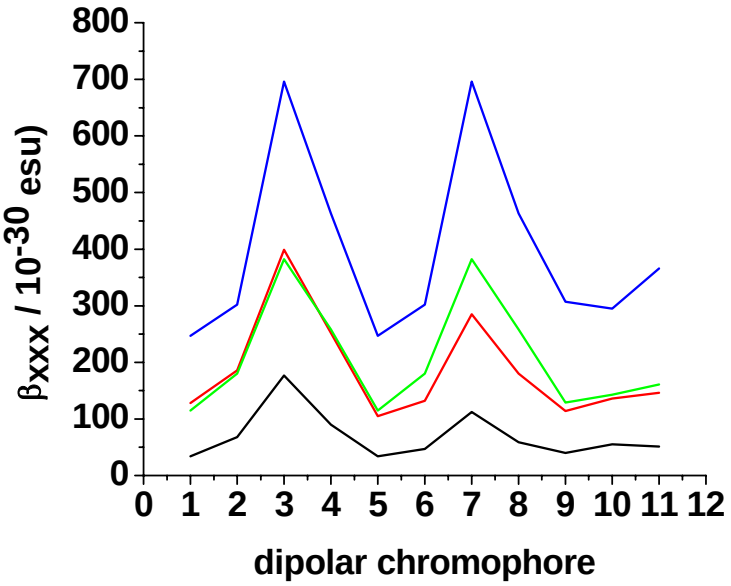

*<u>Figure 19:</u> Theoretical static long axis components of the second-order polarizability (β_{xxx}) calculated with the SOS method as a function of dipolar chromophores **1** to **11** for Breitung's chemical structures: (i) as reported in Ref. {52} (red); (ii) when the TCV and the dicyanovinyl acceptor groups are replaced by the TCF (green); and (iii) when the TCV and the dicyanovinyl acceptor groups are replaced by the TCP (blue); and β values reported by Breitung in Ref. {64} are also plotted (black).*

While our computational calculations reproduce the trends reported by Breitung, the magnitudes of β are not reproduced in spite of testing the CI active spaces, molecular conformations, numbers of electronic excited states in the SOS expression, including the dispersion of β, and using the Ohno-Klopman instead of the Mataga-Nishimoto potential for electron repulsion. As our β values are larger than those reported by Breitung by a factor between 2 and 3, the main reason for this discrepancy appears to be a different definition of the β value (Taylor vs. Power series) (note that the dipolar

chromophores substituted by the TCP have higher β values than the ones substituted by the TCF for the reason given in chapter 4).

Since similar trends are found, another investigation is done by considering chromophores **12** to **15**, for which the concept suggesting the insertion of auxiliary donor and acceptor into the π-bridge to significantly enhance the β value is tested. The chemical structures of the dipolar D-D′-π-A (**12**), D-π-D′-A (**13**), D-π-A′-A (**14**), and D-A′-π-A (**15**) chromophores are presented in Figure 20 (the matched cases are the ones taken into consideration here because they yield highest β values compared to their mismatched analogues).

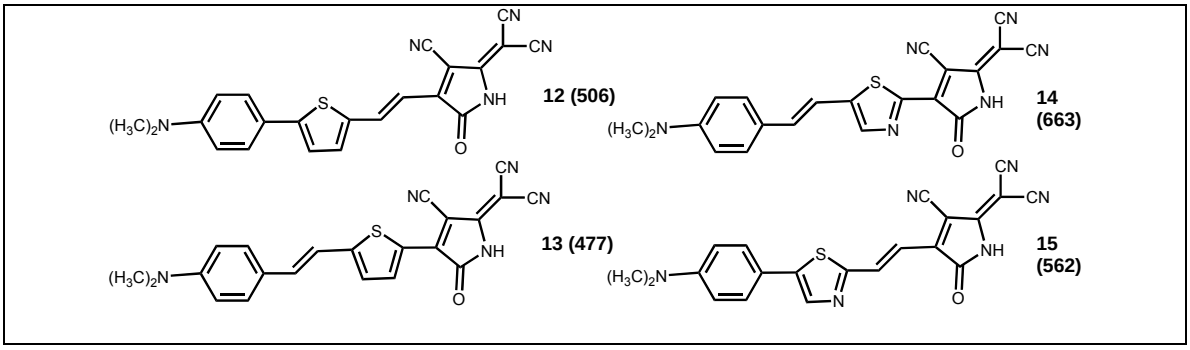

*<u>Figure 20:</u> Chemical structures for dipolar chromophores **12** to **15** (the β_{xxx} components calculated with the FF method are reported in parentheses).*

The theoretical transition energies (E_{ge}), optical absorption maxima ($\lambda_{\max}$), ground state dipole moments (μ_{gg}), long axis components of the second-order polarizability (β_{xxx}), and product of the β_{xxx} components and the μ_x components are calculated with the SOS and/or FF methods for **12** to **15** and are reported in Table 9.

Table 9: Theoretical transition energies (E_{ge}), optical absorption maxima (λ_{max}), ground state dipole moments (μ_{gg}), static long axis components of the second-order polarizability (β_{xxx}), and product of the β_{xxx} components and the μ_x components calculated with the SOS and/or FF methods for dipolar chromophores **12** to **15**.

	E_{ge} (eV)	λ_{max} (nm)	μ_{gg} (D)	β_{xxx} (10^{-30} esu) SOS	β_{xxx} (10^{-30} esu) FF	β_{xxx} μ_x (10^{-48} esu) SOS
12	2.29	542	11.3	496	506	4559
13	2.23	557	10.4	463	477	3877
14	2.08	596	8.6	696	663	5640
15	2.24	553	8.0	586	562	4336
14	***2.08***	***596***	***8.6***	***696***	***663***	***5640***

For all the dipolar chromophores, the trends and magnitudes obtained for the β_{xxx} components from the SOS method are consistent with those obtained with the FF method.

The β_{xxx} components of **14** and **15**, in which the thiazole bridging unit is inserted into the π-bridge, are higher (β_{xxx} (**14**) = 663×10^{-30} esu and β_{xxx} (**15**) = 562×10^{-30} esu) than when a thiophene bridging unit is inserted (β_{xxx} (**12**) = 506×10^{-30} esu and β_{xxx} (**13**) = 477×10^{-30} esu). Interestingly, the position of the thiophene bridging unit has almost no effect, while the β_{xxx} component is nearly 20% higher when the thiazole bridging unit is next to the acceptor group than when it is closer to the donor group. A conformational origin for these differences is excluded because the same behavior is observed when the π-bridge of these dipolar chromophores is constrained to remain fully coplanar.

In order to understand the molecular origin of the trends observed for the β_{xxx} components, the β-charges obtained from the FF method are plotted for **12** to **15** in Figure 21.

12

13

14

15

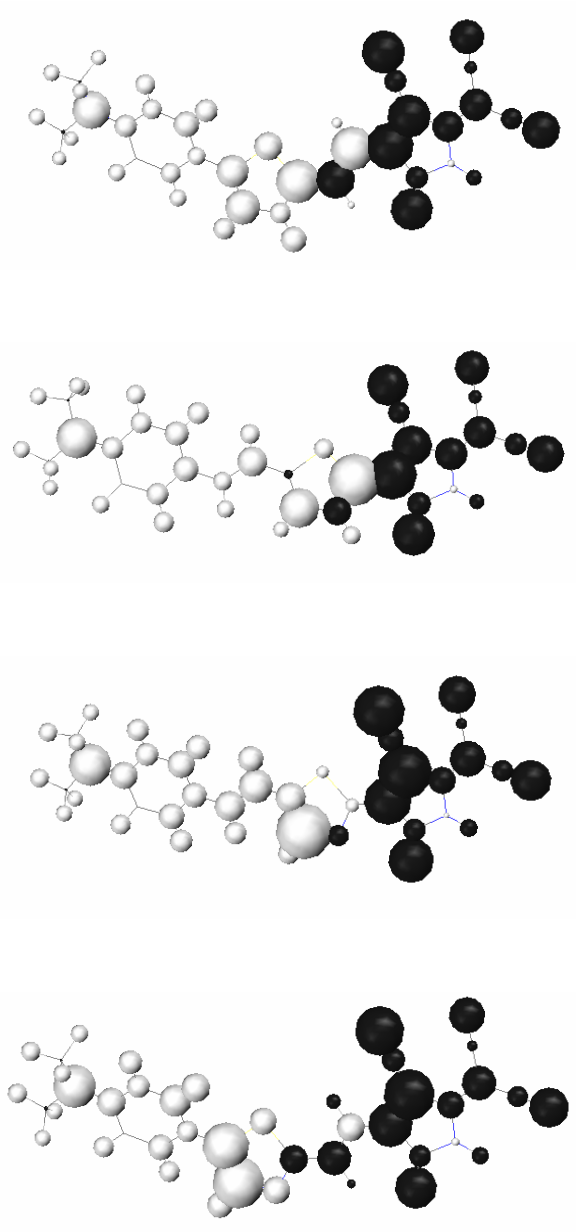

*<u>Figure 21:</u> Second derivatives of the atomic charge (β-charges) for dipolar chromophores **12** to **15** (from top to bottom). The circle size is proportional to the magnitude of the β-charge and the circle shading indicates its sign (positive β-charges are in black circles and negative ones in white).*

From the plots in Figure 21, two factors are seen to be responsible for the two- to nearly three-fold increase of the β_{xxx} component from **4** (TCP-based dipolar chromophore of chapter 4 section (4.1.) with β_{xxx} (**4**) = 255×10^{-30} esu) to **12**-**15**: (i) the magnitudes of the β-charges, in particular in the acceptor group, are much larger in **12**-**15**; and (ii) due to the greater length of the dipolar chromophores, the corresponding β-moments are further increased. Point (i) is, at least partly, explained by the observation that the β-charges on the auxiliary donor and acceptor are mostly negative and relatively large. Invoking the rule that the sum over all β-charges of the dipolar chromophore must be zero, this paves the way for larger positive β-charges on the main acceptor group. Comparing the two dipolar chromophores containing a thiophene π-bridge (**12** and **13**), very similar β-charge patterns are found, which is consistent with the nearly identical β_{xxx} components. In contrast to **14** and **15**, especially in **14**, both the negative β-charges along the π-bridge and the positive β-charges of the acceptor group are significantly increased, which gives rise to the larger β_{xxx} component of **14**.

In summary, the Sum-Over-States (SOS) and Finite-Field (FF) methods have been carried out in order to evaluate the second-order polarizability of dipolar chromophores, for which auxiliary donor (thiophene) and acceptor (thiazole) are incorporated into the π-bridge. This insertion yields higher second-order polarizabilities than TCP-based dipolar chromophore whose π-bridge is a simple vinylene unit; however, the position of the thiophene and thiazole affects it in a different way (the position of the thiophene has almost no effect, while the second-order polarizability is nearly 20% higher when the thiazole is next to the acceptor group than when it is closer to the donor group).

3.5. EFFECT ON SECOND-ORDER POLARIZABILITY OF NATURE OF π-BRIDGE OF DIPOLAR CHROMOPHORES – INSERTION OF TWO AUXILIARY DONORS AND/OR ACCEPTORS

In Ref. {52}, Breitung *et al.* have also systematically investigated by quantum-chemical computational calculations the effect on β of the order in which the auxiliary donor (thiophene bridging unit) and acceptor (thiazole bridging unit) are inserted into the π-bridge of dipolar chromophores. The two main observations were that:

- the magnitude of the increase in the β value depends substantially on the regiochemistry of the thiazole bridging unit;
- the large β values of matched A'–matched A' exceeds those of D'–matched A' analogues, which, in turn, exceed those of D'– D' analogues.

Breitung's work extends to more complex dipolar chromophores using modified donor and acceptor groups and more extended π-bridges, to develop new guidelines for the rational design of new efficient NLO chromophores; the dipolar chromophores investigated in this chapter are grouped into three series: chromophores **1** to **8** (Figure 22), are related to Breitung's dipolar chromophores, but differ from them in having different donor (4-(dimethylamino)-phenyl) and acceptor (TCF) groups, and a more extended π-bridge. The present donor group has the advantage of increasing the overall stability compared to a mere dimethylamine, while the present acceptor group holds the promise of decreasing the electrostatic interactions among dipolar chromophores in a polymer host. The insertion of auxiliary donor and acceptor into the π-bridge leads to four possible structural motifs: D–D'–A'–A (**1** and **6**), D–A'–A'–A (**2** and **8**), D–D'–D'–A

(**3**), D–A'–D'–A (**4** and **7**). The difference between **1** and **6**, **2** and **8**, and **4** and **7** stems from the position of the nitrogen atom in the thiazole bridging unit ("matched" vs. "mismatched) (**5**, in which the thiophene bridging unit of **3** is replaced by a dialkoxy thiophene is also considered).

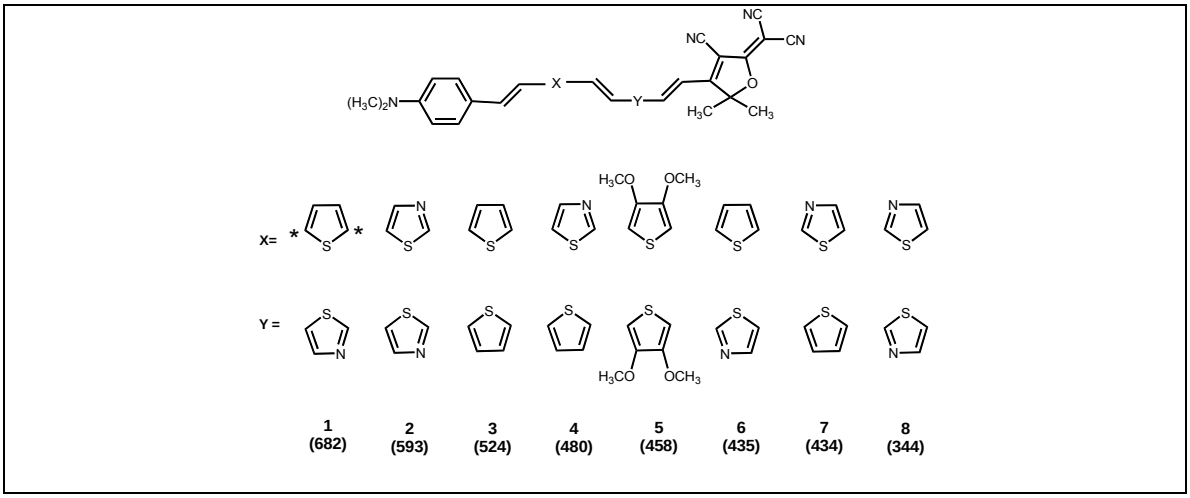

*Figure 22: Chemical structures for dipolar chromophores **1** to **8** (the points of attachment of the auxiliary donors and acceptors are shown by the two stars and remain the same for all dipolar chromophores; the β_{xxx} components obtained with the SOS method are reported in brackets).*

As, depending on the order of the auxiliary donor and acceptor, in certain cases, a significant increase of the β value is observed in the dipolar chromophores investigated by Breitung compared to those presented in this chapter, chromophores **9** to **16** (Figure 23), are then considered: we start from the strongest and weakest dipolar chromophores from Breitung's work (**9** and **13** respectively) and in several steps (**9** to **16**) alter the chemical structure of these dipolar chromophores to finally arrive at **1** to **8**.

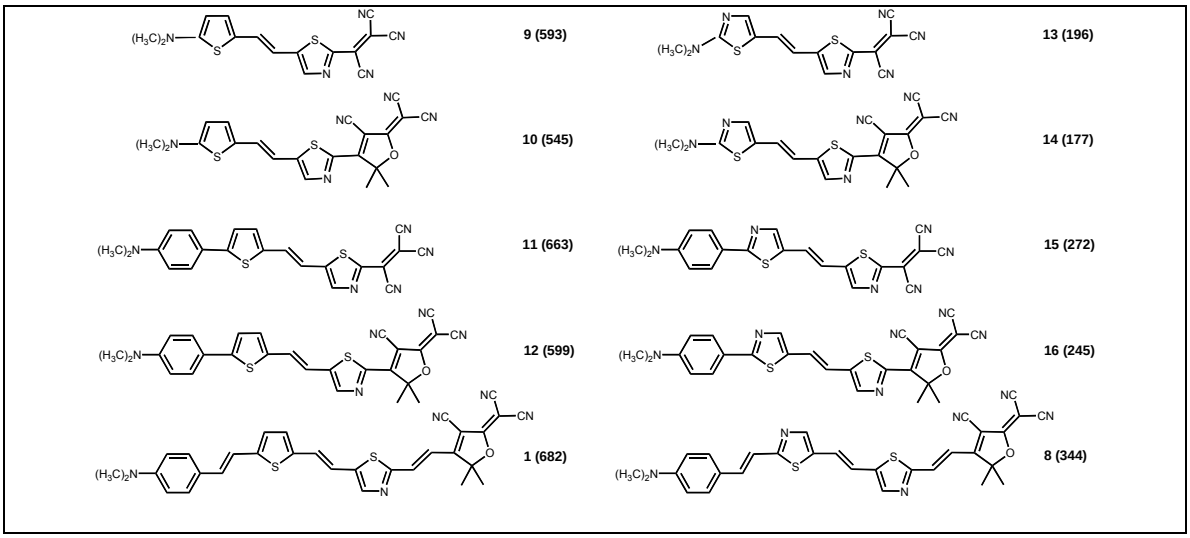

*<u>Figure 23:</u> Chemical structures for dipolar chromophores **9** to **16** (the β_{xxx} components obtained with the SOS method are reported in brackets).*

Additionally, the effect on β of the length of the π-bridge is investigated considering chromophores **17** to **22** (Figure 24). They are characterized by a varying number of vinylene units and/or different positions of the vinylene units relative to the auxiliary donor and acceptor. As far as their order is concerned, **17**-**22** are restricted to the D'–matched A' structural motif, which yields the highest β value among **1**-**8**.

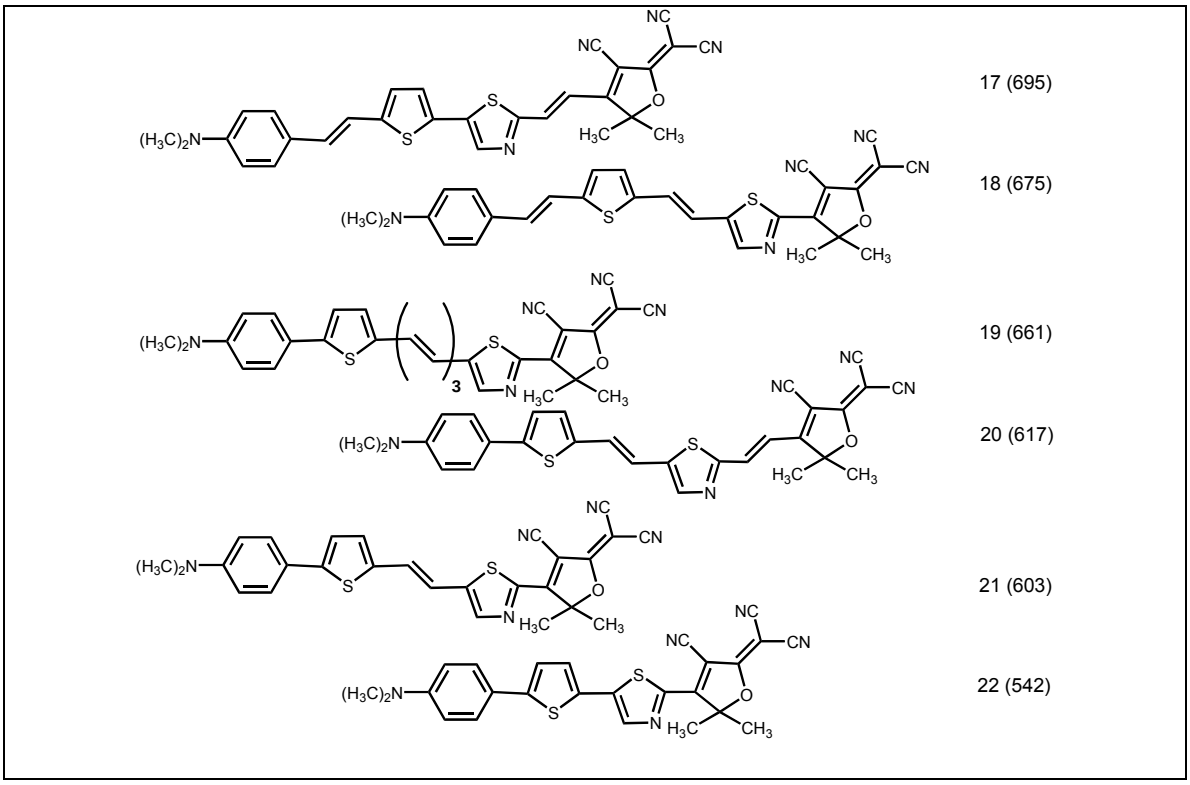

*<u>Figure 24:</u> Chemical structures for dipolar chromophores **17** to **22** (the β_{xxx} components obtained with the SOS method are reported in brackets).*

As in part I, the magnitudes of β are not reproduced for **9** and **13** (where our choice of dipolar chromophores overlaps with Breitung's); again, the main reason for the discrepancy appears to be a different definition of the β value (Taylor vs. Power series). The theoretical transition energies (E_{ge}), optical absorption maxima ($\lambda_{\max}$), ground state dipole moments (μ_{gg}), long axis components of the second-order polarizability (β_{xxx}), and product of the β_{xxx} components and the μ_x components calculated with the SOS method are reported for **1** to **8**, **9** to **16**, and **17** to **22** in Tables 10, 11, and 12 respectively.

Table 10: Theoretical transition energies (E_{ge}), optical absorption maxima (λ_{max}), ground state dipole moments (μ_{gg}), static long axis components of the second-order polarizability (β_{xxx}), and product of the β_{xxx} components and the μ_x components calculated with the SOS and/or FF methods for dipolar chromophores **1** to **8**.

	E_{ge} (eV)	λ_{max} (nm)	μ_{gg} (D)	β_{xxx} (10^{-30} esu) SOS	β_{xxx} (10^{-30} esu) FF	$\beta_{xxx}\ \mu_x$ (10^{-48} esu) SOS
1	2.18	568	12.7	682	858	7953
2	2.25	551	13.4	593	691	6387
3	2.27	546	15.7	524	724	7025
4	2.31	536	16.7	480	610	6018
5	2.26	549	18.0	458	636	7148
6	2.31	536	15.1	435	657	6117
7	2.29	542	18.2	434	633	6390
8	2.34	529	17.4	344	561	5310
1	***2.18***	***568***	***12.7***	***682***	***858***	***7953***

Table 11: Theoretical transition energies (E_{ge}), optical absorption maxima (λ_{max}), ground state dipole moments (μ_{gg}), static long axis components of the second-order polarizability (β_{xxx}), and product of the β_{xxx} components and the μ_x components calculated with the SOS and/or FF methods for dipolar chromophores **9** to **16**.

	E_{ge} (eV)	λ_{max} (nm)	μ_{gg} (D)	β_{xxx} (10^{-30} esu) SOS	β_{xxx} (10^{-30} esu) FF	$\beta_{xxx}\ \mu_x$ (10^{-48} esu) SOS
9	2.15	577	10.9	593	519	6343
10	2.18	568	13.1	545	565	6623
11	2.15	575	10.3	663	653	6921
12	2.18	567	13.2	599	692	7432
13	2.50	496	11.0	196	217	2138
14	2.46	503	14.8	177	240	2231
15	2.44	509	12.3	272	345	3336
16	2.40	517	16.2	249	374	3543

Table 12: Theoretical transition energies (E_{ge}), optical absorption maxima (λ_{max}), ground state dipole moments (μ_{gg}), static long axis components of the second-order polarizability (β_{xxx}), and product of the β_{xxx} components and the μ_x components calculated with the SOS and/or FF methods for dipolar chromophores **17** to **22**.

	E_{ge} (eV)	λ_{max} (nm)	μ_{gg} (D)	β_{xxx} (10^{-30} esu) SOS	β_{xxx} (10^{-30} esu) FF	β_{xxx} μ_x (10^{-30} esu) SOS
17	2.17	570	12.9	695	843	8443
18	2.14	580	13.5	675	831	8618
19	2.21	562	13.0	661	840	7485
20	2.22	557	12.3	617	735	6981
21	2.18	567	13.3	603	696	7379
22	2.20	564	13.6	542	590	6919
17	***2.17***	***570***	***12.9***	***695***	***843***	***8443***

For all the dipolar chromophores, the trends and magnitudes obtained for the β_{xxx} component from the FF method are, in general, consistent with those obtained with the SOS method (except for **3** and **6** of series I).

Four main observations are made for **1** to **8**. Firstly, for **1** with a D'–matched A' structural motif, the highest β_{xxx} component is achieved (β_{xxx} (**1**) = 682×10^{-30} esu); it decreases by about 40%, when the auxiliary donor and acceptor are interchanged, matched A'–D' (β_{xxx}(**4**) = 480×10^{-30} esu). Secondly, the values for the β_{xxx} component are higher for D'–A', A'–A', and A'–D' when the thiazole bridging unit is in the matched case rather than mismatched (β_{xxx}(**1**) = 682×10^{-30} esu > β_{xxx}(**6**) = 435×10^{-30} esu for D'–A', β_{xxx}(**2**) = 593×10^{-30} esu > β_{xxx}(**8**) = 344×10^{-30} esu for A'–A', and β_{xxx}(**4**) = 480×10^{-30} esu > β_{xxx}(**7**) = 434×10^{-30} esu for A'–D'). Thirdly, the magnitude of the difference between the matched and mismatched cases depends on the positions of the auxiliary donor and acceptor in the π-bridge: the β_{xxx} component decreases by about 57%, 72%, and 10% in going from

1 to **6**, **2** to **8**, and **4** to **7**, respectively. Finally, the β_{xxx} component is only slightly affected when the thiophene bridging unit in **3** is replaced by the stronger dialkoxythiophene (β_{xxx}(**3**) = 524×10^{-30} esu vs β_{xxx}(**5**) = 458×10^{-30}).

In order to understand the molecular origin of the trends observed for the β_{xxx} components, the β-charges from the FF method are shown for **1**, **2**, **6**, and **8** in Figure 25.

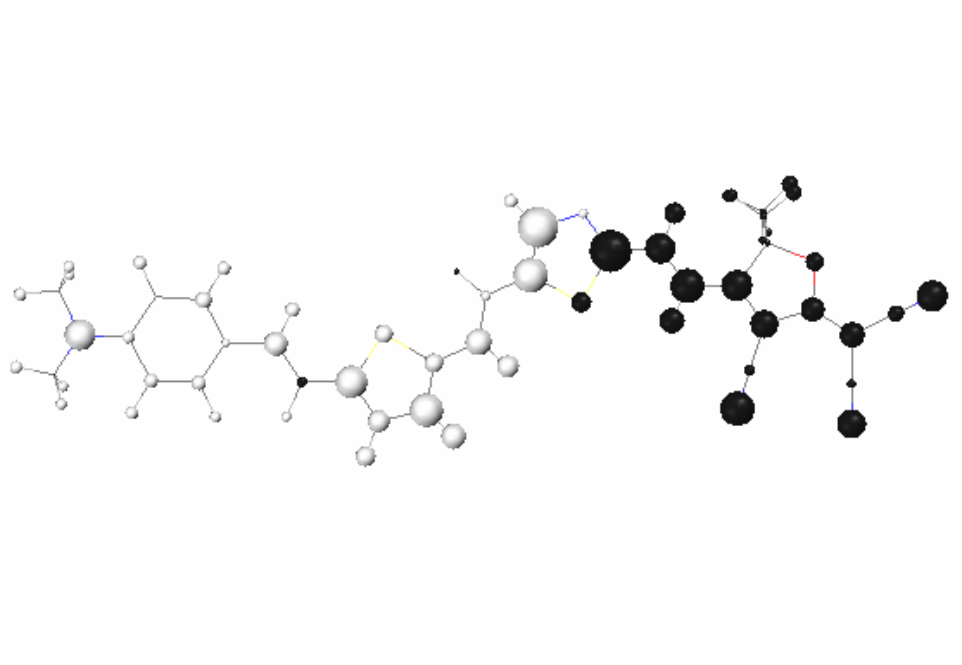

1

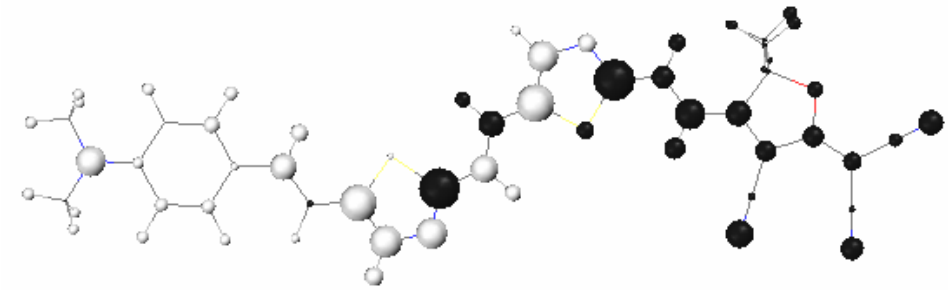

2

*<u>Figure 25:</u> Second derivatives of the atomic charge (β-charges) for dipolar chromophores **1**, **2**, **6**, and **8**. The circle size is proportional to the magnitude of the β-charge and the circle shading indicates its sign (positive β-charges are in black circles and negative ones in white).*

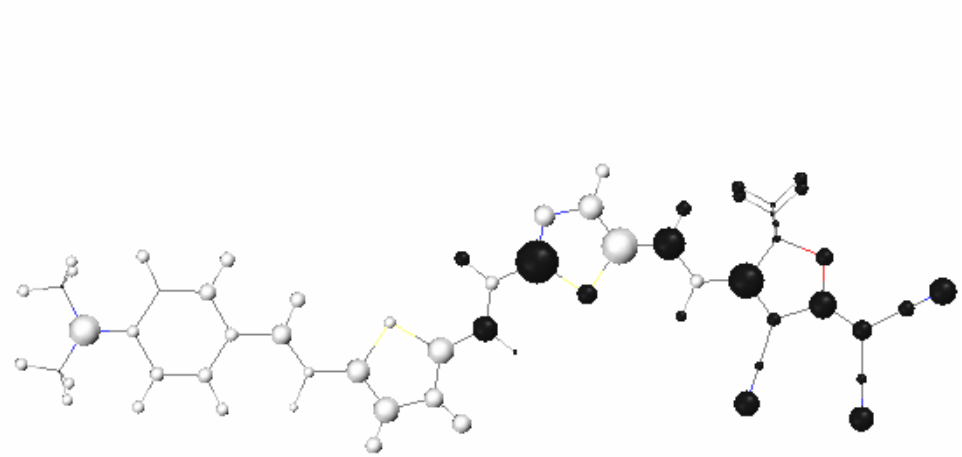

6

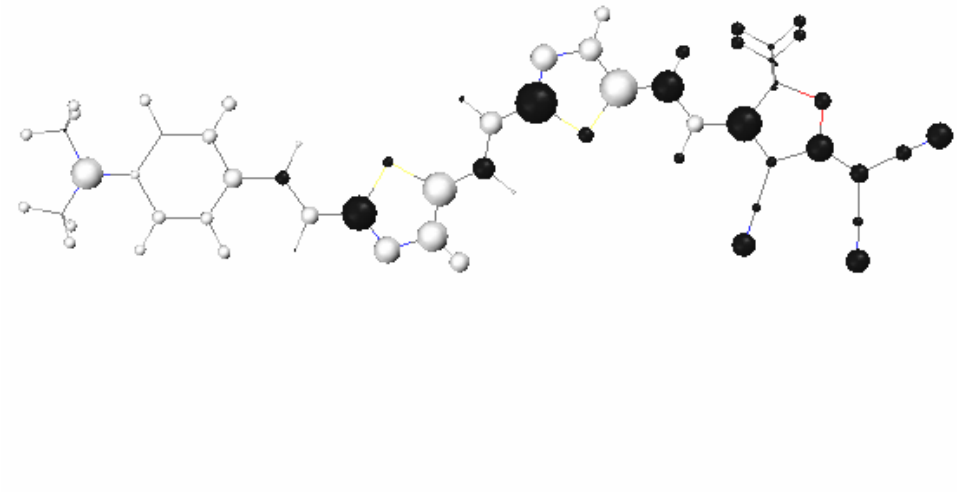

8

Figure 25: continued.

When comparing the plots for **1** and **6**, the influence of the matched vs. mismatched case of the thiazole bridging unit next to the acceptor group becomes obvious: In **1**, the ideal situation is encountered because all the β-charges being positive (black circles) are

on the acceptor group of the dipolar chromophore, while they are all negative (white circles) on the donor group. In contrast, when switching the thiazole bridging unit to the mismatched case (**6**), the distribution of the β-charges is also reversed; this results in partial cancellations of the associated β-moments in the summation. Moreover, the magnitudes of the β-charges on each atom are bigger in **1** than in **6**. In **2**, the β-charges on the thiazole bridging unit in the matched case next to the acceptor group are distributed properly; in this dipolar chromophore, however, the advantageous pattern of the β-charges seen in **1** is disturbed by the thiazole bridging unit next to the donor group. All unfavorable effects discussed above come together for the mismatched A'-mismatched A' structural motif in **8**, where the negative effect of the thiazole bridging unit next to the donor group is even enhanced by its orientation.

Although the trend in the β_{xxx} component is the same in **1** to **8** and in Breitung's dipolar chromophores, the magnitude by which the β_{xxx} component varies is different (independent of the methodological issues discussed above). The effect is most pronounced when comparing **1** (β_{xxx}(**1**) = 682×10^{-30} esu) and **8** (β_{xxx}(**8**) = 344×10^{-30} esu) with their Breitung equivalents **9** (β_{xxx}(**9**) = 593×10^{-30} esu) and **13** (β_{xxx}(**13**) = 196×10^{-30} esu). While the β_{xxx} component decreases only by a factor of 2 from **1** to **8**, it shows a three-fold decrease from **9** to **13**. At this point, the question arises as to which of the structural segments by which our dipolar chromophores differ from the Breitung's ones is responsible for this observation. In order to answer this question, the chemical structures of **9** and **13** are modified in several steps to reach **1** and **8**, yielding series II in Figure 22. When the acceptor group is changed from the TCV to the TCF, the β_{xxx} component does not significantly change; in fact it even slightly decreases. However, when the

donor group is changed from the dimethylamine to the 4-(dimethylamino)-phenyl, when extending the π-bridge by a phenylene bridging unit, the β_{xxx} component changes by 39 % (41%) when going from **13** (**14**) to **15** (**16**), while it increases by only 12% (10%) from **9** (**10**) to **11** (**12**). Finally, the β_{xxx} component is more significantly affected for mismatched A'–mismatched A' than for D'–matched A' when the number of vinylene units is increased (14% from **12** to **1** vs. 38% from **16** to **8**). Consequently, the β_{xxx} component increases by only 15% for D'–matched A' when different donor and acceptor groups and more extended π-bridge are considered; while the increase is 75% for the mismatched A'-mismatched A'. The increase of the length of the π-bridge, which appears to be the main reason for the increased of the β_{xxx} component in our dipolar chromophores, affects the β_{xxx} component of the mismatched A'-mismatched A' much more profoundly than the "ideal" D'–matched A'. However, although the increase in the β_{xxx} component is only 15% for the ideal D'–matched A' (**1**) relative to Breitung's dipolar chromophore (**9**), **1** offers additional advantages over **9**; In particular the TCF allows for the linkage of bulky substituents to the CH_3 groups (particularly important for the fabrication of commercial devices, as it helps in preventing the formation of large electrostatic interactions typical of planar dipolar chromophores).

Also for the Breitung's dipolar chromophores, **9** and **13**, additional insight are obtained from the plots of the β-charges in Figure 26.

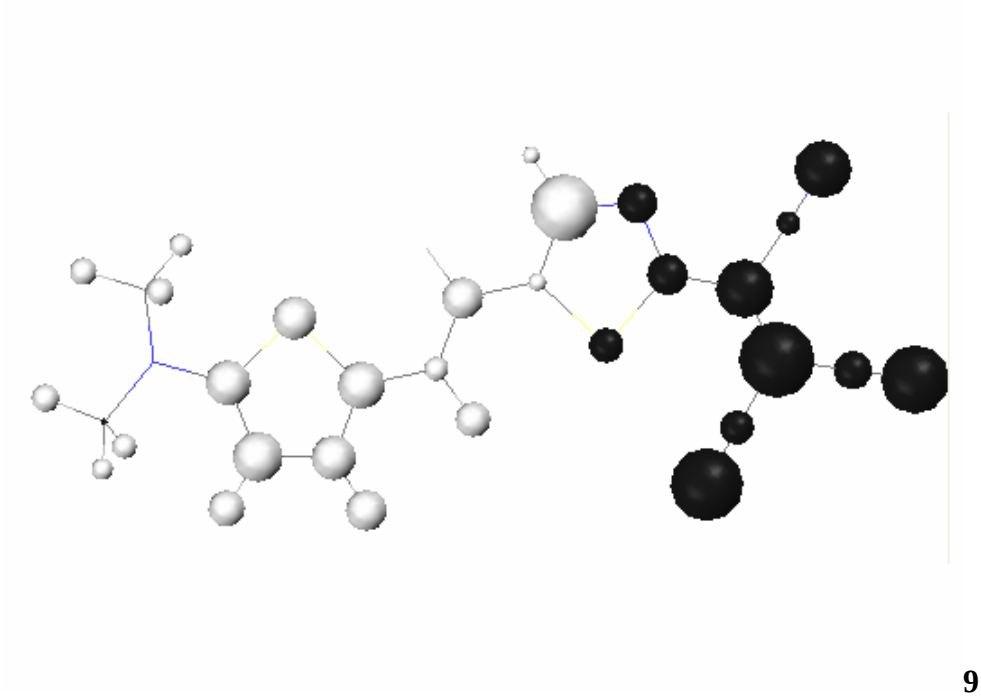

9

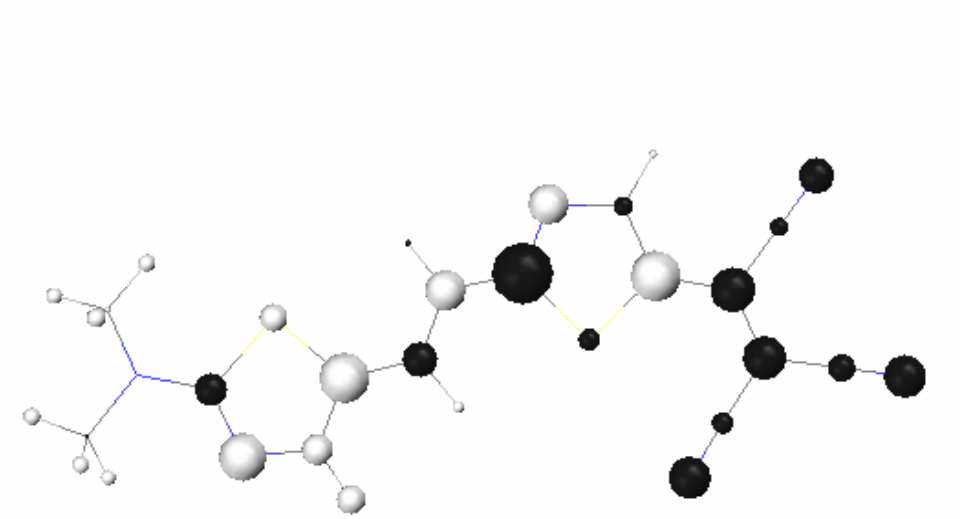

13

*<u>Figure 26:</u> Second derivatives of the atomic charge (β-charges) for dipolar chromophores **9** and **13**. The circle size is proportional to the magnitude of the β-charge and the circle shading indicates its sign (positive β-charges are in black circles and negative ones in white).*

The large β_{xxx} component of **9** is rationalized by the fact that the β-charges on the donor and acceptor groups are significantly larger than in **1**; this compensates for the reduced length of the π-bridge. As far as **13** is concerned, the distribution of the β-charges along the π-bridge is strongly reminiscent of the situation in **8**. However, the smaller size of the donor and acceptor groups together with the strongly reduced β-charges on those groups (compared to **9**), result in a much stronger decrease in β_{xxx} component for the mismatched A'-mismatched A' in the Breitung's dipolar chromophores.

For zero, one, and two vinylene units in the π-bridge (i.e., going from **22** to **21** to **17**), a continuous increase in the β_{xxx} component with the length is observed. Again, the β-charges (in Figure 27) are useful for rationalizing this trend.

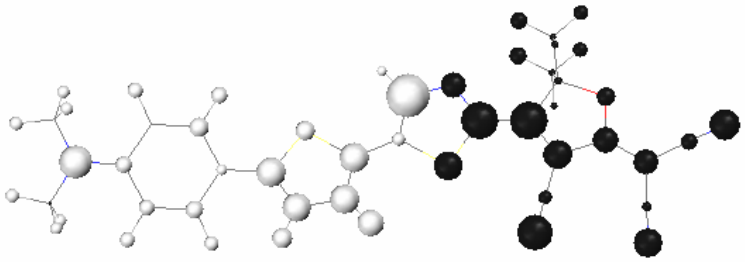

22

*<u>Figure 27:</u> Second derivatives of the atomic charge (β-charges) for dipolar chromophores **17**, **21**, and **22**. The circle size is proportional to the magnitude of the β-charge and the circle shading indicates its sign (positive β-charges are in black circles and negative ones in white).*

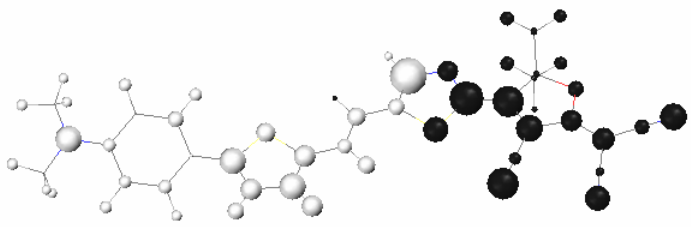

21

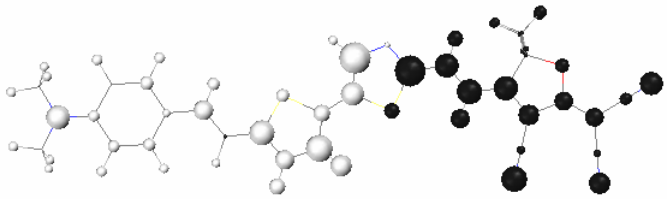

17

Figure 27: continued.

Independently of the length of the π-bridge, a favorable β-charge pattern is preserved with all positive (negative) β-charges close to the acceptor (donor) groups of the dipolar chromophores. Moreover, the change in magnitude of the β-charges remains small when the number of vinylene units increases. In combination with the elongation of the π-bridge, this results in an increase of the β-moments and thus the β_{xxx} components. This trend is further enhanced by favorable β-charges on the vinylene unit connecting the thiazole bridging unit and the acceptor group in **1**.

The fact that the β_{xxx} component for **17** with two vinylene units is already in the same range as for the dipolar chromophores with three vinylene units (**1** and **19**) suggests that the β_{xxx} component saturates with chain length of the π-bridge. This is a positive finding in terms of overall stability since extended polyenes suffer from chemical and thermal instabilities. However, dipolar chromophores with directly linked thiazole bridging unit and acceptor group are likely to present considerably synthetic challenges.

Whenever the thiophene bridging unit is adjacent to the donor group (specifically the phenylene bridging unit) (i.e., in **19**, **20**, **21**, and **22**), a twist of about 25° between those bridging units is observed, which reduces the effective conjugation. This, for example, explains why the β_{xxx} component is slightly smaller in **19** than in **1**. In fact, when considering a planar conformation of **19**, its β_{xxx} component approaches that of **1** (SOS: $\beta_{xxx}=678\times10^{-30}$ esu; FF: $\beta_{xxx}=867\times10^{-30}$ esu). For the dipolar chromophores with two vinylene units (**17**, **18**, and **20**), a stronger dependence of the β_{xxx} component is found on the actual positions of the vinylene units. In part, this is again explained by the twist, i.e., the β_{xxx} component in **20** increases upon planarization (SOS: $\beta_{xxx}=645\times10^{-30}$ esu; FF: $\beta_{xxx}=772\times10^{-30}$ esu).

In summary, the Sum-Over-States (SOS) and Finite-Field (FF) calculations have been carried out in order to evaluate the second-order molecular polarizabilities of dipolar chromophores incorporating auxiliary electron-rich (D'), thiophene, and electron-poor (A'), thiazole, into the π-bridge between the 4-(dimethylamino)-phenyl donor (D) group, and the TCF acceptor (A) group. The second-order polarizability strongly depends on the order in which D' and A' are inserted into the π-bridge as well as on the

regiochemistry of the nitrogen atom in the thiazole. The largest second-order polarizabilities are obtained for a D'-matched A' structural motif, while it is by a factor of nearly two smaller in the mismatched A'-mismatched A' one. While the trends are consistent with those found by Breitung et al. [52] for smaller chromophores, the magnitudes of the changes are strongly amplified in the present chromophores. These findings are rationalized using the FF method in the local contribution version. Studying the dependence of the second-order polarizability as a function of the number and position of vinylene units inserted between the D, D', A', and A, an increase of the second-order polarizability is observed when going from zero to one and eventually to two vinylene units. This trend is again understood with the FF method in the local contribution version.

CHAPTER 4 THIRD-ORDER NONLINEAR OPTICAL DIPOLAR AND QUADRUPOLAR CHROMOPHORES

Two-photon absorbing chromophores are used in applications such as limiting optical power, upconverted lasing, three-dimensional fluorescence microcopy and microfabrication, two-photon photodynamic cancer therapy, or biological caging [15]. This has stimulated research on the rational design, organic synthesis, and optical characterization of new efficient chromophores with large two-photon absorption (2PA) cross-sections (δ); δ is the parameter characterizing the ability of a chromophore to absorb simultaneously two photons of the same energies (degenerate 2PA) or of different energies (non-degenerate 2PA). There is still a need to develop a better understanding of structure-property relationships in order to establish new guidelines for the rational design of new efficient two-photon absorbing chromophores, whereby δ is systematically increased (the position of the 2PA peak can be tuned), and wherein an improved δ is adequately combined with other molecular properties (for example, large fluorescence quantum yield, efficient intersystem crossing), that make those two-photon absorbing chromophores suitable for given applications.

Some strategies to rationally design chromophores with large δ have been previously reported [56]. One of them has involved symmetrically substituted chromophores with the D-π-D structural motif (donor-(π-bridge)-donor). Experimental and theoretical evidence have shown that D-π-D chromophores can have large δ, more than one order of magnitude larger than the corresponding unsubstituted chromophores. This enhancement in δ can be correlated with the intramolecular charge transfer from the

donor groups to the π-bridge. The magnitude of δ can be controlled through a structural modification of the chromophore in such a way as to affect the amount of intramolecular charge transfer. Two other strategies to rationally design chromophores with larger δ have involved the increase of the length of the π-bridge (since the charge can be transferred over a longer distance) and the attachment of acceptor groups as side groups to the π-bridge, to form chromophores with the D-π-A-π-D structural motif (wherein the amount of charge transfer can be increased). Experimental and theoretical evidence have shown that the A-π-D-π-A chromophores can also have large δ. Thus, the charge transfer is effective in enhancing δ irrespective of the direction of the charge transfer (from the ends to the center and from the center to the ends of the chromophores).

Over the past decades, with the aim to rationally design two-photon absorbing chromophores with large δ, various classes of chromophores have been investigated, including quasi-linear D-A-D or A-D-A quadrupolar chromophores incorporating a variety of π-bridges [57], bifluorene and oligofluorene systems [58], dipolar chromophores [59], octupolar chromophores [60], multibranched systems [60], dendrimer systems [61], and porphyrins [62].

4.1. TWO-PHOTON ABSORPTION AT TELECOMMUNICATION WAVELENGTH OF DIPOLAR CHROMOPHORES

A few studies have included chromophores with 2PA peaks extending into the near infra-red (NIR) telecommunication wavelength range (1300-1550 nm) [{63}]. However, to the best of our knowledge and prior to our collaborative work [{6}] with the Marder group at the Georgia Institute of Technology, there have been no measurements of 2PA peaks into the NIR range. While, in principle, chromophores with strong 2PA peaks in this NIR range can be achieved using quadrupolar chromophores, dipolar ones possess some attractive features: (i) appropriate donor and acceptor substitution can lead to relatively low-lying charge transfer one-photon absorption (1PA); (ii) whereas in quadrupolar chromophores the mutually exclusive selection rules for 1PA and 2PA mean that the 2PA peak is typically at a photon energy greater than that corresponding to half the energy of the 1PA peak, in dipolar chromophores the 2PA peak can be anticipated at half the photon energy of the 1PA peak.

Dipolar chromophores containing auxiliary donor (D') and acceptor (A') along the π-bridge between the donor (D) and acceptor (A) groups have previously been studied as second-order NLO chromophores (see chapter 3). In this chapter, three new examples **1** to **3**, whose chemical structures are presented in Figure 28, are synthesized incorporating the pyrrole as an auxiliary donor and the thiazole as an auxiliary acceptor, which has been previously reported to be effective in this role [{64}]. As the acceptor groups, the strong SDS and TCF are used, while the 4-(dibutylamino)-phenly is used as the donor group.

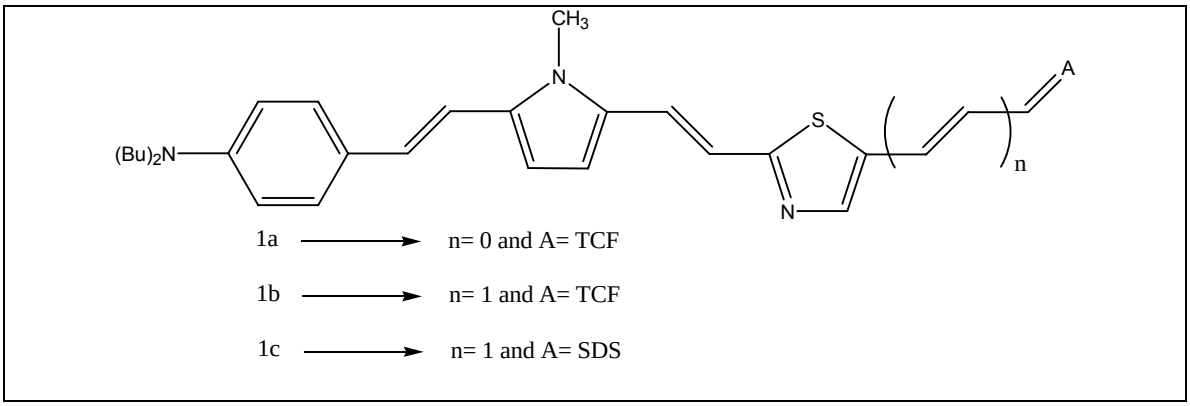

*<u>Figure 28:</u> Chemical structures of dipolar chromophores **1** to **3** (1a, 1b, and 1c of the Figure correspond to **1**, **2**, and **3** respectively).*

The experimental 1PA spectra of **1** to **3** are presented in Figure 29; while the experimental 2PA spectrum of **1**, acquired using a pump-probe technique (a 100 fs white-light continuum source as a probe and a wavelength of 1800 nm as a pump) is presented in Figure 30 [{6}].

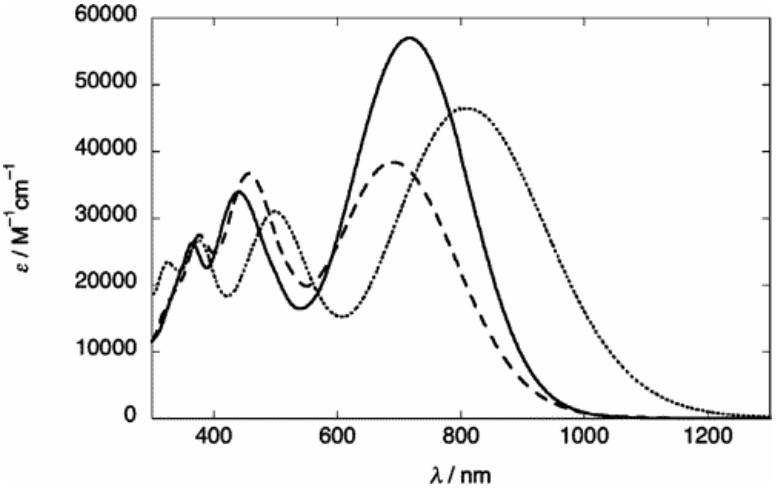

*Figure 29: Experimental 1PA spectra in THF for dipolar chromophores **1** (solid line), **2** (dashed line), and **3** (doted line).*

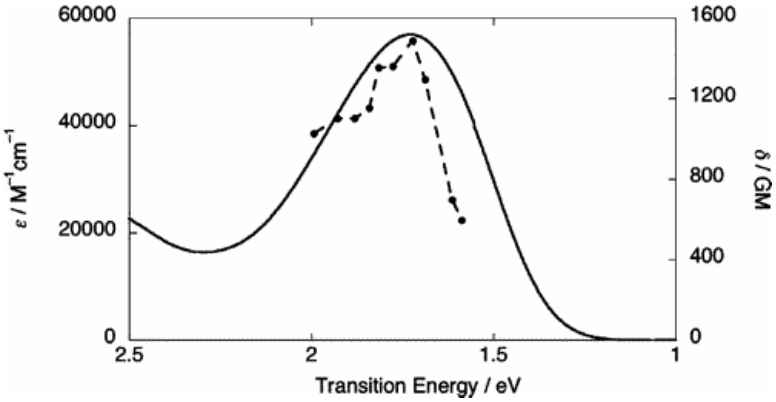

*Figure 30: Experimental 1PA (solid line) and non-degenerate 2PA (broken line) spectra in THF for dipolar chromophore **1**.*

Interestingly, the increase in length of the π-bridge from **1** to **2** results in a slight blue-shift of the main charge transfer transition, together with a decrease in the transition dipole moment term (M_{ge}), whereas a red-shift has been seen with the increase in

length of the π-bridge in many other dipolar chromophores. The origin of this effect is unclear, but the blue-shift is reproduced qualitatively by the computational calculations (see Table 13: E_{ge} (**1**) = 2.43 eV < E_{ge} (**2**) = 2.47 eV).

Although, as expected for a dipolar chromophore, 1PA and 2PA spectra access the same electronic excited state, δ of about 1500 GM is unprecedented for dipolar chromophores, which often display δ ranging from tens to a few hundreds GM, and is similar magnitude to that of some of the most effective 2PA dyes known.

It is important to note that δ obtained using the probe-pump technique refers to a non-degenerate 2PA ($\delta_{non-\deg}$), which, due to pre-resonance enhancement effects, is anticipated to be slightly larger than δ for a degenerate 2PA ($\delta_{\deg}$). Highly correlated quantum-chemical computational calculations are performed to gain insight into the relative magnitudes of the $\delta_{non-\deg}$ and the $\delta_{\deg}$ for **1**; these values are reported in Table 13 along with some electronic terms of interest.

Table 13: Theoretical $\delta_{non-\deg}$, $\delta_{\deg}$, transition energies (E_{ge}), transition dipole moments (M_{ge}), changes in state dipole moment ($\Delta\mu_{eg}$) calculated with the SOS method for dipolar chromophores **1** to **3**.

	E_{ge} (eV)	M_{ge} (D)	$\Delta\mu_{eg}$ (D)	$\delta_{\deg}$ (GM)	$\delta_{non-\deg}$ (GM)
1	2.43	15.2	15.1	752	1224
2	2.47	16.2	17.7	1070	1888
3	2.36	14.0	18.5	904	1113
2	***2.47***	***16.2***	***17.7***	***1070***	***1888***

To a first approximation, within the few-term model, the large transition dipole moment and change in state dipole moment terms associated with the $S_0 - S_1$ transition are held responsible for the large $\delta_{non-\deg}$. The results also show significant differences between $\delta_{non-\deg}$ and $\delta_{\deg}$; the computational calculations clearly indicate that $\delta_{\deg}$ into S_1 in these dipolar chromophores is anticipated to be large. The difference between $\delta_{non-\deg}$ and $\delta_{\deg}$ is smaller in **3** because it has the smallest transition energy, resulting in reduced pre-resonance enhancement effect.

In summary, the D-D'-A'-A dipolar chromophores can act as an efficient 2PA dye in the NIR telecommunication wavelength range (where it finds applications for limiting optical power), and as an efficient 2PA sensitizer for photorefractive composites.

4.2. EFFECT ON TWO-PHOTON ABSORPTION CROSS-SECTION OF NATURE OF π-BRIDGE OF DIPOLAR CHROMOPHORES

Based on the previous observations of strong 2PA in D-D'-A'-A chromophores (see chapter 4), a systematic investigation of the effect on δ of the nature of the π-bridge is of interest in this chapter, i.e. the order in which the auxiliary donor and acceptor are inserted into the π-bridge. Chromophores **1** to **8** , whose chemical structures are presented in Figure 31, are considered since the insertion of auxiliary donor and acceptor into the π-bridge lead to four possible structural motifs: D – D' – A' - A (**1** and **6**), D – D' – D' – A (**2**), D – A' – D' – A (**3** and **7**), D – A' – A' – A (**5** and **8**). The difference between **1** and **6**, **3** and **7**, and **5** and **8** stems from the position of the nitrogen atom in the thiazole bridging unit, whose effect on δ is investigated, since it has previously shown to affect β. For **1** to **8**, the donor and acceptor groups are the 4-(dimethylamino)-phenyl and the TCF, respectively Also, chromophore **4**, for which the thiophene bridging unit in **2** is replaced by another auxiliary donor, dialkoxythiophene, is considered.

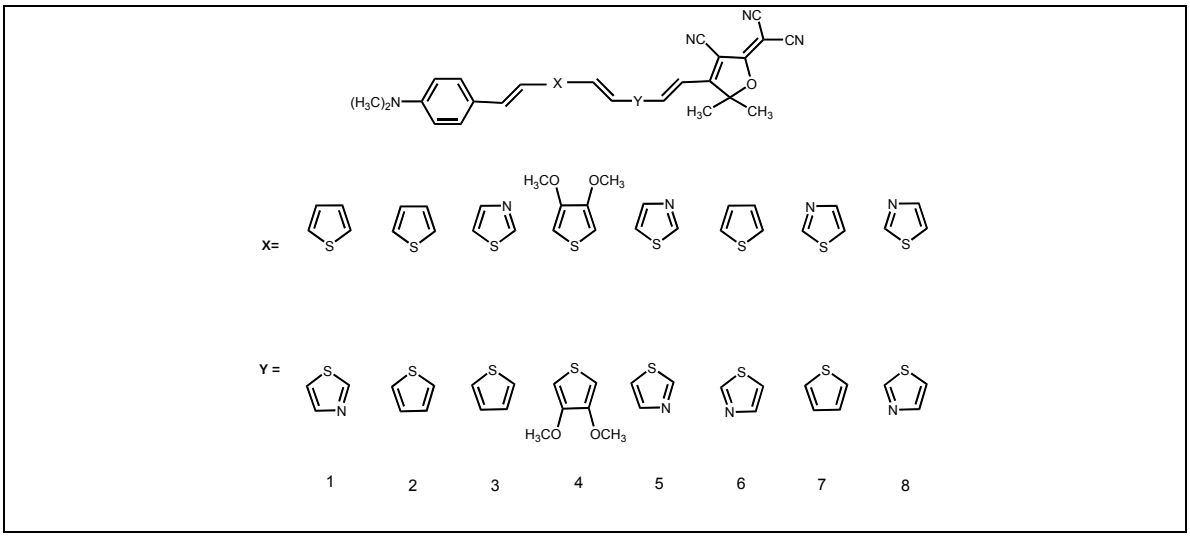

*Figure 31: Chemical structures of dipolar chromophores **1** to **8** (point of attachment of auxiliary donors and acceptors are the same as in Figure 22).*

Additionally, the effect on δ of the length of the π-bridge is investigated by considering chromophores **9** to **14** (Figure 32). They are characterized by a varying number of vinylene units and/or different positions of the vinylene units relative to the auxiliary donor and acceptor. As far as the order of the auxiliary donor and acceptor is concerned, **9**-**14** are restricted to the D–D'–A'–A structural motif, which yields the highest δ.

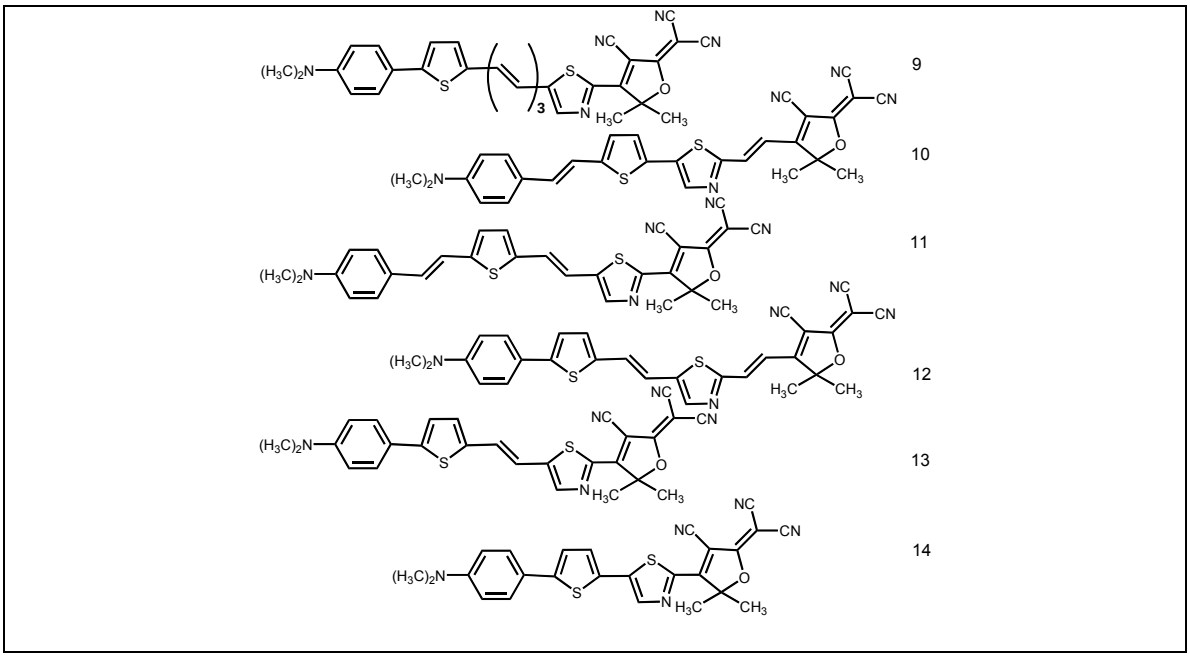

*<u>Figure 32:</u> Chemical structures of dipolar chromophores **9** to **14**.*

The theoretical 2PA spectra, which are reported for **1**, **3**, and **5**-**8** in Figure 33, consist of low-energy (calculated photon-energy range, 0.8 to 1.6 eV) feature with δ of a few thousand GM and much stronger values at higher energy (calculated photon-energy range, 1.6 to 2.2 eV). The low-energy feature is computationally calculated to arise from two 2PA transitions, the strongest one of which is into S_1 for **1** to **5** and into S_2 for **6** to **8**.

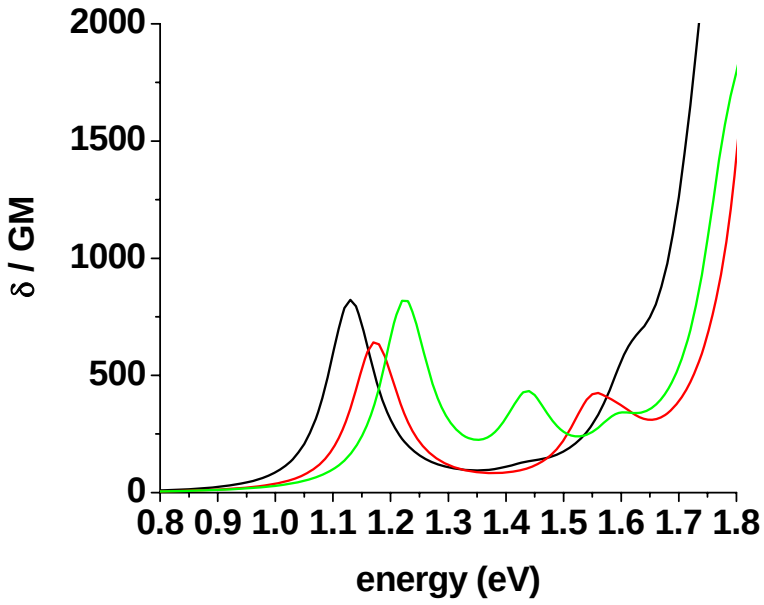

*Figure 33: Theoretical 2PA spectra for dipolar chromophores **1** (black line – top plot), **3** (red line – top plot), **5** (green line – top plot), which are the matched case, and **6** (black line – bottom plot), **7** (red line – bottom plot), **8** (green line – bottom plot), which are the mismatched case.*

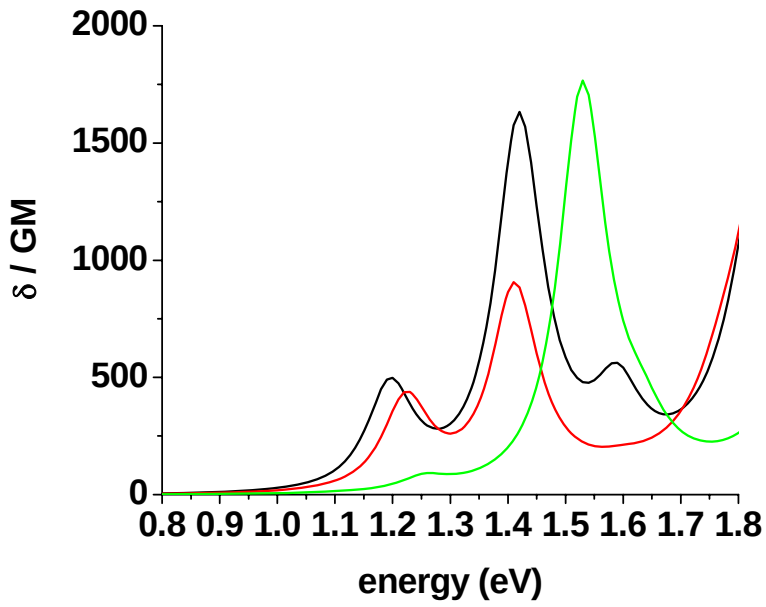

Figure 33: continued.

The theoretical δ for the 2PA into S_1 and S_2 are reported in the Table 14.

Table 14: Theoretical δ calculated with the SOS method for dipolar chromophores **1** to **14** for 2PA into S_1 and S_2 for dipolar chromophores **1** to **14**.

	δ (GM) – 2PA into S_1	δ (GM) – 2PA into S_2
1	830	29
2	828	321
3	817	341
4	699	326
5	648	298
6	451	1608
7	397	863
8	54	1767
9	870	99
10	806	21
11	780	11
12	674	44
13	603	35
14	460	31

In the calculated photon-energy range from 0.8 to 1.3 eV (2PA into S_1), δ is higher when the thiazole bridging unit is in the matched case rather than mismatched (δ (**1**) = 830 GM $>$ δ (**6**) = 451 GM, δ (**3**) = 817 $>$ GM δ (**7**) = 397 GM, δ (**5**) = 648 GM $>$ δ (**8**) = 54 GM). In addition, the difference between the matched and mismatched cases depends on the order in which the auxiliary donor and acceptor are inserted into the π-bridge, the difference being much larger for A' – A' (**5**). Also, for the matched case, δ only significantly changes for the A' – A' (**5**) compared to D' – A' (**1**), D' – D' (**2**), and A' – D' (**3**), which remain similar (δ (**1**) = 830 GM $\approx$ δ (**2**) = 828 GM $\approx$ δ (**3**) = 817 $>$ δ (**5**) = 648 GM).

However, in the calculated photon-energy range from 1.3 to 1.6 eV (2PA into S_2), one observes a somewhat different behavior. Firstly, δ is higher when the thiazole bridging unit is in the mismatched case rather than matched (δ (**1**) = 29 GM vs $<$ (**6**) = 1608 GM, δ (**3**) = 341 GM $<$ δ (**7**) = 863 GM, δ (**5**) = 298 GM $<$ δ (**8**) = 1767 GM). As with 2PA into S_1, the difference between the matched and mismatched cases depends on the order in which the auxiliary donor and acceptor are inserted into the π-bridge; however, in this case the difference is greatest for the D' – A' (**1**). Secondly, for the matched case, δ only significantly changes for D' – A' (**1**) while remaining similar for D' – D' (**2**), A' – D' (**3**), and A' – A' (**5**) (δ (**2**) = 321 GM $\approx$ δ (**3**) = 341 GM $\approx$ δ (**5**) = 298 $>$ δ (**1**) = 29 GM).

Thus, the order in which the auxiliary donor and acceptor are inserted into the π-bridge affects the energy and intensity of the 2PA peak (for instance, 2PA into S_1 (**1**) = 830 GM and into S_2 (**8**) = 1767 GM); and also, for the dipolar chromophores in the mismatched case, the 2PA (**6** to **8**) is stronger into S_2 than into S_1, whereas for **1** to **5**

(the matched case) S_1 is the more strongly absorbing of the two low-energy electronic excited states.

In order to gain further insight into structure-property relationships, the few-term models are often helpful. In general, while in the case of quadrupolar chromophores δ for a given electronic excited state is usually explained with a three-term model (T-term), in dipolar chromophores a two-term model (D-term) is usually used to explain δ. In cases where one or two electronic excited states dominate δ, they are used to identify the important electronic terms responsible for the trends in δ; however, in some cases, the few-term models are of limited use because too many electronic excited states are involved to directly identify their important features giving rise to δ. In order to investigate which electronic excited state dominates δ when the 2PA occurs into S_1 and into S_2 for **1** to **8**, convergence plots are plotted for **1** and **6** taken as illustrative examples to compare the matched and mismatched case in Figure 34. The theoretical δ into an electronic excited state |e'> are plotted versus the number of intermediate electronic excited states, |e>, included in the computational calculation. Each successive point corresponds to the inclusion of another channel for the 2PA; and therefore, the convergence plot enables one to determine which of these channels is most important in determining δ.

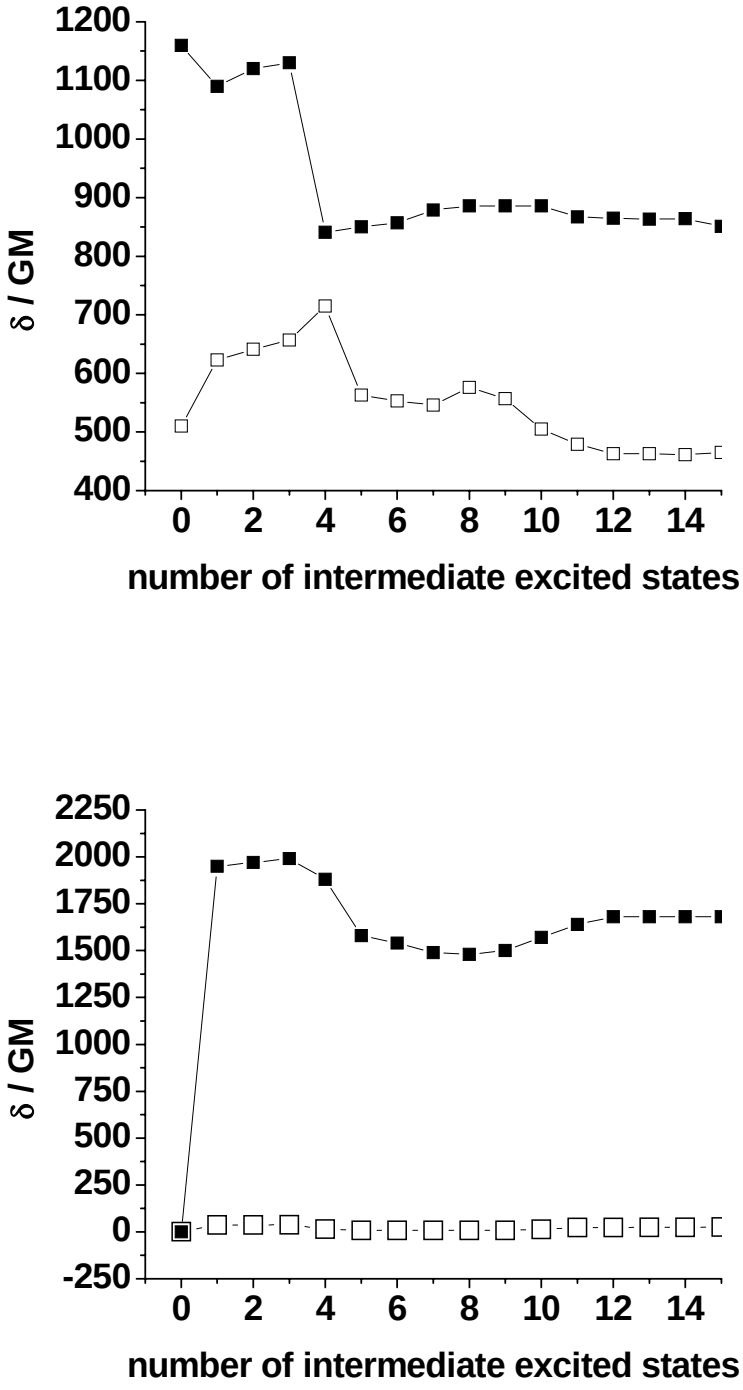

*<u>Figure 34:</u> Convergence plots for dipolar chromophores **1** (black square) and **6** (white square) for 2PA is into S_1 (top plot) and S_2 (bottom plot).*

In both **1** and **6**, the inclusion of more than 15 intermediate electronic excited states does not significantly affect δ (i.e. δ are essentially converged with inclusion of 15 intermediate electronic excited states). For the 2PA into S_1, significant δ are obtained with no intermediate electronic excited states, thus indicating that the 2PA peak is reasonably well-described using the D-term (this is not the case for **8**). In contrast, δ is close to zero for the 2PA into S_2 if no intermediate electronic excited state is included and essentially converged upon the inclusion of one more intermediate electronic excited state, thus indicating that the 2PA peak is well approximated by a T-term involving the S_1 state as an intermediate electronic excited state. Therefore, the two low-energy features are explained by different electronic terms, which are reported for **1** to **8** in Table 15.

Table 15: Theoretical transition energies (E_{ge} and $E_{ge'}$), transition dipole moments (M_{ge} and $M_{ee'}$), state dipole moments (μ_{gg} and μ_{ee}), and changes in state dipole moment ($\Delta\mu_{eg}$) calculated with the INDO/MRDCI method for dipolar chromophores **1** to **8**.

	E_{ge} (eV)	$E_{ge'}$ (eV)	M_{ge} (D)	$M_{ee'}$ (D)	μ_{gg} (D)	μ_{ee} (D)	$\Delta\mu_{eg}$ (D)
1	2.26	2.86	12.2	1.6	12.4	30.9	19.4
2	-	-	-	-	-	-	-
3	2.44	2.87	13.1	8.2	15.9	33.3	20.3
4	-	-	-	-	-	-	-
5	2.34	3.09	11.1	8.0	12.8	31.4	20.6
6	2.39	2.83	14.8	13.9	13.9	23.9	10.5
7	2.44	2.82	14.8	10.1	16.7	26.9	11.9
8	2.50	3.06	14.3	14.1	14.4	17.0	2.7

- not reported because not mentioned in the discussion

For 2PA into S_1, the electronic terms involved are M_{ge}, $\Delta\mu_{eg}$, and E_{ge} (those entering the D-term) and $\Delta\mu_{eg}$ is the term responsible for the higher δ for **1**, **3**, and **5** relative to **6**-**8**, respectively ($\Delta\mu_{eg}$ (**1**) = 19.4 D > $\Delta\mu_{eg}$ (**6**) = 10.5 D; $\Delta\mu_{eg}$ (**3**) = 20.3 D > $\Delta\mu_{eg}$ (**7**) = 11.9; and $\Delta\mu_{eg}$ (**5**) = 20.6 D > $\Delta\mu_{eg}$ (**8**) = 2.7 D). It is important to point out that the larger $\Delta\mu_{eg}$ for the dipolar chromophores in the matched case arises from the fact that the dipole moment of the electronic excited state |e> is much bigger for **1**, **3**, and **5** than for **6**-**8**; the ground state dipole moments are similar independently of the regiochemistry of the thiazole bridging unit. In contrast, for the 2PA into S_2, the electronic terms involved are M_{ge}, $M_{ee'}$, E_{ge}, and $E_{ge'}$ (those entering the T-term) and $M_{ee'}$ is the term responsible for the higher δ for **6**-**8**, relative to **1**, **3**, and **5**, respectively ($M_{ee'}$ (**1**) = 1.6 D < $M_{ee'}$ (**6**) = 13.9 D; $M_{ee'}$ (**3**) = 8.2 D < $M_{ee'}$ (**7**) = 10.1; and $M_{ee'}$ (**5**) = 8.0 D < $M_{ee'}$ (**8**) = 14.1 D).

As for **1** to **8**, the theoretical 2PA spectra, which are reported for **1** and **14** taken as illustrative example of **9** to **14** in Figure 35, consist of low-energy (calculated photon-energy range, 0.8 to 1.6 eV) feature with δ < 1000 GM and a much stronger value at higher energy (calculated photon-energy range, 1.6 to 2.2 eV).

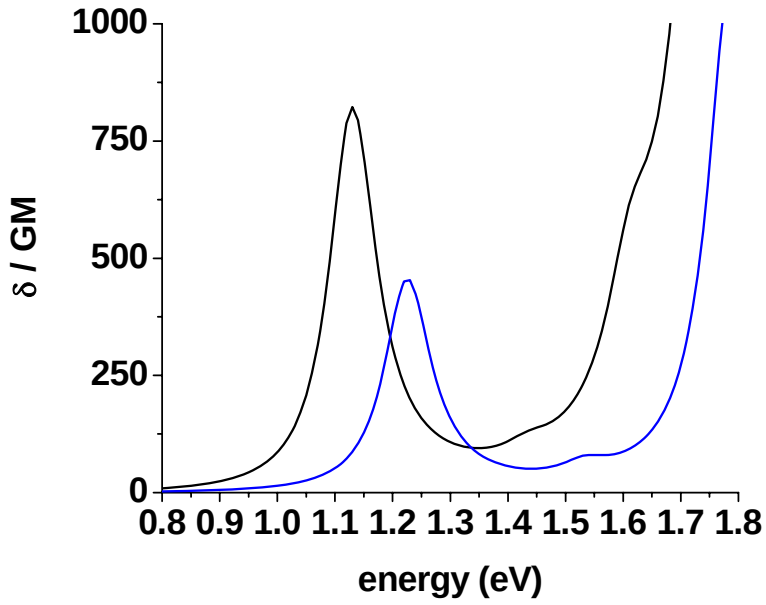

*Figure 35: Theoretical 2PA spectra for dipolar chromophores **1** (black line) and **14** (blue line).*

In common with **1**, in these dipolar chromophores with shorter π-bridge, there is only one significant low-energy 2PA peak (into S_1) for **9** to **14**; i.e. the 2PA peak into S_2 is consistently weak (< 100 GM). Although the energy value at which the 2PA occurs is independent of the number of vinylene units, it does affect its intensity as follows: the reduction of the π-bridge from that in **1** only significantly affects δ in the cases of **13** and **14** where the D, D', A', and A are connected with one vinylene unit (**13**) or where the D, D', A', and A are all linked directly with no vinylene unit (**14**) (δ (**1**) = 830 GM > δ (**13**) = 603 GM and δ (**14**) = 460 GM). Therefore, the number and position of the vinylene units in the other dipolar chromophores have a relatively minor effect on δ; the fact that δ for the dipolar chromophores with two vinylene units is already close to those with three suggests that δ is essentially saturated as a function of the polyene length. This is an

encouraging finding in terms of applications since, as mentioned earlier, extended polyenes often suffer from chemical and thermal instabilities.

The structure-property relationship is then established for **9**, **13**, and **14** using the convergence plots, which reveal that the low-energy 2PA peak is reasonably well-described using the D-term. It allows us to obtain a clear picture of the direct correlation between the decrease in δ and the decrease in number of vinylene units based on the electronic terms involved in the D-term, M_{ge}, $\Delta\mu_{eg}$, and E_{ge}, which are reported for **9**, **13**, and **14** in Table 16.

Table 16: Theoretical transition energies (E_{ge} and $E_{ge'}$), transition dipole moments (M_{ge} and $M_{ee'}$), state dipole moments (μ_{gg} and μ_{ee}), and changes in state dipole moment ($\Delta\mu_{eg}$) calculated with the INDO/MRDCI method for dipolar chromophores **9**, **13**, and **14**.

	E_{ge} (eV)	$E_{ge'}$ (eV)	M_{ge} (D)	$M_{ee'}$ (D)	μ_{gg} (D)	μ_{ee} (D)	$\Delta\mu_{eg}$ (D)
9	2.31	-	12.6	-	-	-	19.1
13	2.37	-	11.6	-	-	-	17.0
14	2.45	-	10.8	-	-	-	15.8

- not reported because not mentioned in the discussion

The M_{ge}, $\Delta\mu_{eg}$, and E_{ge}, terms all work in concert to give an increase of δ for the elongated chromophore **9** relative to **13** and **13** relative to **14** (M_{ge} (**9**) = 12.6 D > M_{ge} (**13**) = 11.6 D > M_{ge} (**14**) = 10.8 D; $\Delta\mu_{eg}$ (**9**) = 19.1 > $\Delta\mu_{ge}$ (**13**) = 17.0 D > $\Delta\mu_{ge}$ (**14**) = 15.8 D; and E_{ge} (**9**) = 2.31 eV < E_{ge} (**13**) = 2.37 eV < E_{ge} (**14**) = 2.45eV).

In summary, The Sum-Over-States (SOS) methods have been carried out in order to evaluate the two-photon absorption cross section of dipolar chromophores incorporating auxiliary electron-rich (D'), thiophene, and electron-poor (A'), thiazole into the π-bridge, which connect a donor (D) and an acceptor (A) groups. These dipolar chromophores are predicted to exhibit two low-energy 2PA transitions. The order in which D' and A' are inserted into the π-bridge affects the energy and intensity of these 2PA transitions. In addition, the regiochemistry of the thiazole affects whether 2PA is stronger into S_1 or S_2. Convergence plots of two-photon absorption cross-section versus the number of intermediate excited states included in the computational calculations reveal that multiple few-state terms contribute to the two-photon absorption cross-section. However, in the case of 2PA into S_1, the 2PA peak is reasonably well-described using a two-level D-term; while for 2PA into S_2, the 2PA peak is well-approximated by a tree-level T-term where S_1 is the intermediate state. These observations reveal that increased $\Delta\mu_{eg}$ is the parameter responsible for the higher two-photon absorption cross-section into S_1 of dipolar chromophores with thiazole in the matched case relative to that for the mismatched case (the bigger $\Delta\mu_{eg}$ for the chromphores in the matched case arises from the fact that the dipole moment of the excited state |e> is much bigger for the matched than the mismatched case; while the dipole moment of the ground-state are similar independent of the regiochemistry of the thiazole); whereas $M_{ee'}$ is the parameter responsible for the higher two-photon absorption cross-section into S_2 for the dipolar chromophores in the mismatched case. Finally, in dipolar chromophores with shorter length, there is one significant low-energy value at which 2PA occurs independently of the number of vinylene units, for the shorter examples show significantly reduced two-photon absorption cross-sections.

4.3. TWO-PHOTON ABSORPTION FOR QUADRUPOLAR CHROMOPHORES

In previous studies, it has been shown that quadrupolar chromophores have large δ [55]. In this chapter, a collaborative (experimental and theoretical) investigation of new quadrupolar chromophores with the A–D-D–A structural motif is done by considering chromophores **1** to **7**, whose chemical structures are presented in Figure 36. Strong acceptor groups, the TCF (**1** and **2**), the CF_3-TCF (**3-5**), and the SDS (**6** and **7**) are conjugated through polyene linkages to E-1,2-bis(3,4-dibutoxythien-2-yl)ethylene and E-1,2-bis(N-hexylpyrol-2-yl)ethylene donor groups.

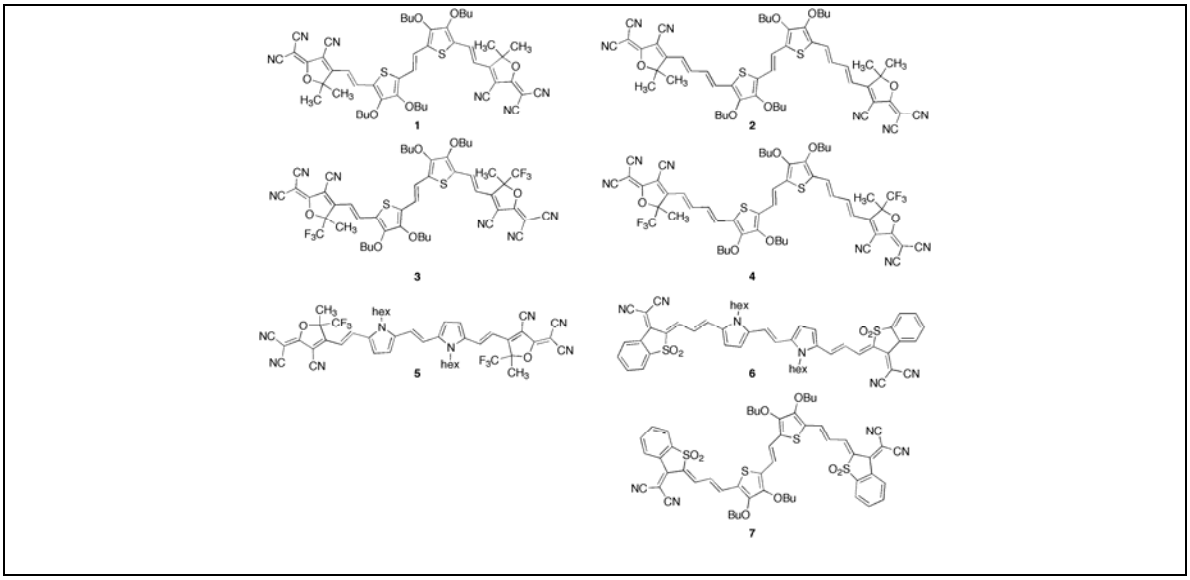

*Figure 36: Chemical structures of quadrupolar chromophores **1** to **7**.*

The experimental 1PA and degenerate 2PA spectra, obtained using the Z-scan technique, are shown for **1**-**7** in Figure 37; the corresponding electronic terms are reported for **1**-**7** in Table 17.

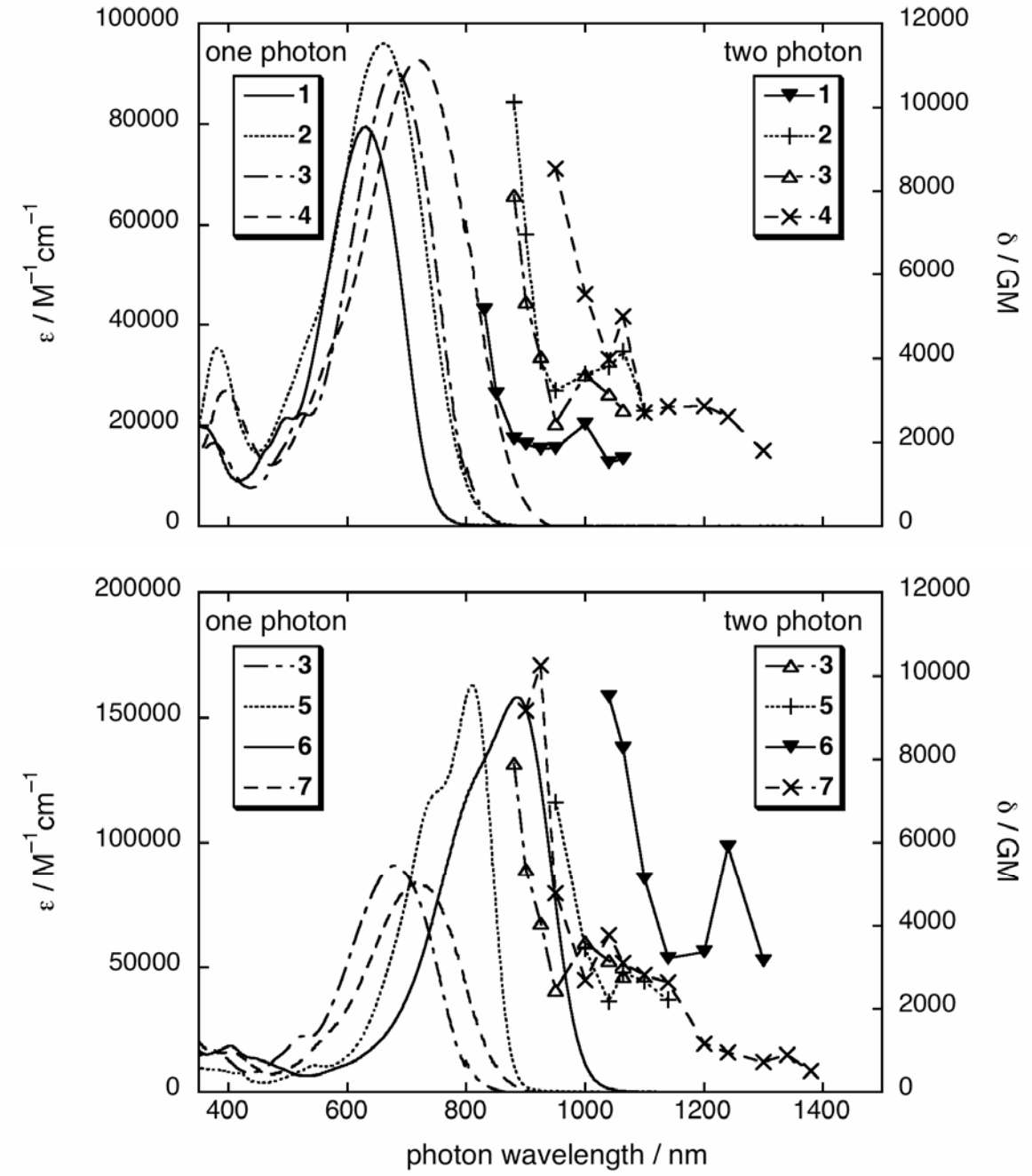

*Figure 37: Experimental 1PA and degenerate 2PA spectra, obtained using the Z-scan technique, for quadrupolar chromophores **1** to **4** (top plot) allowing comparison of the effect of the strength of the acceptor group (**1** vs. **3** and **2** vs. **4**) and the length of the π-bridge (**1** vs. **2**; **3** vs. **4**); **3** and **5** to **7** (bottom plot), allowing comparison of the CF_3-TCF and the SDS (**3** vs. **7**, **5** vs. **6**) and of the pyrrole and dialkoxythiophene auxiliary donors (**3** vs. **5**, **6** vs. **7**).*

Table 17: Experimental 1PA and 2PA electronic terms for quadrupolar chromophores **1** and **7**.

	$\lambda_{max}^{(1)}$ (nm)[a]	$E_{max}^{(1)}$ (eV)[b]	M_{ge} (D)[c]	$\lambda_{max}^{(2)}$ (nm)[d]	$E_{max}^{(2)}$ (eV)[e]	δ_{max} (GM)[d]
1	616	2.01	13.7	1000	2.48	2400
2	661	1.88	15.8	1064	2.33	4200
3	679	1.82	14.9	1000	2.48	3600
4	718	1.73	16.3	1064	2.33	5000
5	811	1.53	17.4	1064	2.33	2900
6	889	1.39	19.2	1240	2.00	5900
7	719	1.72	14.5	1040	2.38	3800
6	***889***	***1.39***	***19.2***	***1240***	***2.00***	***5900***

[a] low-energy 1PA peak ($\lambda_{max}^{(1)}$), [b] energy of the 1PA peak ($E_{max}^{(1)}$), [c] transition dipole moment of the transition from the ground state to excited-state (M_{ge}), [d] low-energy 1PA peak ($\lambda_{max}^{(2)}$), and δ_{max} are the approximate photon wavelength for the low-energy 2PA peak and the corresponding cross-section, respectively, according to Z-scan measurements (1 GM = 1 $\times$ 10^{-50} cm^4 s/photon-molecule), [e] energy of the 1PA peak ($E_{max}^{(2)}$) is the approximate total two-photon excitation energy (twice the photon energy at the given wavelength).

The 1PA peak is shifted to smaller transition energy by 0.09-0.13 eV when the π-bridges between the auxiliary donors and each acceptor group of **1** and **3** are each extended with an additional vinylene unit. The 1PA peak is also red-shifted (0.15-0.19 eV) when the TCF is replaced by the CF_3-TCF. The maxima are red-shifted still further when the CF_3-TCF is replaced by the SDS. The replacement of the auxiliary 3,4-dibutoxythiophene donors with the auxiliary N-hexylpyrrole leads to a red shift (0.29-0.33 eV) of the 1PA peak. Overall, however, a plot of the optical absorption maxima against electrochemical gap does not reveal a clear linear relationship; this is not surprising

since the CI description of the lowest energy 1PA transitions obtained by computational calculations (INDO/MRDCI) reveal that these 1PA transitions are considerably more complex than simple HOMO-LUMO transition.

The degenerate 2PA (Z-scan) spectra for **1**-**7** are similar in that they all show a poorly resolved low-energy 2PA peak with δ ranging from 2500-5900 GM in the measured photon wavelength range 1000-1300 nm, this 2PA peak appearing as a shoulder of a much stronger one lying close to, or beyond, the 1PA absorption edge. As shown in Figure 35, the measurable high-energy 2PA peaks are in excess of 5000 GM and large δ of greater than 2000 GM are accessed over a measured photon-energy range of ca. 0.5 eV. The δ for the low-energy 2PA peaks are of similar magnitude to those previously measured using the two-photon-induced fluoresence technique for bis(styrylbenzene) chromophores with alkoxy groups imparting donor character to the π-bridge and the SDS (ca. 4400 GM) or the N,N-diethylthiobarbituric acid (ca. 1750 GM) acceptor groups; however, the transitions in the quadrupolar chromophores investigated here are somewhat red-shifted relative to these previously studied chromophores.

Comparing **1** to **2** and **3** to **4**, it is seen that the extension of the π-bridges by one vinylene unit results in both a lowering of the low-energy 2PA state energy (comparable to the shift in 1PA state energy) and an increase in δ into that 2PA state by 40-70%. It is also observed that **3** and **4** show low-energy δ somewhat larger than their analogues (**1** and **2** respectively). On replacement of the 3,4-dialkoxythiophenes with the more strongly donating auxiliary pyrrole, the energy of the 2PA state is lowered; δ decreases between **3** and **5**, but increases between **7** and **6**.

In order to gain more insight into the trends seen in the energy and strength of the electronic transitions when the chemical structure is varied, quantum-chemical computational calculations are performed on **1-7** (with butyl and hexyl groups replaced by methyl groups to simplify the computational calculations). The variation in the bond length alternation in the π-bridges among the quadrupolar chromophores is rather small. The π-bridges of these quadrupolar chromophores are calculated to be more-or-less planar, with the largest deviations from planarity (except in **7**) being in the dihedral angles between the planes of the auxiliary donors and the planes of the central vinylene units (8-10 ° for **1-4**; 12-16 ° for **6**; 19 ° for **5**).

The 1PA transition energies are overestimated, as is typical for the MRDCI method; however, the theoretical trend fits the experimental trend reasonably well if the two pyrrole-based quadrupolar chromophores, **5** and **6**, are excluded; the transition energies are more severely overestimated in these two quadrupolar chromophores regardless of whether SCI or MRDCI schemes are used.

The theoretical 2PA spectra are reported for **1**, **2**, and **3** in Figure 38 and are similar to the experimental ones, which are reported for **1**-**3** in Figure 37 (they are plotted again like in Figure 37 but as a function of the energy rather than the wavelength for the sake of simplicity of comparison with the theoretical spectra in Figures 39, 40, and 41).

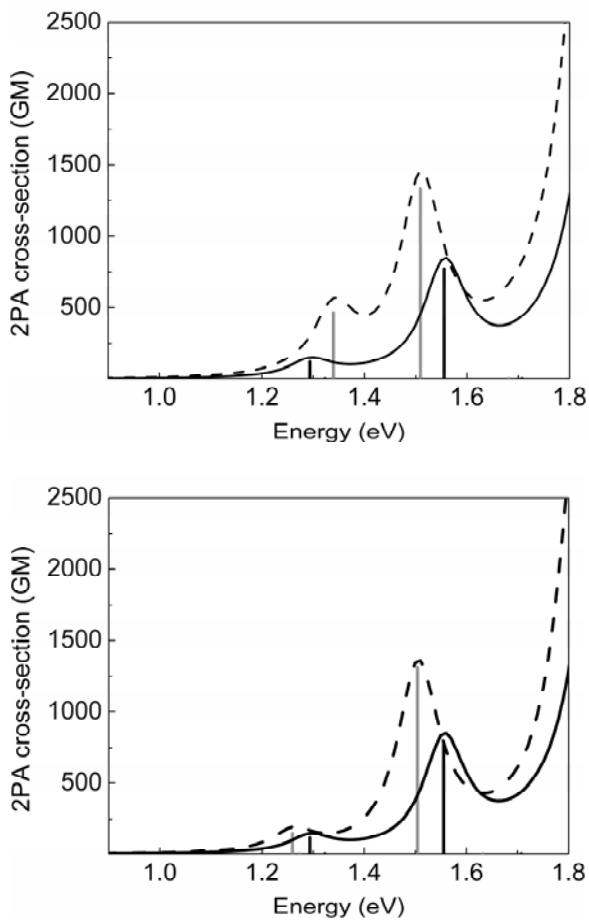

*<u>Figure 38:</u> Theoretical 2PA spectra for quadrupolar chromophores **1**, **2**, and **3**: **1** with **2** (top plot), and **3** (bottom plot). The curved profiles (**1** solid line; **2**,**3** broken line) represent δ calculated with the SOS method and the vertical bars correspond to δ calculated with the 2PA-tensor.*

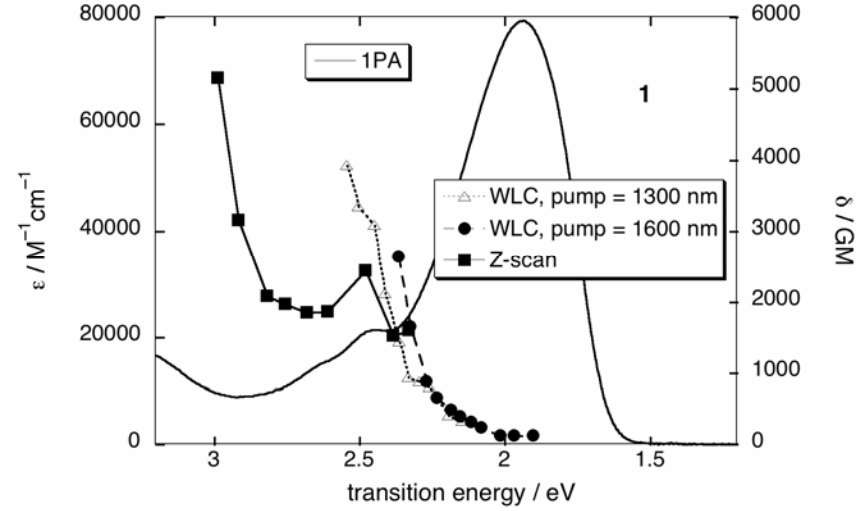

*Figure 39: Experimental 1PA spectra for quadrupolar chromophores **1** (solid line), compared with degenerate 2PA spectra obtained using Z-scan technique (black square, solid line), and with non-degenerate 2PA spectra obtained using the WLC with pump wavelengths of 1400 and 1600 nm (white triangle and black ball).*

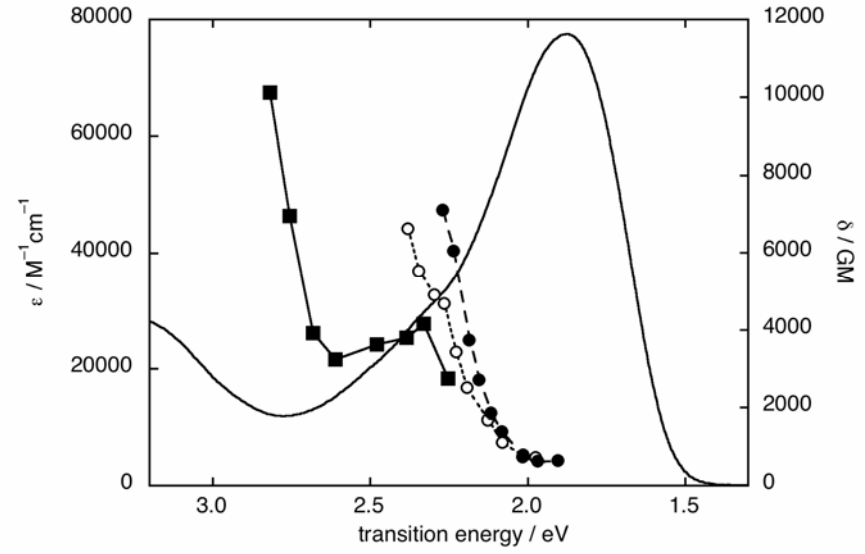

*Figure 40: Experimental 1PA spectra for quadrupolar chromophores **2** (solid line), compared with degenerate 2PA spectra obtained using Z-scan technique (black square, solid line), and with non-degenerate 2PA spectra obtained using the WLC with pump wavelengths of 1400 and 1600 nm (white ball and black ball).*

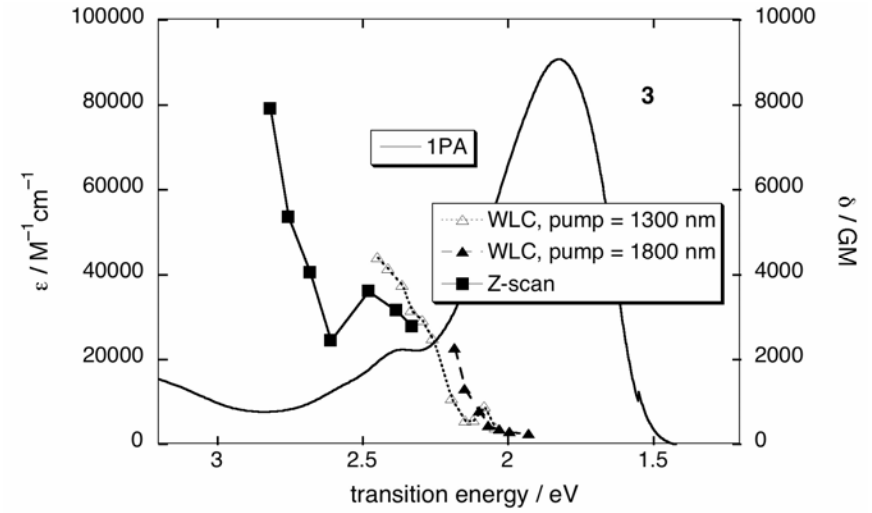

*Figure 41: Experimental 1PA spectra for quadrupolar chromophores **3** (solid line), compared with degenerate 2PA spectra obtained using Z-scan technique (black square, solid line), and with non-degenerate 2PA spectra obtained using the WLC with pump wavelengths of 1400 and 1600 nm (white triangle and black triangle).*

The theoretical 2PA spectra consist of a low-energy (calculated photon-energy range, 1.0 to 1.7 eV) feature (or features) with δ of a few thousand GM and a much stronger value at higher energy (calculated at photon energies of 1.7 to 2.2 eV). The computational calculations also reveal that for **1**-**4** and **7**, there are in fact two significant 2PA peaks in the low-energy range, the lower energy of which is the weaker for **1-4**, but stronger for **7**. This is consistent with the observation of the low-energy shoulders in **4** and **7** in the experimental 2PA spectra, although for **7** the intensity ratio for those peaks/shoulders appears to be reversed. This is, however, hard to quantify, as the experimentally stronger low-energy features sit as a shoulder on the much stronger high-energy feature.

The theoretical transition energies (E_{ge}) and δ calculated with the SOS method and the 2PA tensor for **1** to **7** are reported in Table 18.

Table 18: Theoretical transition energies (E_{ge}) and δ calculated with the SOS method and the 2PA-tensor for quadrupolar chromophores **1** to **7**.

	S_1		S_2		S_3	
	E	δ	E	δ	E	δ
1	2.59	118	2.64	a	3.11	773
2	2.58	a	2.68	464	3.02	1334
3	2.52	150	2.55	a	3.01	1310
4	2.49	a	2.62	797	2.90	1881
5	2.44	a	2.75	2002	–	–
6	2.25	a	2.53	3781	–	–
7	2.21	a	2.46	2203	2.84	1489
6	***2.25***	***a***	***2.53***	***3781***	***–***	***–***

[a]One-photon-allowed, i.e. two-photon-forbidden, transition

The computational calculations suggest that the lowest 2PA-allowed electronic exicted state for **1**-**4** and **7** is rather close in energy to that of the lowest 1PA-allowed electronic excited state; for two of these quadrupolar chromophores (**1** and **3**) the 2PA electronic excited state is slightly lower in energy, whereas, in the other quadrupolar chromophores, S_1 is the lowest 1PA-allowed and 2PA-forbidden electronic excited states. For **5** and **6**, there is only one 2PA-allowed electronic excited state (S_2), which lies significantly above the lowest 1PA-allowed electronic excited state (S_1). As previously, the absolute transition energies are systematically overestimated by the computational calculations, in part because of the overcorrelation of the ground state with the MRDCI scheme; however, the trends are reasonably well-reproduced given the limited resolution in the experimental spectra.

The δ into S_3 (**1**-**4** and **7**) or S_2 (**5** and **6**) increases on extending the π-bridge from **1** to **2** and from **3** to **4**, and also as the strength of the acceptor group increases from **1** to **3** and from **2** to **4**. In addition, the replacement of the CF_3-TCF with the SDS leads to an

increased δ (**7** vs. **3**; **6** vs. **5**). Also, **5** and **6** give higher δ than their analogues (**3** and **7**), consistent with experimental results in the case of **6** vs. **7**, but not in the case of **5** vs. **3**. In general, δ (for the chosen broadening, which appears consistent with the experimental 2PA peak widths) are around a factor of two smaller than those measured by Z-scan. The magnitude of the latter are, however, affected by the stronger overlap with the high-energy 2PA peaks. Another reason for the smaller δ arises from the overestimated electronic excited state energies. If the experimental 1PA and 2PA state energies are considered rather than the values derived from the three-term model for the quadrupolar chromophores (vide infra), δ increase due to the reduced detuning term ($E_{ge} - \frac{E_{ge'}}{2}$).

In order to gain further insight into the structure-property relationships, the few-term models have proven helpful. For quadrupolar chromophores, δ is typically approximated by the T-term (equation [38] – chapter 3) ($\delta_T \prec \frac{\left(\frac{E_{ge'}}{2}\right)^2 M_{ge} M_{ee'}}{\left(E_{ge} - \frac{E_{ge'}}{2}\right)^2}$), for which M_{ge} is the transition dipole moment between (g) and the dominant 1PA electronic excited state (e), $M_{ee'}$ is the transition dipole moment between the 1PA electronic excited state (e) and the 2PA electronic excited state (e'), and $E_{ge} - \frac{E_{ge'}}{2}$ is the so-called detuning energy.

The 2PA peak corresponding to the $S_0 \rightarrow S_3$ transition for **1**-**4** and **7** is reasonably well-described using a three-term model; only the S_1 (**1** and **3**) or S_2 (**2**, **4**, and **7**) 1PA-

allowed intermediate electronic excited states must be considered. In contrast, the 2PA into S_1 of **1** and **3** or into S_2 of **2**, **4** and **7** has a more complex origin with several intermediate electronic excited states contributing significantly to δ. In the convergence plot in Figure 38, the variations seem to be of similar magnitude for both electronic excited states. The description of the 2PA into S_2 of **5** and **6** also requires multiple intermediate states. This is illustrated for the example of **4** in Figure 42, in which δ plotted as a function of the number of intermediate electronic excited states for the 2PA into S_2 and S_3. While for the 2PA into S_2, contributions from several intermediate electronic excited states are evidently important, in the case of the 2PA into S_3, similar δ are calculated with a single intermediate electronic excited state than with a large number; i.e. contributions from additional intermediate electronic excited states besides S_1 essentially cancel one another.

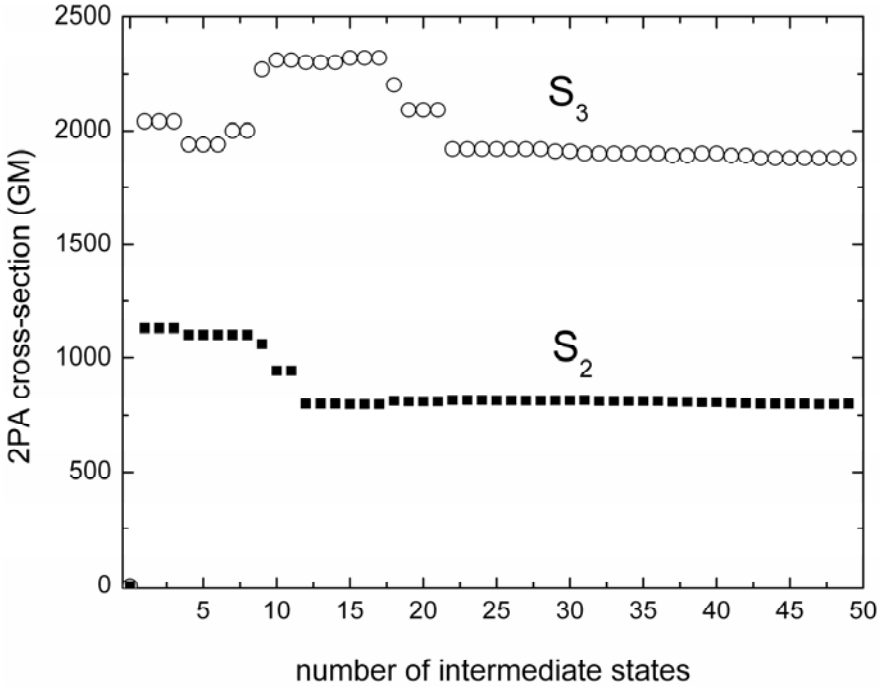

*<u>Figure 42:</u> Convergence plots for quadrupolar chromophores **4** for 2PA is into S_2 (black square) and S_3 (white ball).*

Since the 2PA into S_3 of **1-4** and **7** are particularly well-described by the three-term model, the observed trends in the following are discussed on the basis of the involved electronic terms (transition dipole moments and transition energies), which are reported for **1**-**4** and **7** in Table 19.

Table 19: Theoretical transition energies (E_{ge} and $E_{ge'}$), transition dipole moments (M_{ge} and $M_{ee'}$), and δ calculated with the SOS method for quadrupolar chromophores **1** to **4** and **7** for 2PA into S_3 (e') where (e) denotes S_1 (**2**, **4**, **7**) or S_2 (**1** and **3**) 1PA-allowed intermediate electronic excited state.

	E_{ge} (eV)	$E_{ge'}$ (eV)	$E_{ge} - \frac{E_{ge'}}{2}$ (eV)	M_{ge} (D)	$M_{ee'}$ (D)	δ (GM)
1	2.64	3.11	1.09	13.5	10.1	773
2	2.58	3.02	1.07	15.3	12.2	1334
3	2.55	3.01	1.05	13.9	12.9	1310
4	2.49	2.90	1.04	15.7	14.1	1881
7	2.21	2.84	0.79	14.6	10.8	1489
4	***2.49***	***2.90***	***1.04***	***15.7***	***14.1***	***1881***

From these electronic terms, it becomes obvious that the increase in δ, when replacing the TCF with the CF_3-TCF (i.e., when going from **1** to **3** and from **2** to **4**) is largely due to an increased coupling between the 1PA-allowed and the 2PA-allowed electronic excited states (i.e., an increase in $M_{ee'}$). Increasing the length of the π-bridge (i.e., comparing **1** and **2** as well as **3** and **4**), results in a comparable increase of M_{ge} and $M_{ee'}$. In **1** to **4**, changes in the detuning energy play practically no role. This is significantly different in **7**, where the decreased detuning energy compensates for $M_{ee'}$ being significantly smaller than in **2**, **3**, and **4** resulting in a comparable δ.

In summary, the quadrupolar chromophores A-D'-D'-A with the TCF, CF_3-TCF and SDS and electron-rich bis(heterocycle)ethylene donors (heterocycle = dialkoxythiophene, pyrrole) display strong 2PA in the wavelength range of 1000 to 1300 nm. All of them show strong 2PA peaks (cross-sections from 2400 to 5900 GM) in this low-energy wavelength range with even higher two-photon absorption cross-section (from 5200 to 10100 GM) accessible at higher energies due to the onset of a much stronger 2PA peak

at higher energy. For each quadrupolar chromophore, two-photon absorption cross-sections of over 2000 GM are accessed over photon-energy of ca. 0.5 eV. The trends observed in the transition energies and cross-sections of the low-energy 2PA features are correlated to features of the chemical structures and are generally reproduced well using computational calculations. The observed 2PA peaks are attributed to 2PA into S_2 and S_3 for thiophene-based and pyrrole-based quadrupolar chromophores respectively. In the former class of chromophores, the 2PA into S_3 is well described by a three-level T-term with the one-photon state the only significant intermediate electronic excited state.

CHAPTER 5 CONCLUSION

The Sum-Over-States (SOS) and Finite-Field (FF) (in the local contribution version) methods are carried out in order to evaluate the second-order polarizability (β) of dipolar chromophores incorporating a variety of five-membered heterocyclic rings (primary acceptor end group, A). To obtain a clear picture of the relationship between the chemical structure and the nonlinear polarizability, the FF method is applied and allowed us to provide an explanation for why the furan- and pyrrole-based acceptor groups (TCF and TCP) are good candidates for electro-optic and photonic fields since the pattern of the β-charges reflects an efficient intramolecular charge transfer from the donor to the acceptor groups, nearly without cancellation of the β-moments on neighboring atoms.

The TCP-based dipolar chromophore gives the highest β among the acceptor groups investigated in this dissertation. In general, the TCF and TCP yield β superior to previously developed acceptor groups (SDS, TCI, BBA, and TCV); this is explained by the fact that in the latter groups, significant parts of the acceptor group appear to be relatively inactive in terms of contributing β-moments. Although the TCP-based dipolar chromophore yields highest β, TCF-based ones are increasingly used because the TCP-based dipolar chromophores form large electrostatic dipolar interactions among each other, thus leading to a reduced second-order electrical susceptibility (it becomes impossible to apply the poling process to align the TCP-based dipolar chromophores in a noncentrosymmetric fashion).

In order to clarify the role of the oxygen atom in the TCF, it is replaced by a variety of groups X, for which β increases as the inductive electron-withdrawing ability of the group X increases (SiH_2, CH_2, SO, and SO_2). However, there is a deviation from this trend when the group X possesses either a π electron-donating or electron-withdrawing character. The π electron-withdrawing groups X (C=O and $C=CHNO_2$, and to a lesser extent $C=CH_2$) have higher β than expect based on the inductive electron-withdrawing ability of these groups X alone. Since the trends in β is well-described using the two-term model, the origin of these increased β are traced to stabilizing contributions from the local LUMOs of these fragments to the molecular LUMO, leading to reduced transition energies and increased changes in state dipole moment. The local HOMOs of the π electron-donating groups X (NH, S, and O) contribute to the molecular LUMO in a destabilizing fashion, leading to increased transition energies, reduced changes in state dipole moment, and reduced β.

When an auxiliary electron-withdrawing group, A' (thiazole) is inserted into the π-bridge (one vinylene unit) of a TCP-based dipolar chromophore, β increases by a factor of more than 2. This is remarkable since the origin of that increase is not simply found in the increased of the length of the π-bridge.

The dipolar chromophore investigated next are such that the auxiliary donor, thiophene, and acceptor, thiazole, are inserted into the π-bridge between the 4-(dimethylamino)-phenyl donor group and the TCF. It is found that the magnitude of β strongly depends on the order in which the auxiliary donor and acceptor are inserted into the π-bridge as well as on the regiochemistry of the nitrogen atom in the thiazole. The largest β are

obtained for the D-D'-matched A'-A structural motif, while β is by a factor of nearly two smaller for the D-mismatched A'-mismatched A'-A one. While the trends are consistent with those found by Breitung et al. [59] for smaller chromophores, the magnitudes of the changes are strongly amplified in the present chromophores. These findings are rationalized using the FF method. Studying the dependence of β as a function of the number and position of vinylene units inserted between the D, D', A', and A, an increase of β is observed when going from zero to one and eventually to two vinylene units. This trend is again understood from the FF method. A saturation of β is observed when adding a third vinylene unit to the π-bridge. This is a positive finding in terms of overall stability since extended polyenes suffer from chemical and thermal instabilities.

The Sum-Over-States (SOS) method and the 2PA tensor are carried out in order to evaluate the two-photon absorption cross-section (δ) and it is found that the dipolar chromophores with the D-D'-A'-A structural motif act as efficient 2PA dyes in the NIR telecommunication wavelength range, and as efficient 2PA sensitizers for photorefractive composites. Therefore, the investigation is extended to dipolar chromophores incorporating auxiliary donor, thiophene, and acceptor, thiazole, into the π-bridge, which connect the donor and acceptor groups (4-(dimethylamino)-phenyl group and TCF, respectively). These dipolar chromophores are predicted to exhibit two low-energy 2PA peaks. The order in which the auxiliary donor and acceptor are inserted into the π-bridge affects the energy and intensity of these two 2PA peaks. In addition, the regiochemistry of the thiazole affects whether the 2PA is stronger into S_1 (matched case) or S_2 (mismatched case).

Convergence plots of δ versus the number of intermediate electronic excited states included in the computational calculations reveal that multiple few-term models contribute to δ. However, in the case of the 2PA into S_1, the 2PA peak is reasonably well-described using a two-term model (D-term); while for the 2PA into S_2, the 2PA peak is well-approximated by a tree-term model (T-term) where S_1 is the intermediate electronic excited state. These observations reveal that $\Delta\mu_{eg}$ is the electronic term responsible for the higher δ into S_1 for the dipolar chromophores in the matched case relative to that for the mismatched (the bigger $\Delta\mu_{eg}$ for the dipolar chromphores in the matched case arises from the fact that the dipole moment of the electronic excited state |e> is much bigger for the matched case than the mismatched one; while the ground state dipole moment is similar independently of the regiochemistry of the thiazole); whereas $M_{ee'}$ is the electronic term responsible for the higher δ into S_2 for the dipolar chromophores in the mismatched case. Finally, in dipolar chromophores with shorter π-bridge, there is one significant low-energy 2PA peak independently of the number of vinylene units, for the shorter examples show significantly reduced δ.

The quadrupolar chromophores with the A-D'-D'-A structural motif with strong acceptor groups (TCF, CF_3-TCF and SDS) and auxiliary bis(heterocycle)ethylene donors (heterocycle = dialkoxythiophene, pyrrole) display strong 2PA peak in the wavelength range of 1000 to 1300 nm. All of them show strong 2PA peaks (δ from 2400 to 5900 GM) in this low-energy range with even higher δ (from 5200 to 10100 GM) accessible at higher energies due to the onset of a much stronger peak at higher energy. The trends observed in the transition energies and δ of the low-energy 2PA peaks are correlated to features of the chemical structures and are generally reproduced well using

computational calculations. The observed 2PA peaks are attributed to absorption into S_3 and S_2 states for thiophene-based and pyrrole-based quadrupolar chromophores respectively. In the former class of quadrupolar chromophores, the 2PA into S_3 is well described by a three-term model with the one-photon state the only significant intermediate electronic excited state.

REFERENCES

[1] C. M. Isborn, A. Leclercq, F. D. Vila, J. L. Brédas, B. E. Eichinger, and B. H. Robinson, "Comparison of hyperpolarizabilities calculated with various quantum mechanical methods", submitted for publication (referred to in chapter 2).

[2] A. Leclercq, E. Zojer, S.-H. Jang, S. Barlow, V. Geskin, A. K.-Y. Jen, S. R. Marder, and J. L. Brédas, J. Chem. Phys. **124**, 044510 (2006) (referred to in chapter 3, sections 3.1, 3.4).

[3] S.-H. Jang, J. Luo, N. M. Tucker, A. Leclercq, E. Zojer, M. A. Haller, T.-D. Kim, J.-W. Kang, K. Firestone, D. Bale, D. Lao, J. B. Benedict, D. Cohen, W. Kaminsky, B. Kahr, J. L. Brédas, P. Reid, L. R. Dalton, and A. K.-Y. Jen, Chem. Mater. **18**, 2982 (2006) (referred to in chapter 3, section 3.1).

[4] A. Leclercq, S. Barlow, E. Zojer, K. Schmidt, S.-H. Jang, A. K.-Y. Jen, S. R. Marder, and J. L. Brédas, "Quantum-chemical investigation of second-order polarizability of dipolar chromophores incorporating the TCF acceptor end group: Influence of competing inductive and resonance contributions from the oxygen atom", in preparation (referred to in chapter 3, section 3.2).

[5] A. Leclercq, E. Zojer, K. Schmidt, S.-H. Jang, S. Barlow, V. Geskin, A. K.-Y. Jen, S. R. Marder, and J. L. Brédas, "Role of thiophene auxiliary electron-donor and thiazole electron-acceptor in dipolar chromophores: Quantum-chemical investigation of second-order polarizability", in preparation (referred to in chapter 3, section 3.5).

[6] L. Beverina, J. Fu, A. Leclercq, E. Zojer, P. Pacher, S. Barlow, E. W. Van Styrland, D. J. Hagan, J. L. Brédas, and S. R. Marder, J. Am. Chem. Soc. **127**, 7282 (2005) (referred to in chapter 4, section 4.1).

[7] A. Leclercq, E. Zojer, K. Schmidt, S.-H. Jang, S. Barlow, V. Geskin, A. K.-Y. Jen, S. R. Marder, and J. L. Brédas, "Role of thiophene auxiliary electron-donor and thiazole electron-acceptor in dipolar chromophores: Quantum-chemical investigation of the two-photon absorption cross-section", in preparation (referred to in chapter 4, section 4.2).

[8] S. Zheng, A. Leclercq, J. Fu, L. Beverina, L. A. Padilha, E. Zojer, K. Schmidt, S. Barlow, J. Luo, A. K.-Y. Jen, Y. Yu, Z. Shuai, E. W. Van Styrland, D. H. Jagan, J. L. Brédas, and S. R. Marder, "Two-photon absorption in quadrupolar bis(acceptor)-

terminated chromophores with electron-rich bis(heterocycle)vinylene bridges", in preparation (referred to in chapter 4, section 4.3).

[9] F. Wang, A. W. Harper, M. S. Lee, and L. R. Dalton, Chem. Mater. **11**, 2286 (1999).

[10] S. R. Marder, J. W. Perry, and W. P. Schaeffer, Science **245**, 626 (1989).

[11] D. M. Burland, R. D. Miller, and C. A. Walsh, Chem. Rev. **94**, 31 (1994).

[12] S. Thayumanavan, J. Mendez, and S. R. Marder, J. Org. Chem. **64**, 4289 (1999).

[13] S. Gilmour, R. A. Montgomery, S. R. Marder, L.-T. Cheng, A. K.-Y. Jen, Y. Cai, J. W. Perry, and L. R. Dalton, Chem. Mater. **6**, 1603 (1994).

[14] D. S. Chemla and J. Zyss, Eds., Nonlinear Optical Properties of Organic Molecules and Crystals (New York, 1987); J.L. Brédas and R. R. Chance, Eds., Conjugated Polymeric Materials: Opportunities in Electronics, Optoelectronics, and Molecular Electronics (Dordrecht, 1990); S. R. Marder, J. E. Sohn, and G. D. Stucky, Eds., Materials for Nonlinear Optics (Washington, 1991); P. N. Prasad and D. J. Williams, Introduction to Nonlinear Optical Effects in Molecules and Polymers (New York, 1991); D. R. Kanis, M. A. Ratner, and T. J. Marks, Chem. Rev. **94**, 195 (1994).

[15] W. Denk, J. H. Strickler, and W. W. Webb, Science **248**, 73 (1990); J. E. Ehrlich, X. L. Wu, Ys. L. Lee, Z. Y. Hu, H. Rockel, S. R. Marder, and J. W. Perry, Opt. Lett. **22**, 1843 (1997); B. H. Cumpston, S. P. Ananthavel, S. Barlow, D. L. Dyer, J. E. Ehrlich, L. L. Erskine, A. A. Heikal, S. M. Kuebler, I.-Y. S. Lee, D. Maccord-Maughon, J. Qin, H. Rockel, M. Rumi, X.-L. Wu, S. R. Marder, and J. W. Perry, Nature **398**, 51 (1999); A. Abbotto, L. Beverina, R. Bozio, S. Bradamante, C. Ferrante, G. A. Pagani, and R. Signorini, Adv. Mater. **12**, 1963 (2000); G. S. He, P. P. Markowicz, T.-C. Lin, and P. N. Prasad, Nature **415**, 767 (2002); W. Zhou, S. M. Kuebler, K. L. Braun, T. Yu, J. K. Cammack, C. K. Ober, J. W. Perry, and S. R. Marder, Science **296**, 1106 (2002); D. R. Larson, W. R Zipfel, R. M. Williams, S. Clark, M. P. Bruchez, F. W. Wise, and W. W. Webb, Science **300**, 1434 (2003).

[16] A. Szabo and N. S. Ostlund, Modern Quantum Chemistry: Introduction to Advanced Electronic Structure Theory (New York, 1996).

[17] Gaussian 98 (Revision A.11), M. J. Frisch, G. W. Trucks, H. B. Schlegel, G. E. Scuseria, M. A. Robb, J. R. Cheeseman, V. G. Zakrzewski, J. A. Montgomery, Jr., R. E. Stratmann, J. C. Burant, S. Dapprich, J. M. Millam, A. D. Daniels, K. N. Kudin, M. C. Strain, O. Farkas, J. Tomasi, V. Barone, M. Cossi, R. Cammi, B. Mennucci, C. Pomelli, C. Adamo, S. Clifford, J. Ochterski, G. A. Petersson, P. Y. Ayala, Q. Cui, K. Morokuma, P. Salvador, J. J. Dannenberg, D. K. Malick, A. D. Rabuck, K.

Raghavachari, J. B. Foresman, J. Cioslowski, J. V. Ortiz, A. G. Baboul, B. B. Stefanov, G. Liu, A. Liashenko, P. Piskorz, I. Komaromi, R. Gomperts, R. L. Martin, D. J. Fox, T. Keith, M. A. Al-Laham, C. Y. Peng, A. Nanayakkara, M. Challacombe, P. M. W. Gill, B. Johnson, W. Chen, M. W. Wong, J. L. Andres, C. Gonzalez, M. Head-Gordon, E. S. Replogle, J. A. Pople, Gaussian, Inc., Pittsburgh PA, (2001).

[18] M. J. S. Dewar, E. G. Zoebisch, E. F. Healy, and J. J. P. Stewart, J. Am. Chem. Soc. **107**, 3902 (1985).

[19] J. A. Pople, D. L. Beveridge, and P. A. Dobosh, J. Chem. Phys. **47**, 2026 (1967).

[20] N. Mataga and K. Nishimoto, Z. Phys. Chem. **13**, 140 (1957).

[21] K. Ohno, Theoret. Chim. Acta **2**, 219 (1964).

[22] M. C. Zerner, G. H. Loew, R. F. Kichner, and U. Mueller-Westerhoff, J. Am. Chem. Soc. **102**, 589 (1980).

[23] J. Orr and J. F. Ward, Mol. Phys. **20**, 513 (1971).

[24] S. Dahne, Science **199**, 1163 (1978).

[25] K. C. Rustagi and J. Ducuing, Opt. Commun. **10**, 258 (1974).

[26] S. R. Marder, C. B. Gorman, F. Meyers, J. W. Perry, G. Bourhill, J. L. Brédas, and B. M. Pierce, Science **265**, 632 (1994).

[27] J. L. Oudar and D. S. Chemla, J. Chem. Phys. **66**, 2664 (1977); J. L. Oudar, J. Chem. Phys. **67**, 446 (1977).

[28] J. R. Heflin, K. Y. Wong, O. Zamani-Khamiri, and A. F. Garito, Phys. Rev. B **38**, 1573 (1988); S. N. Dixit, D. Guo, and S. Mazumdar, Phys. Rev. B **43**, 6781 (1991).

[29] H. D. Cohen and C. C. J. Roothaan, J. Chem. Phys. **43**, 34 (1965).

[30] P. Chopra, L. Carlacci, H. F. King, and P. N. Prasad, J. Phys. Chem. **93**, 7120 (1989).

[31] M. N. Nakano, I. Shigemoto, S. Yamada, and K. Yamaguchi, J. Chem. Phys. **103**, 4175 (1995).

[32] V. M. Geskin and J. L. Brédas, J. Chem. Phys. **109**, 6163 (1998); V. M. Geskin, C. Lambert, and J. L. Brédas, J. Am. Chem. Soc. **125**, 15651 (2003).

[33] G. Bourhill, J. L. Brédas, L. -T. Cheng, S. R. Marder, F. Meyers, J. W. Perry, and B. G. Tieman, J. Am. Chem. Soc. **116**, 2619 (1994).

[34] S. R. Marder, D. N. Beratan, and L. T. Cheng, Science **252**, 103 (1991); L. R. Dalton, A. W. Harper, R. Ghosn, W. H. Steier, M. Ziari, H. Fetterman, Y. Shi, R. V. Mustacich, A. K.-Y. Jen, and K. J. Shea, J. Chem. Mater. **7**, 1060 (1995).

[35] M. He, T. M. Leslie, and J. A. Sinicropi, Chem. Mater. **14**, 2393 (2002).

[36] M. Ahlheim, M. Barzoukas, P. V. Bedworth, M. Blancahrd-Desce, A. Fort, Z. Y. Hu, S. R. Marder, J. W. Perry, C. Runser, M. Staehin, and B. Zysset, Science **271**, 335 (1996).

[37] S. S. Sun, C. Zhang, L. R. Dalton, S. M. Garner, A. Chen, and W. H. Steier, Chem. Mater. **8**, 2539 (1996).

[38] M. Dorr, R. Zentel, R. Dietrich, K. Meerholz, C. Brauchle, C. Wichern, S. Zippel, and P. Boldt, Macromolecules **31**, 1454 (1998).

[39] L. R. Dalton, Opt. Eng. **39**, 589 (2000); M. He, T. M. Leslie, and J. A. Sinicropi, Chem. Mater. **14**, 4662 (2002); M. He, T. M. Leslie, J. A. Sinicropi, S. M. Garner, and L. D. Reed, Chem. Mater. **14**, 4669 (2002); S. Liu, M. Haller, H. Ma, L. R. Dalton, S.-H. Jang, and A. K.-Y. Jen, Adv. Mater. **15**, 603 (2003); Y. Liao, B. E. Eichinger, K. A. Firestone, M. Haller, J. Luo, W. Kaminsky, J. B. Benedict, P. J. Reid, A. K-.Y. Jen, L. R. Dalton, and B. H. Robinson, J. Am. Chem. Soc. **127**, 2758 (2005).

[40] G. F. Hennion, and E. J. Watson, J. Org. Chem. **23**, 658 (1958); F. W. Breitbeil, and J. L. Schranz, J. Org. Chem. **44**, 4649 (1979).

[41] R. A. Carboni, D. D. Coffman, and E. G. Howard, J. Am. Chem. Soc. **80**, 2838 (1958); A. J. Fatiadi, Synthesis **165**, 265 (1978).

[42] D. Villemin and L. Liao, Syn. Comm. **31**, 1771 (2001); C. Zhang, L. R. Dalton, M.-C. Oh, H. Xhang, and W. Steier, Chem. Mater. **13**, 3043 (2001).

[43] M. Halik, W. Wenseleers, C. Grasso, F. Stellacci, E. Zojer, S. Barlow, J.L. Brédas, J. W. Perry, and S.R. Marder, Chem. Comm. **1490**, 1490 (2003); E. Zojer, W. Wenseleers, M. Halik, C. Grasso, S. Barlow, J. W. Perry, S.R. Marder, and J.L. Brédas, ChemPhysChem. **5**, 982 (2004).

[44] B. Domercq, C. Grasso, J. L. Maldonado, M. Halik, S. Barlow, S. R. Marder, and B. Kippelen, J. Phys. Chem. B **108**, 8647 (2004); C. Risko, E. Zojer, P. Brocorens, S. R. Marder, and J. L. Brédas, Chem. Phys. **313**, 151 (2005).

[45] B. H. Robinson, L. R. Dalton, A. W. Harper, A. Ren, F. Wang, C. Zhang, G. Todorova, M. Lee, R. Aniszfeld, S. Garner, A. Chen, W. H. Steier, S. Houbrecht, A. Persoons, I. Ledoux, J. Zyss, and A. K.-Y. Jen, Chem. Phys. **245**, 35 (1999).

[46] R. W. Taft and I. C. Lewis, J. Am. Chem. Soc. **80**, 2436 (1958); S. Ehrenson, R. T. C. Brownlee, and R. W. Taft, Prog. Phys. Org. Chem. **10**, 1 (1973).

[47] values of σ_I taken or interpolated from J. March, Advanced Organic Chemistry (New york, 1985) and from T. H. Lowry and K. Schueller Richardson, Mechanism and Theory in Organic Chemistry, 3rd Ed., (New York, 1987).

[48] B. F. Levine and C. G. Bethea, J. Chem. Phys. **66**, 2664 (1977); S. J. Lalama and A. F. Garito, Phys. Rev. A **20**, 1179 (1979).

[49] J. L. Oudar and H. Le Person, Opt. Commun. **15**, 268 (1975); K. D. Singer and A. F. Garito, J. Chem. Phys. **75**, 3572 (1981).

[50] K. Staub, G. A. Levina, S. Barlow, T. C. Kowalczyk, H. Lackritz, M. Barzoukas, A. Fort, and S. R. Marder, J. Chem. Mater. **13**, 825 (2003).

[51] K. D. Singer, J. E. Sohn, L. A. King, H. M. Gordon, H. E. Katz, and C. W. Dirk, J. Opt. Am. B **6**, 1339 (1989); L.-T. Cheng, W. Tam, S. H. Stevenson, G. R. Meredith, G. Rikken, and S. R. Marder, J. Phys. Chem. **95**, 10631 (1991); L.-T. Cheng, W. Tam, S. R. Marder, A. E. Stiegman, G. Rikken, and C. W. Spangler, J. Phys. Chem. **95**, 10643 (1994).

[52] E. M. Breitung, C.-F. Shu, and R. McMahon, J. Am. Chem. Soc. **122**, 1154 (2000).

[53] C. R. Moylan, R. D. Miller, R. J. Twieg, K. M. Betterton, V. Y. Lee, T. J. Matray, and C. Nguyen, Chem. Mater. **5**, 1499 (1993).

[54] P. R. Varanasi, A. K.-Y. Jen, J. Chandrasekhar, I. N. N. Namboothiri, and A. Rathna, J. Am. Chem. Soc. **118**, 12443 (1996).

[55] F. Wurthner, C. Thalacker, R. Matschiner, K. Lukaszuk, and R. Wortmann, Chem. Commun. **1998**, 1739 (1998); S. Beckmann, K.-H. Etzbach, P. Kramer, K. Lukaszuk, R. Matschiner, A. J. Schmidt, P. Schuhmacher, R. Sens, G. Seybold, R. Wortman, and F. Wurthner, Adv. Mater. **11**, 536 (1999).

[56] M. Albota, D. Beljonne, J. L. Brédas, J. E. Ehrlich, J.-Y. Fu, A. A. Heikal, S. E. Hess, T. Kogej, M. D. Levin, S. R. Marder, D. McCord-Maughon, J. W. Perry, H. Röckel, M. Rumi, G. Subramaniam, W. W. Webb, and X.-L. Wu, Science **281**, 1653 (1998).

[57] M. Halik, W. Wenseleers, C. Grasso, F. Stellacci, E. Zojer, S. Barlow, J. L. Brédas, J. W. Perry, and S. R. Marder, Chem. Commun. **1490**, 1490 (2003).

[58] B. A. Reinhardt, L. L. Brott, S. J. Clarson, A. G. Dillard, J. C. Bhatt, R. Kannan, L. Yuan, G. S. He, and P. N. Prasad, Chem. Mater. **10**, 1863 (1998); L. Ventelon, L. Moreaux, J. Mertz, and M. Blanchard-Desce, Chem. Commun. **1999**, 2055 (1999); M.Rumi, J. E. Ehrlich, A. A. Heikal, J. W. Perry, S. Barlow, z. Hu, D. McCord-Maughon, T. C. Parker, H. Rockel, S. Thayunanavan, S. R. Marder, D. Beljonne, and J. L. Brédas, J. Am. Chem. Soc. **122**, 9500 (2000); E. Zojer, D. Beljonne, T. Kogej, H. Vogel, S. R. Marder, J. W. Perry, and J. L. Brédas, J. Chem. Phys. **116**, 3646 (2002).

[59] K. D. Belfield, D. J. Hagan, E. W. Van Stryland, K. J. Schafer, and R. A. Negres, Org. Lett. **1**, 1575 (1999) ; L. Antonov, K. Kamada, K. Ohta, and F. S. Kamounah, Phys. Chem. Chem. Phys. **5**, 1193 (2003).

[60] B. R. Cho, K. H. Son, S. H. Lee, Y.-S. Song, Y.-K. Lee, S.-J. Jeon, J. H. Choi, H. Lee, M. J. Cho, J. Am. Chem. Soc. **123**, 10039 (2001) ; D. Beljonne, W. Wenseleers, E. Zojer, Z. Shuai, H. Vogel, S. J. Pond, J. W. Perry, S. R. Marder, and J. L. Brédas, Adv. Funct. Mater. **12**, 631 (2002).

[61] S.-J. Chung, K.-S. Kim, T.-C. Lin, G. S. He, J. Swiatkiewicz, and P. N. Prasad, J. Phys. Chem. B 103, 10741 (1999); M. Drobizhev, A. Karotki, Y. Dzenis, A. Rebane, Z. Suo, and C. W. Spangler, J. Phys. Chem. B **107**, 7540 (2003).

[62] M. Drobizhev, Y. Stepanenko, Y. Dzenis, A. Karotki, A. Rebane, P. N. Taylor, and H. L. Anderson, J. Am. Chem. Soc. **126**, 15352 (2004).

[63] P. Kaatz and D. P. J. Shelton, Opt. Soc. Am. B **16**, 998 (1999); X. Wang, D. Wang, G. Y. Zhou, W. Yu, Y. Zhou, Q. Fang, and M. Jiang, J. Mater. Chem. **11**, 1600

(2001); B. R. Cho, M. J. Piao, K. H. Son, S. H. Lee, S. J. Yoon, S.-J. Jeon, and M. Cho, Chem. Eur. J. **8**, 3907 (2002); T. E. O. Screen, J. R. G. Thorne, R. G. Denning, D. G. Bucknall, and H. L. Anderson, J. Am. Chem. Soc. **124**, 9712 (2002); H. Lei, Z. L. Huang, H. Z. Wang, X. J. Tang, L. Z. Wu, G. Y. Zhou, D. Wang, and Y. B. Tian, Chem. Phys. Lett. **352**, 240 (2002); C. Martineau, G. Lemercier, C. I. Andraud, X. Wang, M. Bouriau, and P. L. Baldeck, Synth. Met. **138**, 353 (2003).

[64] C.-F. Shu and Y.-Y. Wang, J. Mater. Chem. **8**, 833 (1998).